REPUBLIC OF TURKEY
YILDIZ TECHNICAL UNIVERSITY
GRADUATE SCHOOL OF NATURAL AND APPLIED SCIENCES

CONTRA PREPARATION APPROACHES TO OBTAIN ALGINATE HYDROGELS AS ADSORBENTS

SERAP HAFIZOĞLU

MSc. THESIS
DEPARTMENT OF BIOENGINEERING
PROGRAM OF BIOENGINEERING

ADVISER
ASSOC. PROF. DR. M. MURAT ÖZMEN

İSTANBUL, 2019

REPUBLIC OF TURKEY

YILDIZ TECHNICAL UNIVERSITY

GRADUATE SCHOOL OF NATURAL AND APPLIED SCIENCES

CONTRA PREPARATION APPROACHES TO OBTAIN ALGINATE HYDROGELS AS ADSORBENTS

A thesis submitted by Serap HAFIZOĞLU in partial fulfillment of the requirements for the degree of **MASTER OF SCIENCE** is approved by the committee on 25.07.2019 in Department of Bioengineering, Bioengineering Program.

Thesis Adviser

Assoc. Prof. Dr. M. Murat ÖZMEN

Yıldız Technical University

Approved By the Examining Committee

Assoc. Prof. Dr. M. Murat ÖZMEN

Yıldız Technical Univeristy

Prof. Dr. İbrahim IŞILDAK

Yıldız Technical University

Assoc. Prof. Dr. Suzan ABDURRAHMANOĞLU

Marmara Univeristy

This study was supported by the Scientific Research Projects Coordination Department of Yıldız Technical University under grant of FYL-2018-3432 and by the Scientific and Technological Research Council of Turkey (TUBITAK) under grant of 2210-C National Post-Graduate Scholarship Program for Priority Areas.

ACKNOWLEDGEMENTS

Firstly, I would like to express my gratitude to my supervisor, Assoc. Prof. Dr. M. Murat ÖZMEN, for advising, supporting, and dedicating a generous amount of time and effort for me throughout my studies. His guidance helped me at all times of composing this thesis.

I would like to thank my labmates for their endless support during my thesis works, especially to Tayfun ACAR, Damla GÖKKAYA and Zeynep ÇAĞLAR. I also wish to express my thanks to my dear friends and other labmates, especially Tugçe ŞEN, Şeyma KADAYIFÇI, Dr. Burcu UCAR ACAR, Pelin PELİT ARAYICI, Seçil KAYA,Yağmur BOZKURT, İlke ŞAHİN and Kübra BÜYÜKBAYRAKTAR. I also appriciate support of Assist. Prof. Dr. Murat TOPUZOĞULLARI and Assoc. Prof. Dr. Serap DERMAN as advisers in the laboratory. I would like to extend my thanks to all of the people of the Department of Bioengineering at Yıldız Technical University for all their support and understanding during my studies.

Last but not least, I would like to offer my most gratitude to my beloved fiance, Yusuf Ersagun SEZEN, my parents and brother for their endless support and encouragement. Without their love and understanding, I would not have completed my master study.

July, 2019

Serap HAFIZOĞLU

TABLE OF CONTENTS

Page

LIST OF FIGURES x

LIST OF TABLES xiii

ABSTRACT xiv

ÖZET xvi

CHAPTER 1

INTRODUCTION 1

1.1 Literature Review 1

1.2 Objective of the Thesis 3

1.3 Hypothesis 3

CHAPTER 2

GENERAL INFORMATION 5

2.1 DYES 5

2.1.1 Definition and Classification of Dyes 5

2.1.1.1 Methylene Blue as a Basic Dye 6

2.1.2 Dye Pollution as an Emerging Environmental Problem 7

2.2 STRATEGIES FOR DYE REMOVAL 7

2.3 ADSORPTION AS A STRATEGY FOR DYE REMOVAL 8

2.3.1 The Factors Affecting Adsorption Process 9

2.3.2 Adsorption Equilibrium: Isotherm Models 9

2.3.3 Adsorption Kinetics: Kinetic Models 13

2.3.4 Adsorption Thermodynamics 15

2.4 ADSORBENT MATERIALS FOR DYE REMOVAL 15

2.4.1 Hydrogels as Adsorbents for Dye Removal 16
2.4.1.1 Alginate Hydrogels as Adsorbents for Dye Removal 17
2.4.1.2 Composite Alginate Hydrogels as Adsorbents for Dye Removal . 20
2.4.2 Macroporous Hydrogels as Adsorbents for Dye Removal 22
2.4.2.1 Macroporous Hydrogel Synthesis via Post-Crosslinking Strategy 22
2.4.2.2 Macroporous Hydrogel Synthesis via Cryogelation Technique ... 23

CHAPTER 3

MATERIALS AND METHODS 25
3.1 MATERIALS 25
3.2 METHODS 25
3.2.1 Preparation of Macroporous Alginate/MMT Composite Hydrogels . 25
3.2.1.1 By Post-Crosslinking Strategy 25
3.2.1.2 By Cryogelation Technique 26
3.2.2 Characterization Methods for Macroporous Alginate/MMT Hydrogels 277
3.2.2.1 Fourier Transform Infrared (FT-IR) Analysis 27
3.2.2.2 Pore Size and Pore Size Distribution by Scanning Electron Microscopy 27
3.2.2.3 Gel Fraction and Swelling Ratio Measurements 27
3.2.2.4 Mechanical Tests 28
3.2.3 Methylene Blue Adsorption Test 28
3.2.3.1 Batch Adsorption Procedure 28
3.2.3.2 Adsorption Isotherm Models 29
3.2.3.3 Adsorption Kinetics Study 29
3.2.3.4 Adsorption Kinetic Models 29
3.2.3.5 Estimation of Overall Dye Removal Efficiency 29
3.2.3.6 Desorption Study 30

CHAPTER 4

RESULTS AND DISCUSSION 31
4.1 MACROPOROUS ALGINATE/MMT COMPOSITE HYDROGELS PREPARED BY POST-CROSSLINKING STRATEGY 31
4.1.1 FT-IR Analysis of Post-Crosslinked Macroporous Alginate/MMT Composite Hydrogels 32
4.1.2 Pore Size and Pore Size Distributions of Post-Crosslinked Macroporous Alginate/MMT Composite Hydrogels 34
4.1.3 Gel Fraction and Swelling Ratio Measurements of Post-Crosslinked

Macroporous Alginate/MMT Composite Hydrogels 36
4.1.4 Mechanical Testing of Post-Crosslinked Macroporous Alginate/MMT Composite Hydrogels 37
4.1.5 Adsorption of Methylene Blue by Post-Crosslinked Macroporous Alginate/MMT Composite Hydrogels 39
4.1.5.1 Batch Adsorption and Isotherm Models 40
4.1.5.2 Adsorption Kinetics and Kinetic Models 42
4.1.5.3 Dye Removal Efficiency 44
4.1.5.4 Desorption Study 45
4.2 MACROPOROUS ALGINATE/MMT COMPOSITE HYDROGELS OBTAINED BY CRYOGELATION METHOD 46
4.2.1 FT-IR Analysis of Alginate/MMT Composite Cryogels 48
4.2.2 Pore Size and Pore Size Distributions of Alginate/MMT Composite Cryogels 49
4.2.3 Gel Fraction and Swelling Ratio Measurements of Alginate/MMT Composite Cryogels 51
4.2.4 Mechanical Testing of Alginate/MMT Composite Cryogels 51
4.2.5 Methylene Blue Adsorption by Alginate/MMT Composite Cryogels 52
4.2.5.1 Batch Adsorption and Isotherm Models 52
4.2.5.2 Adsorption Kinetics and Kinetic Models 54
4.2.5.3 Dye Removal Efficiency 55
4.2.5.4 Desorption Study 56
4.3 Comparision of Composite Post-Crosslinked Hydrogels and Cryogels. 57
4.4 Conclusion.....60
REFERENCES 63
CIRRICULUM VITAE 76

LIST OF SYMBOLS

q	The amount of dye adsorbed
C	The amount of dye remained in aqueous phase
q_e	The amount of dye adsorbed in equilibrium
C_e	The amount of dye remained in aqueous phase in equilibrium
q_m	Theoretical maximum adsorption capacity
K_L	Langmuir model constant
R_L	Dimensionless constant
C_0	Initial dye concentration
K_F	Freundlich model constant
N	Measure of energetic heterogenecity
t	Defined time
q_t	The amount of dye adsorbed at defined time
k_1	Pseudo-First Order model rate constant
$q_{e,calc}$	The calculated adsorption capacity in equilibrium
k_2	Pseudo-Second Order model rate constant
ΔG	Change in Gibbs free energy
ΔH	Change in Entalphy
ΔS	Change in Entrophy
K_c	Equilibrium constant in thermodynamic modelling
T	Operation temperature
R	Universal gas constant
μm	Micro meter
C_i	Initial dye concentration in experiments
R^2	Correlation coefficient
C_a	The amount of dye adsorbed
C_d	The amount of dye desorbed
M	Dosage of the adsorbent
W_g	Gel fraction
M_0	The weight of samples just after preparation
M_{dry}	The weight of samples in dry state
X_{MMT}	The weight fraction of montmorillonite
q_w	Equilibrium weight swelling ratio with respect to dry state
M_{sw}	The weight of swollen sample in equilibrium

LIST OF ABBREVATIONS

BET	Brunauer-Emmett-Teller
DE	Desorption efficiency
MB	Methylene blue
MMT	Montmorillonite
G	Gluronic acid
M	Mannuronic acid
NHS	N-hydroxysuccunimide
MES	2-(N-Morpholino) ethanesulfonic acid hydrate
Cys	Cystamine
EDC	N-(3-Dimethylaminopropyl)-N’-ethylcarbodiimide hydrochloride
XL	Crosslinker
RE	Removal efficiency
T	Tetrahedral
O	Octahedral
kPa	Kilo Pascal

LIST OF FIGURES

Page

Figure 2.1 Classification of dyes based on chemical structure [44]. 6
Figure 2.2 Chemical structure of MB [48]. 6
Figure 2.3 Components of an adsorption system [50], [51]. 8
Figure 2.4 The relation between dye adsorbed (q_e) and dye remained in solution (C_e) in equilibrium with assumptions that temperature is constant and system is a single-solute [53]. 10
Figure 2.5 C, L, H and S isotherm models observed in various adsorption systems [54] 10
Figure 2.6 Simplified scheme of monolayer adsorption model [56]. 11
Figure 2.7 Different shapes of Freundlich isotherm model due to varying N values [53]. 13
Figure 2.8 Adsorption kinetics models [57]. 14
Figure 2.9 Hydrogel preparation via crosslinking polymerization of water-soluble monomers (a) and crosslinking of water-soluble polymer (b) [66]. 16
Figure 2.10 Dye adsorption via hydrogels 17
Figure 2.11 Monomers, linkages and blocks of alginates [80] 18
Figure 2.12 Schematic drawing of ''Egg-box'' model in alginate hydrogels [80]. 19
Figure 2.13 Schematic representation of the structure of MMT clay clay [89], [90]. 20
Figure 2.14 Crystal violet removal by alginate/bentonite composite hydrogels [103] 21
Figure 2.15 Schematic representation of macroporous hydrogel preparation via post-crosslinking strategy [23], [105]. 22
Figure 2.16 Schematic representation of cryogel preparation from polymeric gel precursor [111] 23
Figure 4.1 Schematic representation of preparation of post-crosslinked alginate/MMT composite hydrogels. 32
Figure 4.2 FT-IR spectra of MMT, alginate, $A_5MMT_0XL_5$ and $A_5MMT_2XL_5$ samples. .. 33
Figure 4.3 Digital images of post-crosslinking of pre-formed alginate/MMT matrices (a), dissolution of alginate/MMT matrices in water (b) and swelling of post-crosslinked hydrogels in water (c). 34
Figure 4.4 Cross-sectional SEM micrographs of $A_5MMT_0XL_5$ and $A_5MMT_2XL_5$ samples (Scale bar: 100 µm above and 2 µm below). 35
Figure 4.5 The effect of MMT on pore size distribution of post-crosslinked

alginate/MMT composite hydrogels. 36
Figure 4.6 The effect of MMT content (a) and crosslinker amount (b) on gel fraction (%) and swelling ratio of post-crosslinked alginate/MMT hydrogels. ((a): Alginate ratio: 5 (w/v) %, crosslinker ratio: 5 (w/v) %, (b): Alginate ratio:5 (w/v) %, MMT ratio: 2 (w/v) %) 37
Figure 4.7 Typical stress-strain curves for post-crosslinked alginate/MMT composite hydrogels with varying MMT content (a) and crosslinker ratio (b). 38
Figure 4.8 The effect of MMT content (a) and crosslinker ratio (b) on elastic moduli of post-crosslinked alginate/MMT hydrogels. ((a): Alginate: 5 (w/v) % and crosslinker concentration: 5 (w/v) %, (b): Alginate: 5 (w/v) % and MMT concentration 2 (w/v) %). 39
Figure 4.9 The effect of MMT onto batch adsorption data and non-linear fit of Langmuir and Freundlich isotherm models.. 41
Figure 4.10 The effect of crosslinker amount onto batch adsorption data and non-linear regression of Langmuir and Freundlich isotherm models. 41
Figure 4.11 The effect of MMT amount on the kinetic data of post-crosslinked alginate/MMT hydrogels and non-linear fit of PFO and PSO kinetics models. 43
Figure 4.12 The effect of crosslinker amount on kinetic data of post-crosslinked alginate/MMT hydrogels and non-linear regression of PFO and PSO kinetics models 43
Figure 4.13 The effect of MMT content (a) and crosslinker ratio (b) on dye removal of post-crosslinked alginate/MMT hydrogels. ((a): Alginate: 5 (w/v) % and crosslinker concentration: 5 (w/v) %, (b): Alginate: 5 (w/v) % and MMT concentration 2 (w/v) %) 45
Figure 4.14 The effect of MMT presence on desorption efficiencies of various eluting agents for MB from post-crosslinked hydrogels. 46
Figure 4.15 Schematic representation of macroporous alginate/MMT composite hydrogel preparation via cryogelation technique. 47
Figure 4.16 Covalent crosslinking of alginate chains with Cys via EDC/NHS coupling of carbodiimide chemistry. Adapted from [138]. 48
Figure 4.17 FT-IR spectrum of alginate, AMMT0 and AMMT3 samples. Crosslinking achieved by alteration of free COO- groups of alginate into amide bonds 49
Figure 4.18 Cross-sectional SEM micrographs of AMMT0, AMMT3 and AMMT5 samples (Scale bar: 100 μm). 50
Figure 4.19 Pore size distributions of alginate/MMT composite cryogels with varying MMT content 50
Figure 4.20 The effect of MMT amount ((w/v) %) on gel fraction (%) and swelling ratio of alginate/MMT composite cryogels 51
Figure 4.21 Typical stress-strain curves for cryogels (a) and elastic moduli of cryogels with varying MMT amount (b) 52
Figure 4.22 Batch adsorption data of cryogels and non-linear fitting of Freundlich and Langmuir isotherm models. 53
Figure 4.23 Non-linear regression of PFO and PSO kinetic models on the MB retention by alginate/MMT composite cryogels (Initial dye concentration: 25 mg L^{-1}, adsorbent dosage: 0.01 g, temperature: 25 °C). 55

Figure 4.24 The effect of MMT content ((w/v) %) on dye removal (%) of alginate/MMT composite cryogels. 56
Figure 4.25 The effect of MMT presence of cryogels on desorption efficiencies of different eluting agents for MB. 57

LIST OF TABLES

Page

Table 2.1 The feasibility of the adsorption based on R_L values [53]. 12
Table 3.1 Sample designations and the amount alginate, MMT and $CaCl_2$. Alginate and MMT were dissolved in 10 mL of water, while $CaCl_2$ dissolved in 100 mL.....26
Table 4.1 The effect of MMT amount of post-crosslinked hydrogels on Langmuir and Freundlich isotherm constants 42
Table 4.2 The effect of crosslinker amount of post-crosslinked hydrogels on Langmuir and Freundlich isotherm constants 42
Table 4.3 The effect of MMT amount on PFO and PSO kinetic parameters for MB adsorption 44
Table 4.4 The effect of crosslinker amount on PFO and PSO kinetic parameters for MB adsorption 44
Table 4.5 Langmuir and Freundlich isotherm constants for MB adsorption onto AMMT0, AMMT3 and AMMT5 composite cryogel adsorbents..... 54
Table 4.6 PFO and PSO kinetic parameters for MB adsorption onto AMMT0, AMMT3 and AMMT5 samples at the initial dye concentration of 25 mg L^{-1}. 55

ABSTRACT

CONTRA PREPARATION APPROACHES TO OBTAIN ALGINATE HYDROGELS AS ADSORBENTS

Serap HAFIZOĞLU

Bioengineering

MSc. Thesis

Thesis Adviser: Assoc. Prof. Dr. M. Murat ÖZMEN

In the past century, dye-utilizing industries have been releasing synthetic dyes to the environment causing serious environmental problems. Therefore, the use and generation of new materials for dye removal by adsorption method have been of great interest. In this thesis, we developed macroporous alginate hydrogels as adsorbents for methylene blue (MB) dye removal. On the contrary to conventional methods, we employed contra preparation approaches such as post-crosslinking approach and cryogelation technique for preparation of macroporous alginate hydrogels. Montmorillonite (MMT) clay was incorporated to gel system to enhance their dye removal characteristics. As much as we aware, there is no study reporting macroporous alginate/MMT hydrogel adsorbents either prepared by post-crosslinking or cryogelation for dye removal.

Firstly, contrary to the conventional crosslinking strategies for macroporous hydrogel preparation, the post-crosslinking approach containing preparation of three-dimensional polymer matrices, followed by ionic crosslinking was utilized to prepare alginate/MMT hydrogel adsorbents. As-prepared post-crosslinked alginate/MMT hydrogels were characterized by FT-IR, SEM, gel fraction, swelling ratio, mechanical tests and MB adsorption tests.

FT-IR results of post-crosslinked hydrogels indicated that the post-crosslinking of the three-dimensional alginate matrices was achieved. SEM images revealed macroporous structure and interconnected porosity of the post-crosslinked hydrogels. Their pore size distributions were ranged between 75 µm and 250 µm. These hydrogels exhibited high water uptake capacity (13 folds of their dry weight) while their gel fractions were reached up to 85%. Post-crosslinked alginate/MMT hydrogels exhibited upward concave stress-strain curve characteristics to elastomers and maximum value of elastic moduli of them was calculated as 48 kPa. The results of MB adsorption tests indicated that, post-crosslinked hydrogels followed monolayer adsorption. The capacity of theoretical maximum adsorption was estimated as 1435.58 mg g^{-1}. They attained dye adsorption equilibrium within 3 hours of contact with MB and physisorption was found to be main driving force in MB removal by post-crosslinked hydrogels.

Although post-crosslinked alginate/MMT hydrogels exhibited remarkable properties and their adsorption efficiency is quite high, they may suffer from degradation under physiological conditions due to ionic crosslinking route as reported in the literature. Therefore, we assumed that covalent crosslinking of alginate chains may overcome the chemical stability issues of ionic crosslinking.

Therefore, in the second part of the study, cryogelation technique involving covalent crosslinking of alginate chains via carbodiimide chemistry was used to prepare alginate/MMT macroporous hydrogels (cryogels). Gel precursors were frozen at a defined sub-zero temperature and crosslinking reactions were conducted at moderately frozen state. The obtained cryogels were characterized by FT-IR, SEM, gel fraction, swelling ratio, mechanical test and adsorption studies for MB removal.

FT-IR results indicated that covalent crosslinking of alginate chains in moderately frozen state was successfully achieved. SEM images indicated the formation of interconnected porosity. Pore size distributions obtained in the range of 50 µm and 300 µm pore diameters. High gelation yield obtained (above 80 %) for all cryogels and they absorbed huge amount of water. Cryogels exhibited upward concave stress-strain curve, typical for elastomers and elastic modulus of them was estimated around 4 kPa. The results of methylene blue adsorption tests showed that cryogels removed 95 % of dye within 24 hours of contact. Maximum adsorption capacity was around 559.95 mg g^{-1}. MB adsorption by cryogels followed chemisorption path, whereby they reached their dye removal equilibrium within 3 hours of contact.

It can be concluded that, macroporous alginate/MMT hydrogels prepared by both post-crosslinking and cryogelation methods showed great performance as adsorbent for dye removal. Therefore, these post-crosslinked hydrogels and cryogels are novel promising alternatives to state-of-art adsorbents for methylene blue recovery.

Keywords: Alginate, macroporous hydrogel, composite, montmorillonite, dye removal.

ÖZET

ADSORBENT OLARAK ALJİNAT HİDROJELLERİNİN ELDESİ İÇİN KONTRA HAZIRLAMA YÖNTEMLERİNİN KULLANILMASI

Serap HAFIZOĞLU

Biyomühendislik Bölümü

Yüksek Lisans Tezi

Tez Danışmanı: Doç. Dr. M. Murat ÖZMEN

Geçtiğimiz yüzyılda boya kullanan endüstriler, ciddi çevresel sorunlara neden olan sentetik boyaları çevreye salmaktadır. Bu nedenle, adsorpsiyon yöntemi kullanılarak boyaların giderimi için yeni malzemelerin kullanımı ve üretilmesi büyük ilgi çekmektedir. Bu tezde, metilen mavisi (MB) boyasının uzaklaştırılması için makro gözenekli aljinat hidrojelleri adsorban olarak geliştirilmiştir. Geleneksel yöntemlerin aksine, bu çalışmada adsorban olarak makro gözenekli aljinat hidrojellerini hazırlamak için sonradan çapraz bağlama ve kriyojelasyon olarak adlandırılan kontra hazırlama teknikleri kullanılmıştır. Boya giderimini artırmak için, montmorillonit (MMT) kili, jel sistemine eklenmiştir. Bildiğimiz kadarıyla, sonradan çapraz bağlama veya kriyojelasyon yöntemleriyle üretilen makro gözenekli aljinat/MMT hidrojellerinin adsorban olarak kullanıldığını raporlayan bir çalışma bulunmamaktadır.

Öncelikle, makro gözenekli hidrojellerin hazırlanması için kullanılan geleneksel yöntemlerin aksine, üç boyutlu polimer matrislerinin hazırlanması ve takiben iyonik çapraz bağlanmasını içeren sonradan çapraz bağlama yaklaşımı, adsorban olarak kullanılacak aljinat/MMT hidrojellerinin hazırlanması için kulanılmıştır. Elde edilen sonradan çapraz bağlı aljinat/MMT hidrojelleri, FT-IR, SEM, jel fraksiyonu, şişme oranı, mekanik test ve adsorpsiyon testleri açısından karakterize edilmiştir.

Sonradan çapraz bağlı hidrojellerin FT-IR sonuçları, sonradan çapraz bağlama yönteminin, üç boyutlu aljinat matrislerinden süngerimsi hidrojel oluşumunu gerçekleştirdiğini göstermiştir. SEM görüntüleri, çapraz bağlanmış hidrojellerin makro gözenekli yapısını ve iç içe bağlantılı gözenekliliğini ortaya koymuştur. Gözenek boyut dağılımları 75 µm ile 250 µm arasında bulunmuştur. Elde edilen hidrojellerin yüksek su tutma kapasitesine sahip olduğu (kuru ağırlıklarının 13 katı kadar) ve jel fraksiyonlarının % 85'e ulaştığı saptanmıştır. Sonradan çapraz bağlı aljinat/MMT hidrojellerinin gerilme-gerinme eğrisi, elastomerlere özgü olan yukarı doğru içbükey olarak saptanmıştır ve bu malzemeler için maksimum elastik modül değeri 48 kPa olarak bulunmuştur. Metilen mavisi adsorpsiyon teslerinin sonuçları, sonradan çapraz bağlı hidrojellerin tek tabakalı adsorpsiyona sahip olduğunu göstermiştir. Teorik maksimum adsorpsiyon kapasitesi 1435.58 mg g^{-1} olarak bulunmuştur. Bu jeller, metilen mavisi ile temas ettikten sonraki 3 saat içinde adsorpsiyon dengesine ulaşmışlardır ve fiziksel sorpsiyonun metilen mavisi giderimi için itici güç olduğu saptanmıştır.

Sonradan çapraz bağlı aljinat/MMT hidrojelleri mükemmel özelliklere sahip olması ve adsorpsiyon veriminin çok yüksek olmasına ragmen, literatürde raporlanan çalışmalara göre, iyonik çapraz bağlanma sebebiyle bu hidrojeller fizyolojik şartlar altında dagradasyona uğrama problem yaşabilirler. Bu sebeple, aljinatın kovalent çapraz bağlanması iyonik çapraz bağlanmadan kaynaklı kimyasal stabilite problemini çözebileceği düşünülmüştür.

Bu yüzden, çalışmanın ikinci kısmında, aljinat zincirlerinin karbodiimid kimyasıyla kovalent çapraz bağlanmasını içeren kriyojelasyon tekniği, makrogözenekli aljinat/MMT hidrojellerinin (kriyojel) hazırlanması için kullanılmıştır. Jel öncüleri, sıfırın altındaki bir sıcaklıkta dondurulmuş ve çapraz bağlanma reaksiyonu donmuş sistemde gerçekleşmiştir. Elde edilen kriyojeller, FT-IR, SEM, jel fraksiyonu, şişme oranı, mekanik test ve MB adsorpsiyonu açısından karakterize edilmiştir.

FT-IR sonuçları, düşük sıcaklıklarda çapraz bağlanma reaksiyonu için karbodiimid kimyasının başarılı bir şekilde işlediğini gösterilmiştir. SEM, iç içe bağlantılı gözenek yapısının oluşumu göstermiştir. Tüm kriyojeller için gözenek boyut dağılımı 50 µm ile 300 µm arasında kaydedilmiştir. Tüm kriyojeller için yüksek jelleşme verimi (% 80'in üzerinde) elde edilmiştir ve yüksek oranda su tutma kapasitelerinin de olduğu saptanmıştır. Kriyojeller, elastomerler için tipik olan içbükey gerilme-gerinme eğrisine sahiptir ve bunların elastik modülü yaklaşık olarak 4 kPa hesaplanmıştır. Metilen mavisi adsorpsiyon testlerinin sonuçları, 24 saat temas sonrası, kriyojellerin boyanın % 95'ini giderdiğini göstermiştir. Langmuir modeli ile maksimum adsorpsiyon kapasitesi 559.95 mg g^{-1} olarak bulunmuştur. Kriyojeller tarafından metilen mavisi adsorpsiyonu, kimyasal adsorpsiyonu izlemiştir ve dengeye boya ile 3 saat temas sonrası ulaşılmıştır.

Sonuç olarak, hem sonradan çapraz bağlama hem de kriyojelasyon yöntemleriyle hazırlanan makro gözenekli aljinat/MMT hidrojelleri boya giderimi için adsorban olarak mükemmel performans göstermişlerdir. Bu sebeple, üretilen bu adsorbanlar metilen mavisinin geri kazanımı için mevcut adsorban hidrojellere alternatif olabilecek yeni ve umut vaad edici malzemelerdir.

Anahtar kelimeler: Aljinat, makrogözenekli hidrojel, kompozit, montmorillonit, boya giderimi.

CHAPTER 1

INTRODUCTION

1.1 Literature Review

Nowadays, with the development of various industries such as textile, paper and cosmetic, synthetic dye effluents in waste waters have been overly increased. These dyes cause serious ecological problems due to their non-biodegradability and toxicity [1], [2]. More damage to environment have been caused by cationic dyes like methylene blue (MB) contrary to anionic or neutral dyes [2], [3]. As MB is widely used to color wool, silk, cotton and paper, these industries release more MB day by day [3]. MB attacks living cells due to its positive charge and most specifically, gives rise to shock, tissue necrosis, vomiting, diarrhea and heart beat increase in humans [3], [4], [5].

Various strategies have been developed to remove synthetic dyes from water for bioremediation. Photodecomposition, coagulation, flocculation, ion-exchange, membrane technologies and chemical oxidizing agents are some of the methods for dye recovery [4]. Among all techniques, adsorption has been found to be superior as it is more economic and effective [4], [5]. Dye removal by adsorption has several advantages such as ease of operation, selectivity and reusability of adsorbents [6]. Therefore, various adsorbents such as activated carbon, agricultural solid by-products, low-cost materials (e.g. natural biopolymers), industrial wastes and inorganic clays have been applied to treat dye contaminated waters [1].

As a natural biopolymer, alginate and its composites are widely studied as adsorbents [7]. Alginate is a linear co-polymeric natural polysaccharide that formed by gylcosidic bonding of α-L-Gluronic acid (G) and β-D-Mannuronic Acid (M) [8]. Thus, the abundance,

biodegradability and anionic structure of alginate make it very versatile adsorbent either in bulk or hydrogel forms in dye removal process [7], [9].

Alginate hydrogels can be produced by ionic or covalent crosslinking strategies. While divalent cations have been used in ionic crosslinking, bifunctional agents can be used as covalent crosslinker. Calcium chloride has major role as ionic crosslinker, because it is cheap and enables fast-crosslinking [10]. However, fast crosslinking results in partially weak and strong crosslinked zones in hydrogel. Therefore, they may undergo degradation under altered physical conditions [11]. Chemical stability and homogenicity can be obtained by using cystamine, adipic acid dihydrazide as chemical crosslinker [12], [13]. Thus, as strategies for alginate hydrogel preparation, post-crosslinking or cryogelation techniques can be applied to tailor porosity and mechanical strength of the alginate gels.

Post-crosslinking is a simple and low-cost method for hydrogel preparation that comprises initial preparation of 3-D polymer matrices in any desired shape, followed by a crosslinking reaction [10]. This method differs from conventional crosslinking in the way of processing polymer matrices as the conventional crosslinking reactions comprises formation of 3D polymer matrice and *in-situ* crosslinking reaction at the same time [14]. Alginate beads are mostly prepared by ionic crosslinking with conventional way; however, this restricts molding property of alginate beads and causes unrestrained topology [11]. Therefore, post-crosslinking yields homogenous structure formation and enables control over obtained gel morphology, size and shape [10]. Due to these unique advantages, post-crosslinked alginate gels have been of great interest as cell culturing matrices [11], [15], tissue engineered scaffolds [15], [16], [17], [18], [19], [20], [21], [22] and thermal insulator [23]. As much as we aware, although there are some studies on post-crosslinked alginate composite hydrogels [21], [23], [24], [25], [26], they were never applied in dye removal. Therefore, there is still a need to investigate post-crosslinked alginate/MMT composite hydrogels as adsorbents to be used to remove dyes.

On the other hand, cryogelation is a simple contradictory technique that consists of *in-situ* crosslinking of polymer chains in moderately frozen state [27]. Freezing of gel precursor results in solvent crystals and unfrozen phase that crosslinking reactions

occur. The obtained macroporou hydrogels (cryogels) possess macroporosity, open pores and high mechanical elasticity that make them very useful in different research areas [28]. Cryogels prepared using alginate have been extensively applied in biological applications in forms of alginate cryo-beads [29], [30], [31], alginate-gelatin and alginate-chitosan cryogels [32], [33], [34], alginate-agarose cryogels [35], [36], [37], [38], methacrylated alginate cryogels [39], [40], [41] and click alginate cryogels [42]. However, there are rare studies in the literature in pristine alginate cryogels. Alginate cryogels from pristine alginate was only prepared by Mooney et al. and used in neural tissue engineering [13]. On the other hand, Uyar et al. prepared alginate materials called quasi-cryogels for dye removal which do not possess the properties of true cryogels such as open porous structure and interconnectivity [7], [43]. Therefore, as much as we aware, there is no study reporting the use of true alginate cryogels either in pristine or composite form for adsorption process.

1.2 Objective of the Thesis

In this thesis, we aim preparation and characterizations of novel adsorbents for MB removal based on alginate macroporous hydrogels. To do so, we applied two seperate techniques, i.e. post-crosslinking approach and cryogelation method to enhance dye removal capacity, to overcome porosity issues and to obtain tough alginate hydrogel adsorbents for MB removal. To further improve dye removal efficiency and mechanical properties, a smectite clay, i.e. montmorillonite (MMT) is incorporated into these macroporous alginate hydrogels. This thesis comprises two parts;

i) Obtaining macroporous alginate/MMT hydrogels by post-crosslinking approach for MB removal.

ii) The second part of the study aims at preparation of macroporous alginate/MMT cryogels to remove MB.

1.3 Hypothesis

In this thesis, we assume that post-crosslinking approach and cryogelation technique may induce porosity, enable tailoring of morphology and enhance mechanical properties of alginate hydrogels as adsorbents for MB.

In the first part of the thesis, we hypothesized that post-crosslinking method may overcome the limitations of bead shape and heterogenicity of obtained in alginate hydrogels as adosrbents synthesized by ionic crosslinking. Therefore, post-crosslinking approach could also enable tailoring of pyhsico-chemical properties, homogenicity and shape of ionically crosslinked alginate hydrogels by imparting open porosity thus may result in enhanced MB removal.

In the second part of the study, we used cryogelation technique that could induce open and interconnected macropore structure in alginate cryogels. We assume that, covalent crosslinking could eliminate detoriation of alginate hydrogels prepared by ionic crosslinking under physicological conditions. Moreover, covalent crosslinking of alginate chains in moderately frozen state may overcome the limitations of ionic crosslinking such as detoriation under physicological conditions that was reported in the literature to be applied in long-lasting applications.

We also envisaged that, incorporation of MMT clay into these macroporous alginate hydrogels could further boost their dye removal characteristics. Taking consideration of alginate, macroporous structure and MMT presence, post-crosslinked alginate/MMT hydrogels and alginate/MMT cryogels would posses great performance in MB removal.

CHAPTER 2

GENERAL INFORMATION

2.1 DYES AND DYE POLLUTION

2.1.1 Definition and Classification of Dyes

Dyes are colored organic compounds that are able to impart their colors to substances they contact [44]. Dyes are made up of two parts; chromophores and auxochromes. While chromophores give specific color, auxochromes are responsible for rendering solubility and affinity of the dyes [45].

Dyes are classified in three main categories including chemical structure, electronic origin of color and fiber type that they color. Chemical classification has been set based on the type of certain chromophore groups (Figure 2.1). The most common chromophore groups are azo, anthraquinone and phytalocyanine [44].

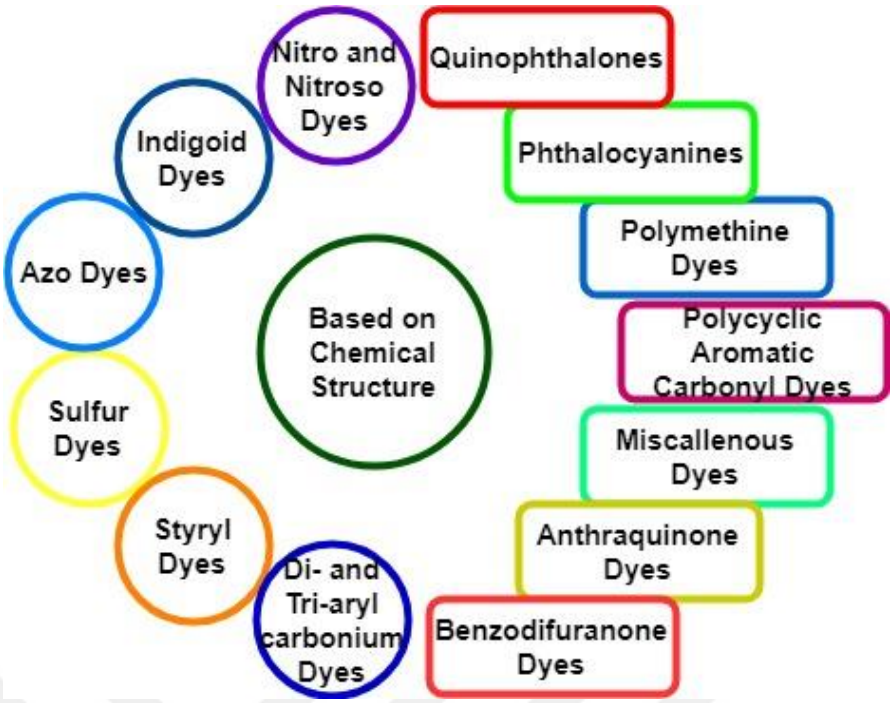


Figure 2.1 Classification of dyes based on chemical structure [44].

Dyes can also be divided into three categories as acidic, basic and neutral dyes based on their solubility in water. Solubility is possible due to availability of caboxyl, hydroxyl, amine and sulfonate groups in auxochromes of the dyes [46]. For example, acidic dyes have carboxyl groups and are negatively charged in water; however, basic dyes utilize amine groups and are positively charged in aqueous media [47].

2.1.1.1 Methylene Blue as a Basic Dye

Methylene blue (MB), or so called basic blue 9, is a positively charged water-soluble dye and is member of di-aryl carbonium dyes. Positive charge is imparted because of the sulfur atom attached to heterocyclic aromatic ring (Figure 2.2) [44].

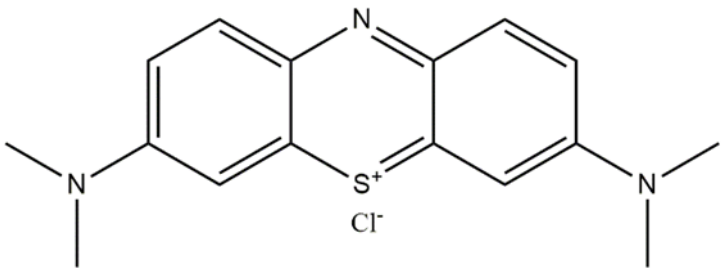


Figure 2.2 Chemical structure of MB [48].

MB is widely used to color wood, paper and textile in such industries [3]. While it has beneficial contributions to our daily life, MB is really harmful for ecological systems.

More specifically, it causes shock, nausea, diarrhea, tissue necrosis, eye burn and heart beat increase in humans [4], [6], [48].

2.1.2 Dye Pollution as an Emerging Environmental Problem

In the last century, there has been a significant increase in dye-utilizing industries. Therefore, the amount of synthetic dye consumed and released has also been increased and resulted in serious environmental pollution [46]. Paper, cosmetic, plastic and textile industries are the pioneers of dye-releasing industries. For example, in textile industry, more than 200.000 tons/year of dye are left to the ground and surface waters [46].

Industrial dyes are resistant to heat, temperature, detergents and they are accumulated where they released. They have chemical stability, hence their biological degradation is quite rare [46]. In fact, they harshly disrupt the entirety of ecological systems, more specifically the marine ecosystem. For example, basic dyes like MB directly attack living cells and deteriorate cell's integrity [4]. Since they sustained in environment, they have to be removed either before or after discharging to the nature [46]. Therefore, several strategies have been developed and applied to treat dye-contaminated waters.

2.2 STRATEGIES FOR DYE REMOVAL

Various procedures have been improved for elimination of dye effluents from waste waters. Some of these methods are photodecomposition, coagulation/flocculation, ion-exchange, ultraviolet radiation, enzymatic degradation, ozonation, membrane filtration, chemical oxidation and adsorption [4], [5], [49]. The efficiency of these methods are affected by the composition of water, amount of dye, operation conditions and by-products while processing [49].

Although these methods have been applied for recovery of dyes, they have some limitations with respect to economical cost, complication of process and production of carcinogenic by-products during operation[49]. Therefore adsorption strategy has been chosen as a more versatile way to extract dyes from waters. Adsorption has several advantages such as being cost-effective, ease of operation, selectivity and reusability of equipments [6].

2.3 ADSORPTION AS A STRATEGY FOR DYE REMOVAL

Adsorption is a mass transfer phenomena where a specific compound accumulates to a defined bulk surface from a fluidic surrounding [45]. The elements of adsorption system is given in Figure 2.3. The bulk material that holds molecules onto its surface is called adsorbent, and the specific compounds that is attached onto adsorbent surface is called adsorbate [50].

Adsorption has been driven by concentration gradient of adsorbate molecules in fluidic phase. Therefore, deposition occurs between fluid phase (gas or liquid) and bulk phase (adsorbate). The unbalanced forces available on the surface of the solid phase or adsorbent yield retaining of adsorbate molecules onto bulk materials [51].

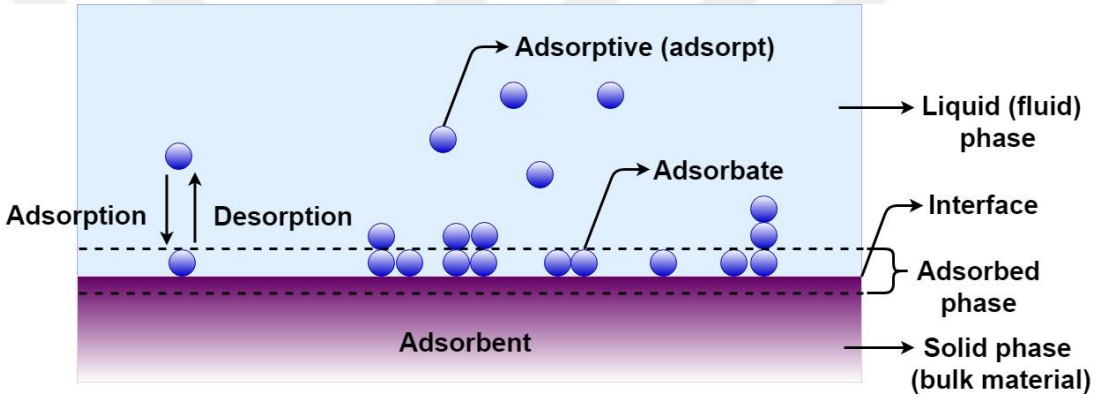


Figure 2.3 Components of an adsorption system [50], [51].

The feasibility of adsorption is determined by unbalanced forces between adsorbate and adsorbent. If adsorbate molecules are released, the process is called desorption. These forces also can be chemical or physical interactions. If the accumulation of adsorbate onto adsorbent is drived by chemical interactions, it is named as chemisorption; if otherwise, the process is defined as physisorption.

Physisorption occurs when attachment of adsorbate is conducted by Van der Waals forces or electrostatic interactions. Therefore, this is thermodynamically reversible. Adsorbate molecules are not attached to certain point and they can move through the surface of adsorbent. On the other hand, in chemisorption, covalent or ionic bonds are formed and yielded thermodynamically irreversible deposition. While mono- or multi-layer adsorption occurs in physisorption, only monolayer adsorption was observed in chemisorption [52].

2.3.1 The Factors Affecting Adsorption Process

The feasibility of the adsorption or adsorption capacity is defined by surface property of the adsorbent, temperature and pH of the environment, initial adsorbate concentration, particle size of adsorbate, solubility, presence of other compounds and flow of fluidic phase [1], [45]. For example, adsorption capacity enhances by increased surface area. Therefore, in recent years, porous adsorbents have taken great attention owing to huge surface area [51].

Adsorption is a thermodynamic phenomenon that is influenced by temperature. If adsorption follows endothermic path, adsorption capacity increases by temperature; if not, adsorption is negatively affected by increasing temperature [1]. pH also alters adsorption capacity, by changing surface of adsorbents or ionization degree of adsorbate molecules. For example, acidic dyes are more ionized by decreasing pH meaning enhanced adsorption capacity [44]. However, adsorption of basic dyes works perfect at high pH values [1].

One should also be note that, both enhanced adsorbate amount and adsorbent concentration result in increased adsorption capacity. After a specific limit of adsorbate amount, adsorbent no longer accepts adsorbate and reaches its equilibrium [1].

2.3.2 Adsorption Equilibrium: Isotherm Models

The state of adsorption equilibrium has been defined as saturation of adsorbent surface with adsorbate molecules [53]. This state is a function of adsorbate concentration, adsorbent amount and temperature. If we assume that temperature is constant, than adsorption equilibrium will be only a function of adsorbate concentration. These whole assumptions are worked in single-solute system. If q_e is defined as dye adsorbed and C_e is assigned as dye amount retained in solution in equilibrium, then we observe a linear relation between q_e and C_e. However, even C_e more increases, q_e stops raising to saturation of active sites of adsorbate (Figure 2.4) [53]. q_e and C_e values can be experimentally determined by altering initial adsorbate concentration with no change in adsorbent amount in constant temperature.

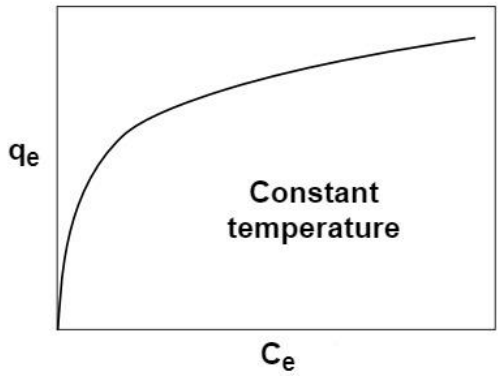


Figure 2.4 The relation between q_e and C_e in equilibrium with assumptions that temperature is constant and system is a single-solute [53].

Before we explain classical isotherm models that used to define adsorption characteristics, we should mention 4 main shapes of general isotherm types; C, L, H and S sorption models purposed by Giles et al. (Figure 2.5) [54]. C isotherm indicates that dye adsorbed (q) and dye remained in the solution (C) is the same in any dye concentration. L isotherm explains that when dye concentration increases, the amount of dye adsorbed reaches to a constant q value. If the initial slope of L isotherm is high, then L isotherm turns into H isotherm. If two or more opposite forces are presented in adsorption, S isotherm will be observed [54].

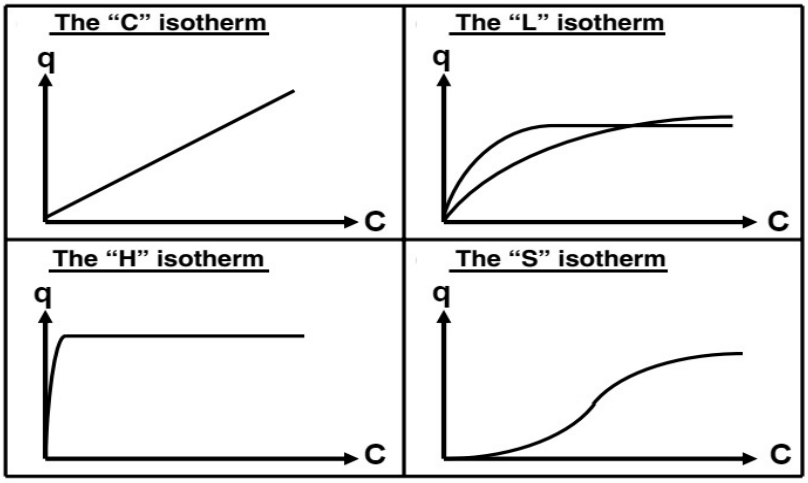


Figure 2.5 C, L, H and S isotherm models observed in various adsorption systems [54].

Adsorption isotherms also can be classified based on the number of parameters/constants that they use. These isotherms are one-parameter, two-parameter and three-parameter isotherm models.

***One-parameter isotherms*:** Also known as irreversible or Henry isotherm models, one-parameter isotherm defines constant q values independent from adsorbate concentration. Linear relationship can be observed between adsorbate amount and adsorbate load. Thus, this model also follows a C isotherm. When adsorbate concentration goes to zero, Henry isotherm has been required to understand the adsorption in thermodynamic manner [53].

***Two-parameter isotherms*:** Most well-known two isotherm models, namely Langmuir and Freundlich are belonging to this class of isotherms. Other two-parameter isotherm models are Dubinin-Radushkevic, Tempkin, Flory-Huggins and Hill [55]. Langmuir and Freundlich models will be explained in detail in following paragraphs, as both models are characteristic of L isotherms.

Langmuir model assumes that active sites for adsorption is equally dispersed over adsorbent and favors monolayer irreversible adsorption (Figure 2.6) [1], [56].

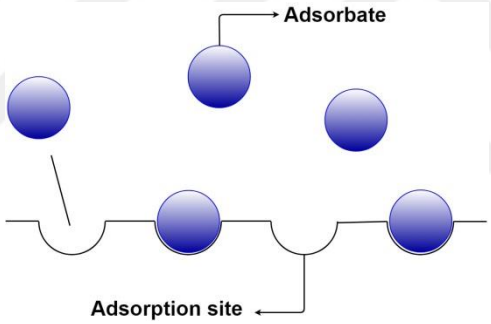


Figure 2.6 Simplified scheme of monolayer adsorption model [56].

The Langmuir model has been explained by following equation (Eq. 2.1):

$$q_e = \frac{q_m K_L C_e}{1 + K_L C_e} \tag{2.1}$$

where q_e is defined as the amount of dye adsorbed in equilibrium (mg g^{-1}), C_e is known as the amount of dye remained in the solution in equilibrium state (mg L^{-1}), q_m is described as the maximum adsorption capacity or theoretical adsorption limit (mg g^{-1}) and K_L is expressed as the Langmuir constant (L mg^{-1}) [7]. There are several linearized forms of this model, some of them are as follows [1], [53]:

$$\frac{C_e}{q_e} = \frac{1}{q_m} C_e + \frac{1}{q_m K_L} \tag{2.1a}$$

$$\frac{1}{q_e} = \frac{1}{q_m K_L} \frac{1}{C_e} + \frac{1}{q_m} \tag{2.1b}$$

Since Langmuir explains monolayer adsorption, dimensionless constant (R_L) calculated from parameters of Langmuir model gives information about the nature of process. R_L can be estimated by following equation (Eq. 2.2):

$$R_L = \frac{1}{1+C_0 K_L} \tag{2.2}$$

As C_0 is the initial dye concentration (mg L^{-1}). The favorability of the adsorption according to R_L values are given in Table 2.1.

Table 2.1 The feasibility of the adsorption based on R_L values [53].

R_L Value	**Feasibility of Adsorption**
>1	Unfavorable
=1	Linear
0<R_L<1	Favorable
=0	Irriversible

Freundlich model is not restricted with monolayer adsorption; in contrast, it favors multilayer and reversible adsorption. The model purposes that active sites for adsorption are not uniformly distributed over adsorbate surface and heterogeneous adsorption is observed where the adsorption heat also non-uniformly deployed [55]. Freundlich model is applied by following equation (Eq. 2.3):

$$q_e = K_F {C_e}^N \tag{2.3}$$

K_F is known as the Freundlich constant that characterizes the strength of the adsorption meaning that higher K_F (mg g^{-1}) value indicates higher amount of adsorbent loading can be done. N is related to the nature of the adsorbent and gives information about the measure of energetic heterogeneity [4]. Linear form of Freundlich model can be stated by (Eq. 2.3a) [1]:

$$lnq_e = lnK_f + N\ lnC_e \tag{2.3a}$$

Based on the value of N, Freundlich isotherm can be in three different shapes as illustrated in Figure 2.7. If N<1; Freundlich model shows L isotherm, if N=1, Freundlich

model becomes C isotherm type, and if N>1; Freundlich model turn into S isotherm model, inevitably [53].

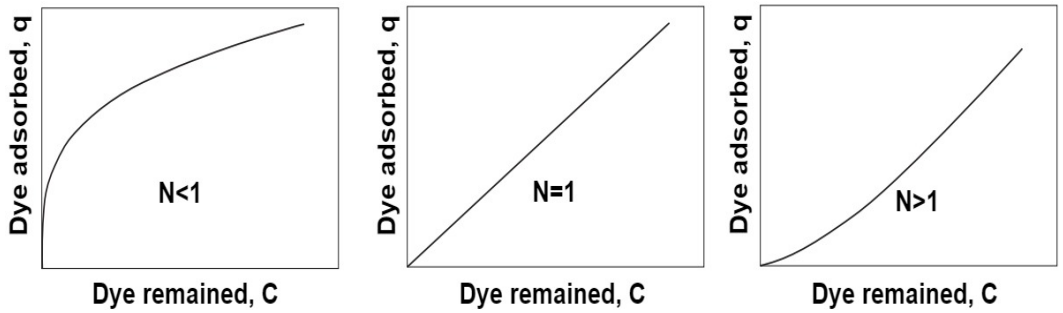


Figure 2.7 Different shapes of Freundlich isotherm model due to varying N values [53].

Three-parameter isotherms: These isotherm model are developed by introducing another parameter into two-parameter isotherm models [53]. These models are Koble-Corrigan, Radke-Prausnitz, Sips, Redlich-Peterson, Toth, Khan and Multilayer physisorption (Brunauer-Emmett-Teller, BET) isotherms [55].

2.3.3 Adsorption Kinetics: Kinetic Models

Since the saturation of adsorbent with adsorbate has not been instantaneously, the time for reaching equilibrium needs to be determined. Therefore, the time progression of reaching equilibrium in adsorption systems is called adsorption kinetics [53].

Mainly adsorption process occurs in three steps; mass transfer via diffusion of adsorbate particles from bulk fluid to exterior surface of adsorbate, inner mass transfer of adsorbate particles to interface where sorption occurs, and the sorption itself. Therefore, models for adsorption kinetics are based on either diffusion or sorption is a rate-limiting step. Mass transfer and adsorption models used to evaluate adsorption kinetics are listed in Figure 2.8. [57].

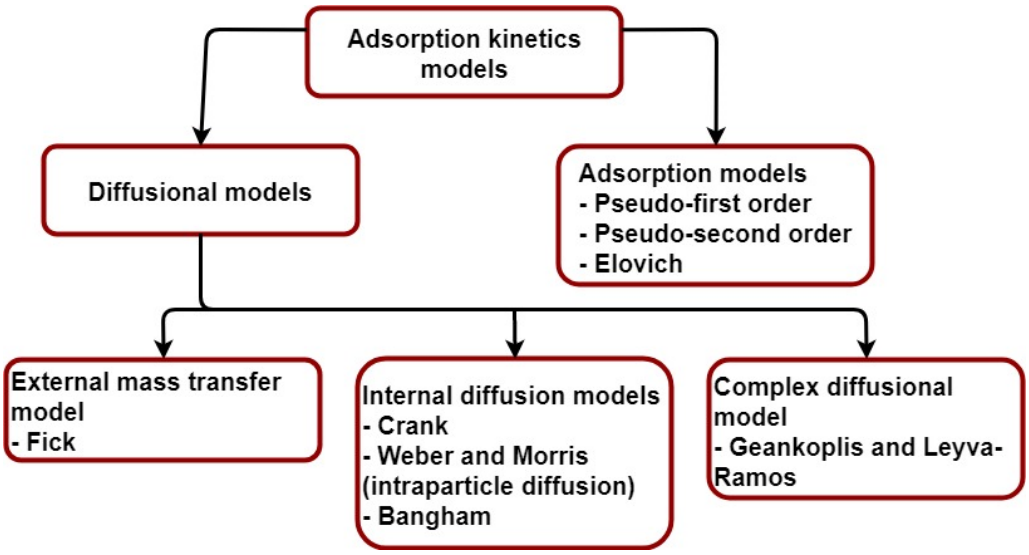


Figure 2.8 Adsorption kinetics models [57].

Pseudo-first order (PFO) kinetic model is generally utilized to identify dye adsorption from waters. It predicts multilayer adsorption, meaning that adsorption has been driven by Van der Waals forces or electrostatic interactions, or physisorption [58], [59]. Non-linear form of Lagergren PFO model is expressed as follows (Eq. 2.4)

$$q_t = q_{e,calc}(1 - e^{-k_1 t}) \tag{2.4}$$

As t is the time intervals (min), q_t is defined as the adsorption capacity at certain time (mg g^{-1}), k_1 is the PFO constant (min $^{-1}$) and $q_{e,calc}$ is the equilibrium adsorption capacity (mg g^{-1}) calculated by regression of PFO model [4]. Linearized form of PFO model is given by Eq. 2.4a:

$$\log(q_{e,calc} - q_t) = \log q_{e,calc} - \frac{k_1}{2.303} t \tag{2.4a}$$

Pseudo-second order (PSO) kinetic model is originated based on the theory that the adsorption has a rate limiting step that covers the sharing or transfer of electrons between adsorbent surface and adsorbate molecules. Mostly monolayer adsorption has been observed since the interaction between adsorbate surface and adsorbent is either ionic or covalent. Therefore, the model has been fictionalized based on chemisorption process [58], [59]. Non-linear form of PSO kinetic model has been provided by Eq. 2.5:

$$q_t = q_{e,calc} + \frac{q_{e,calc}}{(1+q_{e,calc}k_2 t)} \tag{2.5}$$

Where k_2 is known as the PSO kinetic constant (g mg^{-1} min^{-1}). $q_{e,calc}$ and q_e are the same in most cases [5], [58], [59]. Linear form of PSO model has been shown by Eq. 2.5a:

$$\frac{t}{q_t} = \frac{1}{k_2 q_e} + \frac{1}{q_e} t \quad (2.5a)$$

2.3.4 Adsorption Thermodynamics

Thermodynamic modelling of adsorption is considered when testing kinetics models and spontaneity of sorption process [5]. In this way, change of Gibb's free energy (ΔG, kJ mol^{-1}), change of enthalpy (ΔH, kJ mol^{-1}) and change in entropy (ΔS, J mol^{-1} K^{-1}) has been calculated and evaluated. To find these values, adsorption experiments should be completed at varying temperatures. By taking account of C_e and q_e values as function of varying temperature, the equilibrium constant K_c (L g^{-1}) is calculated by Eq. 2.6:

$$K_c = \frac{q_e}{C_e} \quad (2.6)$$

Therefore, K_c has been used to calculate ΔG of adsorption by Eq. 2.7:

$$\Delta G = -R\,T \ln K_c \quad (2.7)$$

where R is defined as the universal gas constant (8.314 J mol^{-1} K^{-1}) and T is the operation temperature (K) [5].

Van't Hoff equation gives relationship between change in enthalpy and entropy for adsorption. Eq. 2.8 summarizes Van't Hoff law.

$$\ln K_c = \frac{\Delta S}{R} - \frac{\Delta H}{RT} \quad (2.8)$$

Adsorption is thermodynamically favorable and spontaneous when ΔG<0, suggesting that the process follows physisorption. When ΔH value is negative, adsorption is exothermic, otherwise it will be attained as endothermic process. ΔS shows the randomness and orderliness of adsorption process [5].

So explained above, various models have been developed for characterization of adsorption process between different adsorbent and adsorbate materials.

2.4 ADSORBENT MATERIALS FOR DYE REMOVAL

The problem of dye pollution and the preference of adsorption to treat dye contaminants have emerged improvement and development of adsorbent materials.

These materials can be either natural or synthetic originated possessing following properties:

- Owing high dye removal capacity and enhanced surface area,
- High mechanical strength and reusability,
- Preferably low-cost and easily generated,
- Having high active sites for dye attachment,
- Chemical stability and non-toxicity [4], [60], [61].

As adsorbent materials, activated carbon, dead or living biomasses (microbial cultures), agricultural-solid by products, zeolites (for example silica and alumina), metal oxides, carbon derived materials (e.g. graphene, graphene oxide), clays and various biopolymers have been extensively applied [48], [62], [63], [64]. These adsorbents have been generated in different shapes and morphologies such as nanoparticle, microparticle, mezoporous material, conventional hydrogels, macroporous hydrogels or composites [62], [63], [65].

2.4.1 Hydrogels as Adsorbents for Dye Removal

Hydrogels are three-dimensional (3D) polymeric networks that retain huge amount of water. Hydrogels can be synthesized by either crosslinking polymerization of water-soluble monomers (Figure 2.9a) or direct crosslinking of water-soluble polymers (Figure 2.9b) [66].

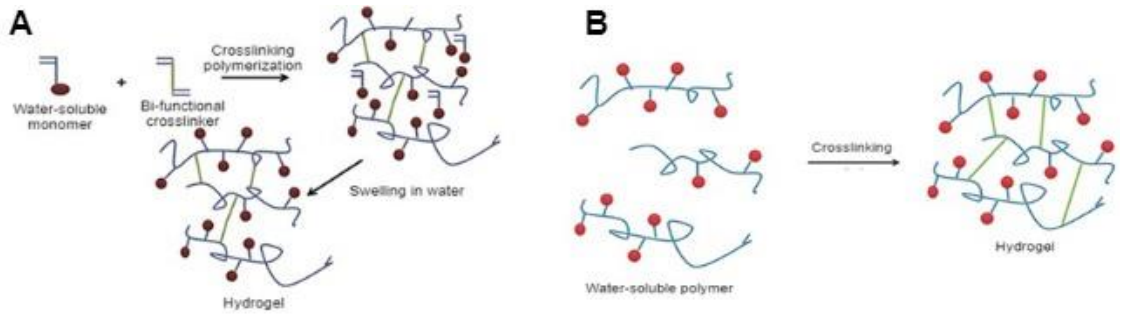


Figure 2.9 Hydrogel preparation via crosslinking polymerization of water-soluble monomers (a) and crosslinking of water-soluble polymer (b) [66].

Hydrogels can be synthesized from water-soluble natural originated or synthetic polymers and they inherently possess the property of what they are made up of.

Therefore, they are widely employed in biomedical, bioseparation and environmental applications [4], [67], [68], [69].

Hydrogels absorb and hold huge amount of water and the compounds dissolved in water permeates into hydrogel matrices. Therefore, they also take attention as adsorbent for removal of various compounds such as heavy metals, phenolic compounds and different types of dyes (Figure 2.11) [70], [71]. For example, anionic hydrogels such as alginate [7], *kappa*-carrageenan [72], poly (acryl amide) [73], cellulose [74], poly (acrylic acid) [75] hydrogels have been studied for cationic dye removal such as MB. On the other hand, cationic hydrogels such as chitosan [76], gelatin [77], poly (aniline) [78] have been applied to remove anionic dyes from polluted waters.

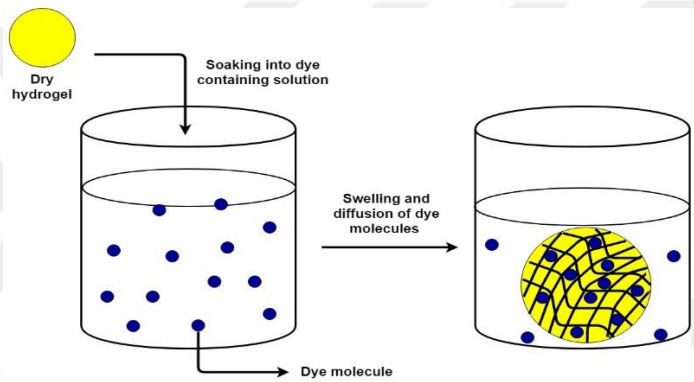


Figure 2.10 Dye adsorption via hydrogels.

Adsorbent hydrogels are mostly synthesized from natural polysaccharide polymers. They are easily extracted as sustainable materials abundant in nature, relatively cost-effective, biodegradable, non-toxic and enabling chemical modifications [79]. Alginate is one of the natural polysaccharide that is widely studied in cationic dye removal.

2.4.1.1 Alginate Hydrogels as Adsorbents for Dye Removal

Alginate is the general name of alginic acid salts has been extracted from seaweeds or bacteria [80]. It is an unbranched anionic copolymer that formed by α-L-Gluronic acid (G) and β-D-mannuronic acid (M) units that are covalently bonded with α- or β-1-4 glycosidic bonds [62]. Monomers, linkages and blocks of alginate are illustrated in Figure 2.12.

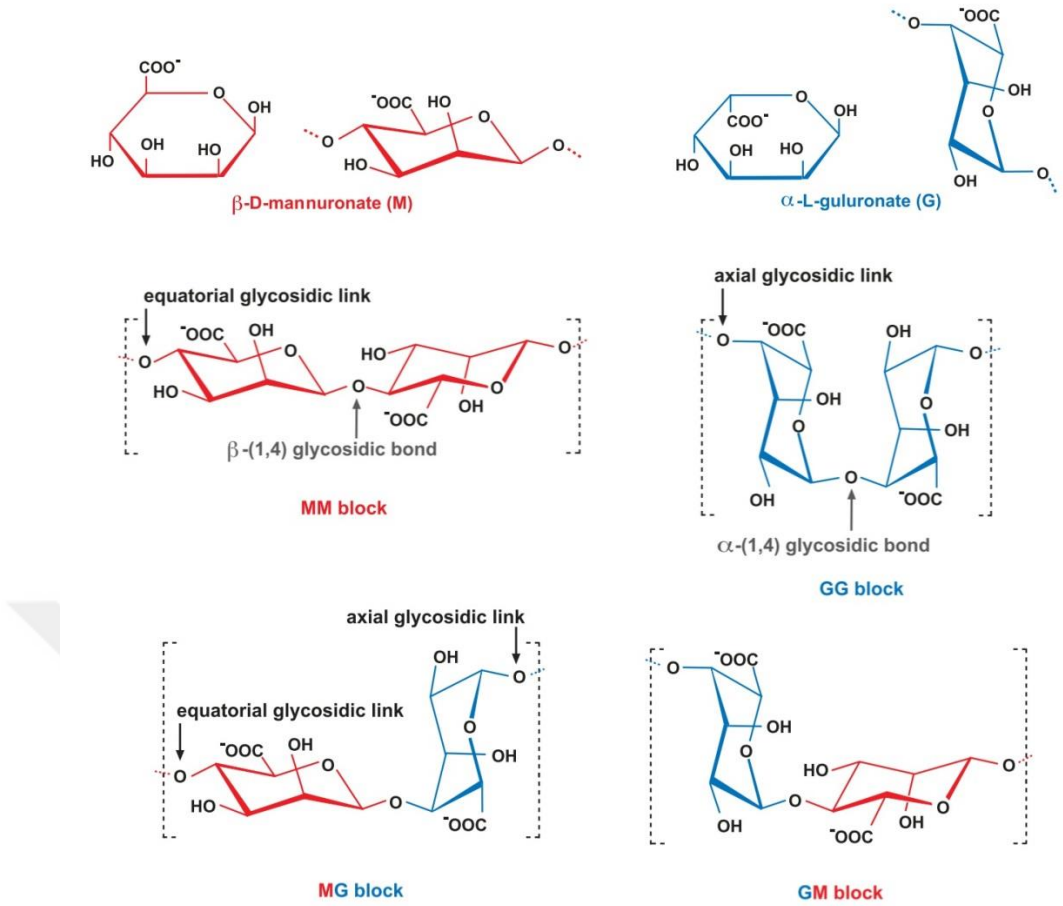


Figure 2.11 Monomers, linkages and blocks of alginates [80].

Alginate forms hydrogels in the entity of divalent cations, such as calcium (Ca^{2+}), where the process called physical crosslinking. When Ca^{2+} is introduced to alginate, carboxylate groups of GG blocks ionically attach with Ca^{2+} ions, forming alginate hydrogels (Figure 2.13). This formation is also named as 'Egg-box' model [80].

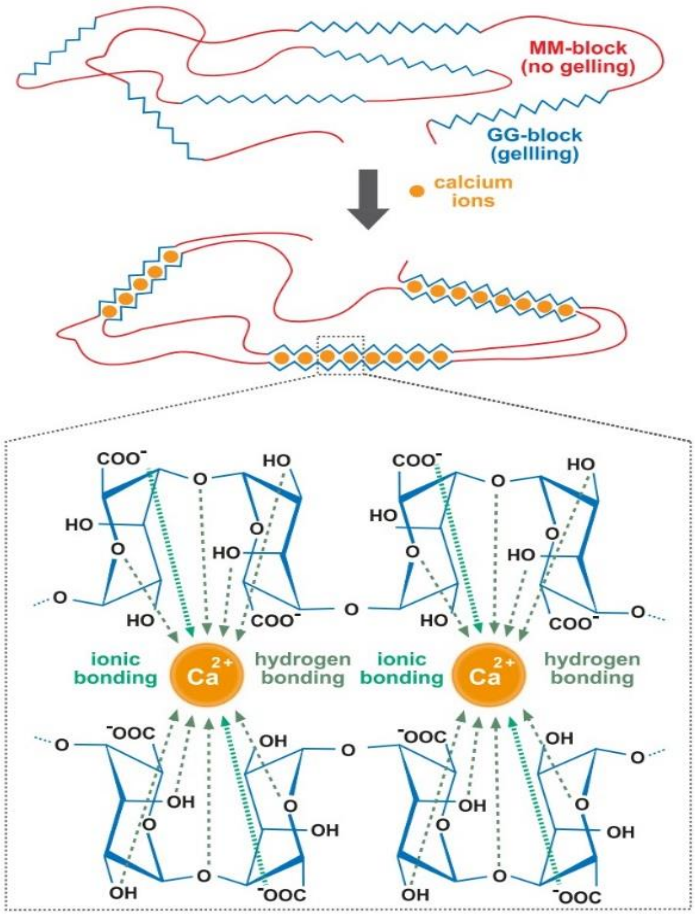


Figure 2.12 Schematic drawing of ‘’Egg-box’’ model in alginate hydrogels [80].

Ionically crosslinked alginate hydrogels still possess free carboxylate groups. Therefore, they become unique materials in recovery of cationic dyes. For example, Dinu et al. [4] and Liu et al. [9] used ionic crosslinked alginate hydrogels for MB removal. Besides, these alginate hydrogels have been also used to remove pesticide [81] and heavy metals [8].

Ionic crosslinking strategy may be useful for adsorption process; however it has some limitations for other applications. This strategy yields strongly crosslinked zones and weakly crosslinked zones (i.e. junction zones). Therefore, this inequality of crosslinking points badly affects their chemical stability under physiological conditions [82].

In covalent crosslinking strategies, more homogenous and chemically stable alginate hydrogels are formed. In this process, cystamine, adipic acid dihydrazide, or glutaraldehyde have been utilized as crosslinker [12], [83]. For example, Zhao et al. used cystamine as crosslinker to form alginate hydrogels [12].

2.4.1.2 Composite Alginate Hydrogels as Adsorbents for Dye Removal

As much as alginate hydrogels exhibited remarkable performance in dye adsorption processes, they still exhibit restrictions with respect to adsorption capacity. To overcome this limitations, various materials have been incorporated into alginate hydrogels to form composite resulting in significantly enhanced dye removal capacity. For example, Lezehari et al. [84] added pillared clays, Li et al. [85] incorporated graphene oxide, Mahmoodi et al. [86] loaded titania nanoparticles and Uyar et al. [7] embedded montmorillonite (MMT) clay into alginate hydrogels to enhance dye removal capacity against cationic dyes. In all of them, clays take attention owing to low-cost, abundance and high water uptake capacity [7].

Clays are finely-grained minerals formed by stack of tetrahedral (T) and octahedral (O) sheets and the centers of these layers are generally occupied with a cation [87]. They hold excessive amount of water and are negatively charged in water due to available hydroxyl groups onto layers. They also possess cation exchange capacity, becoming candidates to form composite hydrogels as adsorbents to remove cationic dye effluents.

MMT is a water-soluble, negatively charged smectite clay, made up of two T and one O layers attached with Al^{3+} or Mg^{2+} (Fig. 2.14). $(Ca_{0.14}Na_{0.02})_{0.16}(Al_{1.66}Mg_{0.36}Fe_{0.04})_{2.08}(Si_{3.90}Al_{0.10})_{4.00}O_{10.00}(OH)_{2.00}1.02H_2O$ is the chemical formulation of MMT, which is never observed in nature. The natural form of MMT is called bentonite; however, bentonite can also comprises feldspar, cristobalite and quartz addition to MMT particles [88].

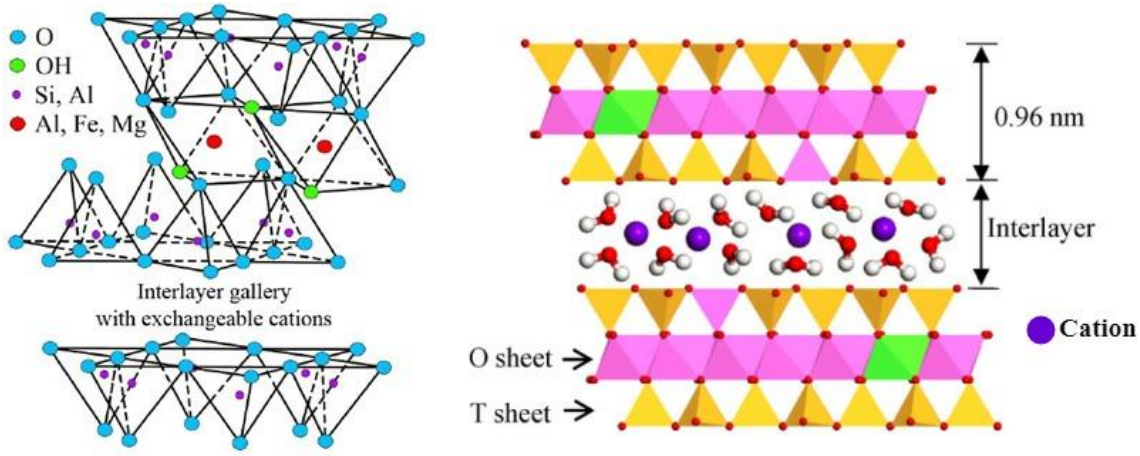


Figure 2.13 Schematic representation of the structure of MMT clay clay [89], [90].

MMT possesses high cation exchange capacity, enhanced surface area, huge water retention capacity [88]. Therefore, MMT either in pure or composite form, is used to remove heavy metals [91], organic pollutant [92], pesticide [93] and synthetic dyes [94].

Previous studies reported that, MMT enhances dye adsorption efficacy of alginate hydrogels. For example, Wang et al. [95] added MMT into alginate/poly (vinyl alcohol)/chitosan hydrogel, Li et al. [96] incorporated modified MMT into alginate hydrogels, Saavedra-Labastida et al. [97] loaded cationic surfactant modified MMT into alginate hydrogels, Remigio-Reyes et al. [98] prepared MMT embedded alginate/chitosan hydrogels, Uyar et al. [7] generated alginate/MMT composite hydrogels, Hassani et al. [99] produced nano-sized MMT loaded alginate hydrogels for improvement of dye removal capacity against cationic dyes. MMT also used to remove anionic dyes. For example, Talep et al. [100] used organophilic MMT loaded alginate hydrogels for anionic dye removal.

Not only MMT but also other clays were employed to enhance dye removal efficiencies of alginate/clay composite hydrogels. For example, alginate/clinoptilolite [4], alginate/hectorite [101], alginate/halloysite [9] and alginate/bentonite [102] composite hydrogels have been successfully applied to treat waters contaminated with cationic dyes. For instance, Fabryanty et al. illustrated enhanced crystal violet as cationic dye removal by alginate/bentonite composite hydrogels (Figure 2.15) [103].

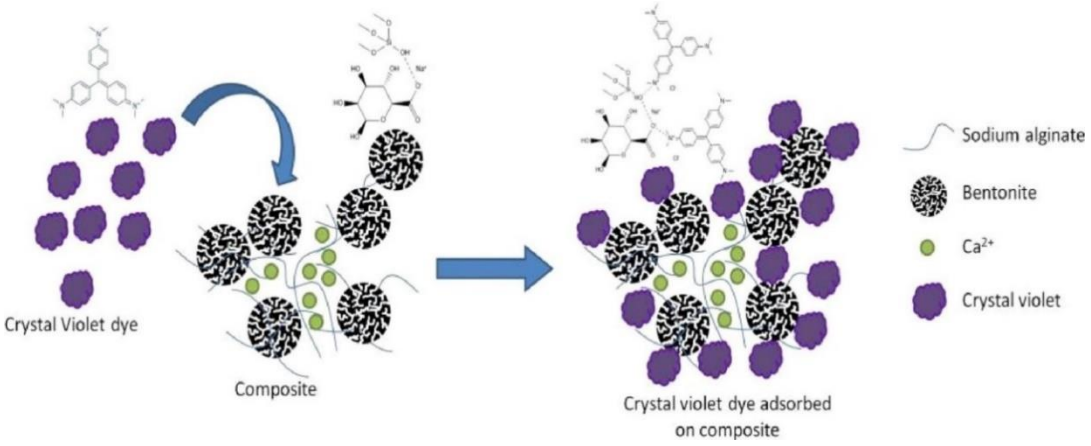


Figure 2.14 Crystal violet removal by alginate/bentonite composite hydrogels [103].

As much as hydrogels either pure or composite form, show super performance in dye removal, they still possess lack of porosity. Therefore, macroporosity has to be induced for further enhancement of dye recovery of the hydrogels.

2.4.2 Macroporous Hydrogels as Adsorbents for Dye Removal

Macroporous hydrogels are specific type of hydrogels where pore size are above 50 nm in diameter [104]. They are very versatile polymeric materials that can be used in different application areas such as biomedical, separation and environmental areas. Since various methods can be applied to prepare macroporous hydrogels, post-crosslinking approach and cryogelation techniques draw attention due to their versatility and simplicity. Both techniques are explained in the following paragraphs in detail.

2.4.2.1 Macroporous Hydrogel Synthesis via Post-Crosslinking Strategy

Post-crosslinking is method to produce macroporous hydrogels in any desired shape and morphology. This method is comprised of two steps; preparation of 3D polymer matrices, later crosslinking at ambient conditions (Figure 2.16) [105]. Polymer matrices can be prepared either by slow freezing or flash freezing followed by subsequent freeze-drying to sustain suitable macroporosity inside. Afterwards, when polymer matrices are soaked into crosslinker solution, polymer matrices are crosslinked forming macroporous hydrogels [106]. After that step, these gels can be dried for further use and storage. Alteration in reactions conditions yield tailoring of shape, internal morphology and mechanical elasticity [105].

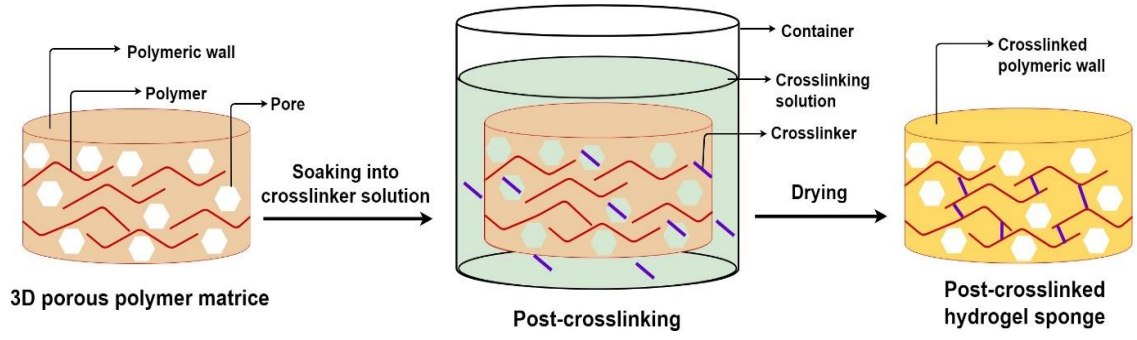


Figure 2.15 Schematic representation of macroporous hydrogel preparation via post-crosslinking strategy [23], [105].

Post-crosslinked macroporous alginate hydrogels are widely employed as cell culturing matrices, tissue engineered scaffolds and non-flammable materials [17], [19], [82], [106]. For example, Katsen-Globa et al. [82] used post-crosslinking strategy to form alginate hydrogels for cell preservation purpose. Petrenkov et al. [107] also used post-

crosslinking strategy to attach gelatin into inner surface of alginate matrices for the same. Nguyern et al. [18] applied post-crosslinking approach for production of porous anti-inflammatory alginate scaffolds. Liu et al. [21] used post-crosslinking strategy for formation of alginate/halloysite nanotube composites. In this regard, this technique has become important for production of macroporous matrices to be used in various applications.

2.4.2.2 Macroporous Hydrogel Synthesis via Cryogelation Technique

Cryogelation is a method to produce of 3D macroporous hydrogels (or cryogels). This method involves preparation of polymeric or monomeric gel precursor, freezing at defined sub-zero temperatures and crosslinking in moderately frozen state (Figure 2.17) [108].

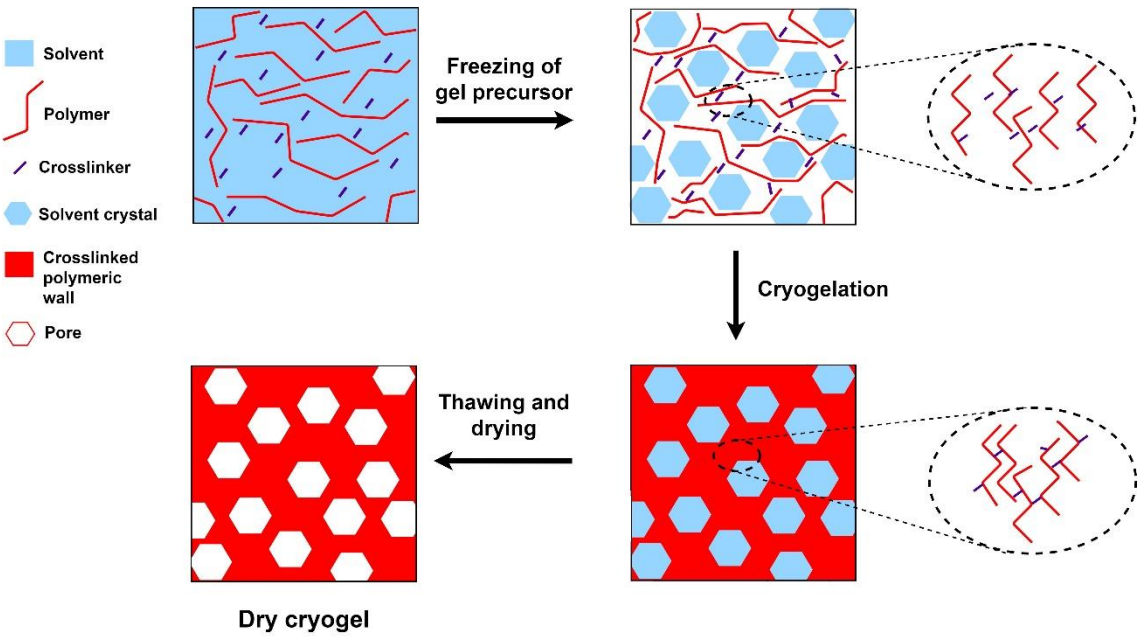


Figure 2.16 Schematic representation of cryogel preparation from polymeric gel precursor [109].

The closer look on the formation of cryogels reveals the creation of macroporosity. Freezing of gel precursor forms in two parts; unfrozen liquid microphase where crosslinking occurs and solvent crystals which act as porogen [110]. Thawing of solvent crystals results in macroporous crosslinked polymeric networks or cryogels.

Cryogels exhibit remarkable properties. They own interconnected porosity which impart super-fast responsiveness when introduced to solvents [111], [112]. They possess

superior mechanical elasticity compared to other hydrogels whereby they can be compressed up to 80% without any crack or deformation [108]. Therefore, cryogels are employed in tissue engineering, separation, biosensor, antibacterial and water treatment applications [36], [113], [114], [115], [116].

Alginate in cryogel systems have been broadly utilized in biomedical applications. For example, alginate/agarose cryogels were applied for biomedical applications [117]. Aginate/laponite injectable cryogels were employed to deliver protein [118]. Alginate/carboxymethyl-cellulose cryogels were used as scaffolds [13]. Poly (ethylene glycol)/alginate/gelatin cryogels were utilized for cell culturing [119]. Injectable alginate cryogels were used as vaccines [39], [40],[41]. These alginate cryogels exhibited greater performance in those applications.

On the contrary to alginate cryogels, various cryogels such as poly (acryl amide)/starch cryogels [5], poly (acryl amide)/chitosan cryogels [120], poly (4-vinyl pyridine)/graphene oxide cryogels [121], poly (2-acrylamido-2-methylpropane sodium sulfonate)/magnentite cryogels [122] and semi-interpenetrating composite cryogels based on starch, poly (acryl amide) and chitosan [123] have been utilized for cationic dye removal from waste waters.

In this thesis, as will be seen below, the two methods, post-crosslinking approach and cryogelation described above will be utilized to produce macroporous alginate/MMT hydrogels as adsorbents to remove MB.

CHAPTER 3

MATERIALS AND METHODS

3.1 MATERIALS

Alginic acid sodium salt from brown algae (Alginate, Sigma-Aldrich), Montmorillonite K10 (MMT, Sigma Aldrich), Calcium Chloride ($CaCl_2$, Merck), Methylene Blue (MB, Sigma-Aldrich), N-Hydroxysuccinimide (NHS, Sigma), 2-(N-Morpholino) ethanesulfonic acid hydrate (MES, Sigma), Cystamine Hydrochloride (Cys, Sigma) and N-(3-Dimethylaminopropyl)-N'-ethylcarbodiimide hydrochloride (EDC, Sigma), Hydrochloric acid (HCl, Merck), Acetic acid (Merck) and Metanol (Merck) were used as received.

3.2 METHODS

3.2.1 Preparation of Macroporous Alginate/MMT Composite Hydrogels

3.2.1.1 By Post-Crosslinking Strategy

Alginate was dissolved in water to obtain 5 (w/v) % alginate solution. Certain amount of MMT was also incorporated into the alginate solution and mixed to form homogenous solution. Then after, the mixtures were drawn into syringes and kept in cryostat (-18°C) for 24 hours and subsequently freeze-dried (-60°C, 24 h). As a result, pre-formed polymer matrices were obtained.

Pre-formed polymer matrices were then inserted into the $CaCl_2$ solutions with varying concentrations for post-crosslinking reaction. The reaction was conducted for 72 hours at stirring speed of 200 rpm at 25°C. After post-crosslinking, macroporous alginate/MMT

hydrogels were washed thoroughly using distilled water, replaced at least 4 times and then they were freeze-dried for storage and further use.

All samples were designated as $A_xMMT_yXL_z$ where x refers to alginate ratio (x (w/v) %), y indicates MMT ratio (y (w/v) %) and z shows $CaCl_2$ ratio (z (w/v) %). As an example, $A_5MMT_0XL_5$ refers to sample containing alginate 5 (w/v) %, MMT 0 (w/v) % and $CaCl_2$ 5 (w/v) %.

Table 3.1 Sample designations and the amount alginate, MMT and $CaCl_2$. Alginate and MMT were dissolved in 10 mL of water, while $CaCl_2$ dissolved in 100 mL.

Sample Code	**Alginate, (w/v) %**	**MMT, (w/v) %**	**$CaCl_2$, (w/v) %**
$A_5MMT_0XL_5$	5	0	5
$A_5MMT_2XL_5$	5	2	5
$A_5MMT_3XL_5$	5	3	5
$A_5MMT_2XL_3$	5	2	3
$A_5MMT_2XL_1$	5	2	1

3.2.1.2 By Cryogelation Technique

Certain amount of alginate, 28 mg NHS, 62 mg MES were dissolved in 2 mL of double distilled water by stirring 40 minutes at 25^0C to obtain molar ratio of COO^-: NHS as 2:1. 3 (w/v) % or 5 (w/v) % MMT was added into solution and the obtained composite cryogels were designated as AMMT3 and AMMT5 according to MMT ratio. Also, control samples were prepared without MMT (named as AMMT0). Later, fresh solution of 112 mg Cys in 100 µL distilled water was added into homogen solution and further mixed for 10 more minutes. Certain amount of EDC was added to the gel precursor and mixed quickly. Then, gel precursor was drawn into disposable syringes, placed into cryostat (-18^0C) and kept there for 48 h for complete gelation. In gel precursor solution, mole ratio of COO^-: NHS: EDC was set to 2:1:2. After gelation at -18^0C, samples were removed from syringes, washed with distilled water and freeze-dried for further use.

3.2.2 Characterization Methods for Macroporous Alginate/MMT Hydrogels

3.2.2.1 Fourier Transform Infrared (FT-IR) Analysis

FT-IR analysis were conducted to ensure crosslinking reaction and MMT presence in composite gels. IR spectra was recorded by FT-IR spectrophotometer (Shimadzu IR-Prestige 21) with Attenuated Total Reflection unit. The spectra of dry samples were taken between 4000 cm^{-1} and 650 cm^{-1} wavenumbers.

3.2.2.2 Pore Size and Pore Size Distribution by Scanning Electron Microscopy

Scanning Electron Microscopy (SEM, Zeiss EVO LS 10) was utilized to evaluate internal morphology and pore structure of dry composite alginate/MMT hydrogels. The specimens were cutted with razor blade then sputter coated with gold-palladium prior to imaging. SEM images were taken in different magnifications in secondary electron mode. Average pore size and pore size distributions were calculated by Image J (NIH) analysis program.

3.2.2.3 Gel Fraction and Swelling Ratio Measurements

To investigate crosslinking efficiency, gel fraction (W_g) of alginate/MMT composite hydrogel was calculated by Eq. (3.1);

$$W_g(\%) = \frac{M_{dry}}{M_0(0.05+X_{MMT})}100 \quad (3.1)$$

Where, M_0 is the weight of samples after preparation (g), M_{dry} is the weight of dry specimens (g) and X_{MMT} is the fraction (w/v) of MMT in reaction medium [4].

Water uptake capacity of composites were estimated by weighing alginate/MMT hydrogels in both equilibrium swollen state and dry state. The equilibrium weight swelling ratio regarding dry state (q_w, g g^{-1}) of the samples was calculated by Eq. (3.2) as follows:

$$q_w = \frac{M_{sw}}{M_{dry}} \quad (3.2)$$

Where M_{sw} is the weight of equilibrium swollen composite gels (g) [124]. All weight measurements were carried out gravimetrically and repeated several times at room temperature.

3.2.2.4 Mechanical Tests

Uniaxial compression test was performed with a load cell via Texture Analyzer TA.HD. Plus (Stable Micro Systems, UK) with the computer analyzer system Texture Exponent 32 at room temperature. Cylindrical samples were compressed up to 80 % of their initial length in swollen state while compression speed was adjusted at 0.1 mm/sec. Elastic modulus of each sampple was estimated by slope of initial linear part of each stress-strain curve [105].

3.2.3 Methylene Blue Adsorption Test

3.2.3.1 Batch Adsorption Procedure

For batch procedure, each dry sample in approximately 0.01 g dosage was soaked into 10 mL of MB solution where the concentration of solution was ranging from 25 mg L^{-1} to 1000 mg L^{-1} for post-crosslinked hydrogels and 25 mg L^{-1} to 2000 mg L^{-1} for cryogels, respectively. Adsorption was operated for 24 hours at a stirring rate of 200 rpm, at 25 °C in magnetic stirrer. The pH of MB solutions before immersing of dry hydrogels were found as 9. After 24 hours, sorbents were removed from medium and dye concentration in the remaining solute was measured using UV-Vis Spectrophotometer (UV-1700 PharmaSpec UV-Vis Spectrophotometer, Schimadzu) at 665 nm. Therefore, the amount of dye sorbed in equilibrium per dry weight (q_e, mg g^{-1}) was evaluted by (Eq. (3.3)):

$$q_e = \frac{(C_i - C_e)V}{M} \tag{3.3}$$

C_i and C_e refer to the dye concentration in aqueous solution before (mg L^{-1}) and after (mg L^{-1}) immersing of adsobents into dye solution. V is the volume of aqueous medium (L) and M is the dosage of dry adsorbent (g) [9].

3.2.3.2 Adsorption Isotherm Models

Two adsorption isotherm models were applied to investigate the mechanism of MB adsorption, namely Freundlich and Langmuir Models. Non-linear form of these models are given above, as Langmuir and Freundlich isotherm models were estimated by Eq. (2.1) and Eq. (2.3), respectively. Dimensionless constant (R_L) for Langmuir model was also calculated by Eq. (2.2).

3.2.3.3 Adsorption Kinetics Study

Kinetic study of MB removal was accomplished by immersing of 0.01 g of dry specimens in 10 mL of MB solution (25 mg L^{-1}). The experiment was conducted for 8 hours at 200 rpm, at 25^0C, at pH 9. Certain amount of MB within time intervals was collected and analyzed by UV-Vis spectrophotometer to obtain C_t which refers to the amount of MB in the solution at the certain time t (min). Time-dependent MB adsorption onto alginate/MMT composite hydrogels is given as (Eq. (3.4)):

$$q_t = \frac{(C_i - C_t)V}{M} \tag{3.4}$$

As q_t is defined as the amount of dye sorbed onto sorbent samples (mg g^{-1}) and C_t refers to the concentration of the MB remaining in solution at defined time t (mg L^{-1}) [5].

3.2.3.4 Adsorption Kinetics Models

PFO and PSO kinetics models were applied to data calculated by Eq. (3.4). Non-linear form of PFO and PSO models as given in Section 2, with Eq. (2.4) and Eq. (2.5), respectively. Parameters of these models are also calculated by non-linear fit of kinetic models onto experimental data.

3.2.3.5 Estimation of Overall Dye Removal Efficiency

Overall dye removal efficiency (RE) of alginate/MMT composite gels were calculated by Eq. (3.5) [7]:

$$RE\ (\%) = \frac{(C_i - C_e)}{C_e} 100 \tag{3.5}$$

3.2.3.6 Desorption Study

Desorption study was elucidated to have an idea of reusability of composite gels for MB removal. To do so, 3 different elutes were prepared, namely 1 M HCl & 90 % methanol, 0.1 M HCl and 0.1 M CH_3COOH where the samples first adsorbed MB for an hour (25 mg L^{-1}, 10 mL) followed by treatment with 10 mL elutes mentioned.

The desorption efficiency (DE) of elutes was calculated as (Eq. (3.6));

$$DE\ (\%) = \frac{C_d}{C_a} 100 \tag{3.6}$$

which C_d refers to dye amount desorbed in elution solutions within contact for an hour (mg L^{-1}) and C_a is the dye amount adsorbed onto hydrogels after contact with MB for an hour (mg L^{-1}) [125].

CHAPTER 4

RESULTS AND DISCUSSION

4.1 MACROPOROUS ALGINATE/MMT COMPOSITE HYDROGELS PREPARED BY POST-CROSSLINKING STRATEGY

In the first part of the thesis, we prepared alginate/MMT macroporous composite hydrogels via post-crosslinking strategy as also shown in Figure 4.1. Post-crosslinking method comprises production of pre-polymer matrices followed by crosslinking of pre-polymer matrices resulting tailored hydrogel matrices in any desired shape and morphology.

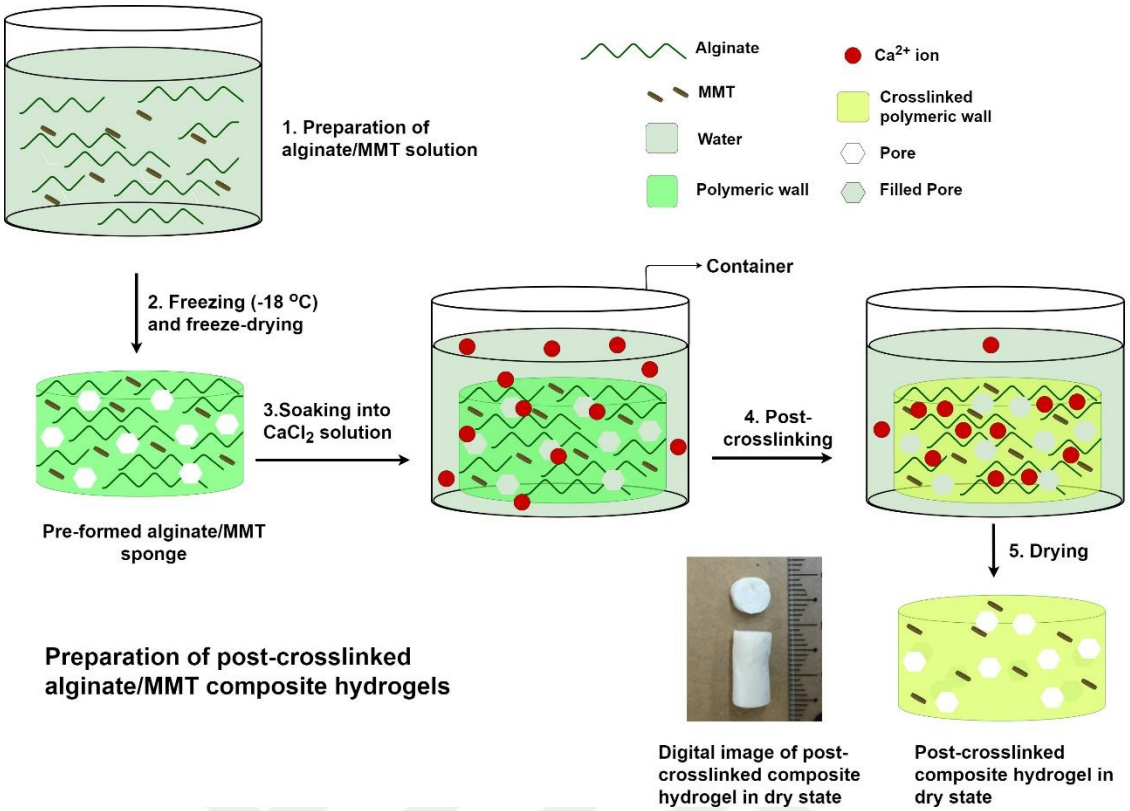


Figure 4.1 Schematic representation of preparation of post-crosslinked alginate/MMT composite hydrogels.

As-prepared post-crosslinked alginate/MMT hydrogels were characterized by FT-IR, gel fraction, swelling ratio, mechnical testing and MB adsorptions. As can be seen below, post-crosslinked macroporous alginate/MMT hydrogels showed remarkable performance in removal of MB.

4.1.1 FT-IR Analysis of Post-Crosslinked Macroporous Alginate/MMT Composite Hydrogels

FT-IR measurements were conducted to investigate crosslinking reaction and MMT incorporation into post-crosslinked alginate hydrogels. Figure 4.2 indicates FT-IR spectra of MMT, alginate, $A_5MMT_0XL_5$ and $A_5MMT_2XL_5$ specimens.

Spectrum of alginate shows stretching vibrations of O-H between 3600 cm^{-1} and 3000 cm^{-1}. The peak observed in the range of 1170–1030 cm^{-1} correspond to the O-C-O bonds, which is typical for polysaccharide rings [126]. While the strong peak at 1594 cm^{-1} is defined as asymmetric stretching of COO^- groups, the peak at 1409 cm^{-1} is identified as symmetric stretching of COO^- groups of sodium alginate, respectively.

IR spectrum of $A_5MMT_0XL_5$ sample differs from alginate due to formation of hydrogel. The spectrum of alginate has bands at 1594 cm^{-1} and 1409 cm^{-1} and these bands turned into 1593 cm^{-1} and 1417 cm^{-1} in the spectra of $A_5MMT_0XL_5$, respectively. This alteration indicates that Na^+ ions linked to G units of alginate were replaced by Ca^{2+} ions forming calcium alginate hydrogel [4].

FT-IR spectrum of $A_5MMT_2XL_5$ indicates broader bands at 1649 cm^{-1} and 1460 cm^{-1} than the spectrum of $A_5MMT_0XL_5$ due to addition of MMT. MMT spectrum involves bands at 3630 cm^{-1} corresponding Si-O-H, 1040 cm^{-1} due to Si-O-Si, 917 cm^{-1} as for Al-Al-O-H and 816 cm^{-1} because of Al-Mg-O-H groups, respectively [126].

Figure 4.3 also illustrates digital images of post-crosslinking of pre-fromed alginate/MMT matrices (Figure 4.3a), dissolution of alginate/MMT matrices in water (Figure 4.3b) and swelling of post-crosslinked hydrogels in water instead of dissolving (Figure 4.3c).post-crosslinking process. As also can be seen from Figure 4.3, post-crosslinking is successfully achieved, while pre-formed alginate/MMT matrices were dissolved in water, post-crosslinked matrices were swellon, instead of dissolving.

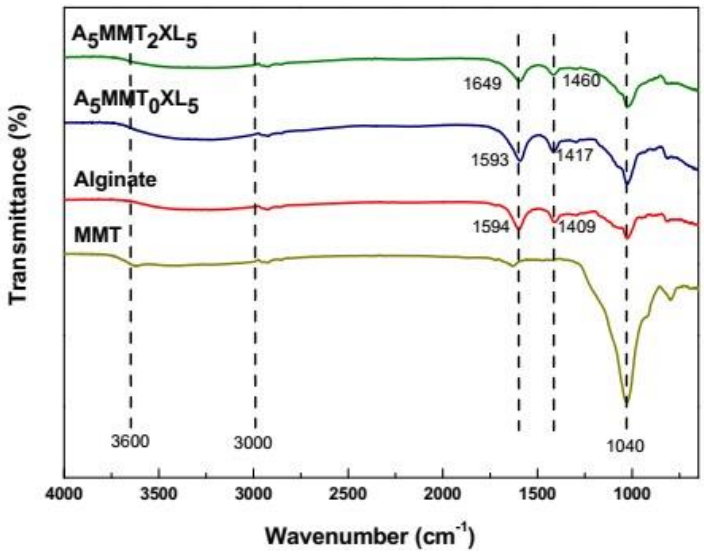


Figure 4.2 FT-IR spectra of MMT, alginate, $A_5MMT_0XL_5$ and $A_5MMT_2XL_5$ samples.

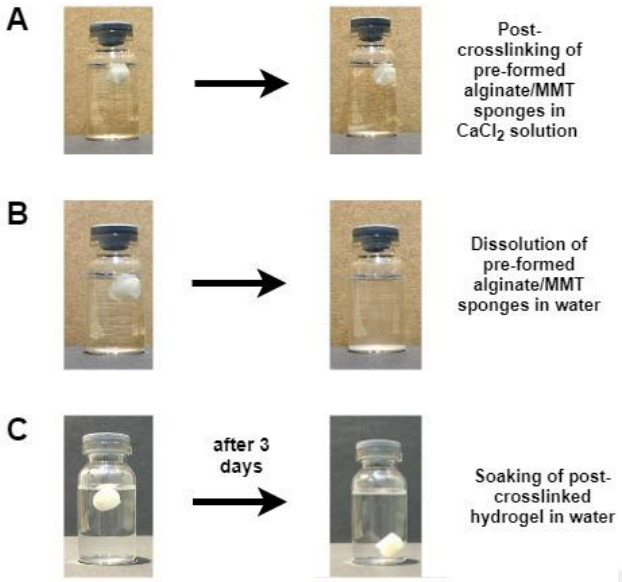


Figure 4.3 Digital images of post-crosslinking of pre-formed alginate/MMT matrices (a), dissolution of alginate/MMT matrices in water (b) and swelling of post-crosslinked hydrogels in water instead of dissolving (c).

4.1.2 Pore Size and Pore Size Distributions of Post-Crosslinked Macroporous Alginate/MMT Composite Hydrogels

SEM measurements were carried out for investigation of internal morphology and evaluation of the effect of MMT on internal morphology of post-crosslinked alginate/MMT composite hydrogels. Figure 4.4 illustrates SEM micrographs of dry specimens taken at different magnifications.

As can be seen in Figure 4.4, both $A_5MMT_2XL_5$ and $A_5MMT_0XL_5$ gels have interconnected and large pores due to freezing of alginate or alginate/MMT solutions and subsequent freeze-drying followed by post-crosslinking. MMT addition caused larger pore formation compared to MMT-free sample ($A_5MMT_0XL_5$). This is due to the fact that, MMT caused depletion in freezing point of water and resulted in comparatively slow freezing compared to MMT-free water [127]. Therefore, in such rate ice crystals may have time to grow more freely resulting larger ice crystals formation as negative replica of pores [128].

According to Figure 4.4, while $A_5MMT_0XL_5$ sample has continuous smooth topology, rough pore surfaces obtained in in $A_5MMT_2XL_5$ sample due to MMT presence.

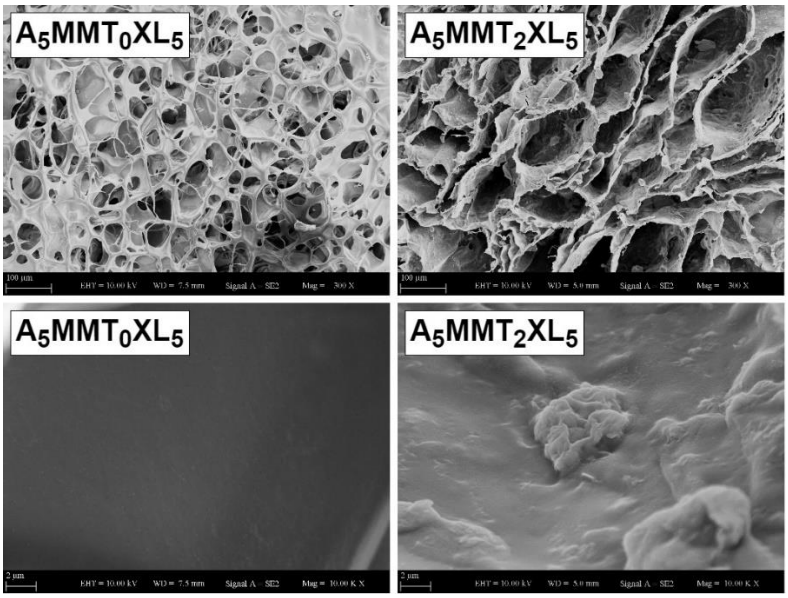


Figure 4.4 Cross-sectional SEM micrographs of $A_5MMT_0XL_5$ and $A_5MMT_2XL_5$ samples (Scale bar: 100 µm above and 2 µm below).

Image J analysis was also conducted to understand the effect of MMT presence on average pore size (µm) and pore size distributions of $A_5MMT_0XL_5$ and $A_5MMT_2XL_5$ samples. Figure 4.5 shows pore size distributions of the samples. According to Figure 4.5, while pore size of $A_5MMT_0XL_5$ sample was ranged between 75 µm to 200 µm, the pore size of $A_5MMT_2XL_5$ sample obtained between 75 µm and 250 µm. For both samples, pore sizes were mostly obtained around 100 µm. Moreover, $A_5MMT_0XL_5$ sample mostly contain smaller pores compared to $A_5MMT_2XL_5$ sample, whereby the average pore size for $A_5MMT_0XL_5$ and $A_5MMT_2XL_5$ samples were found as 120 $\pm$ 27 µm and 162 $\pm$ 50 µm, respectively.

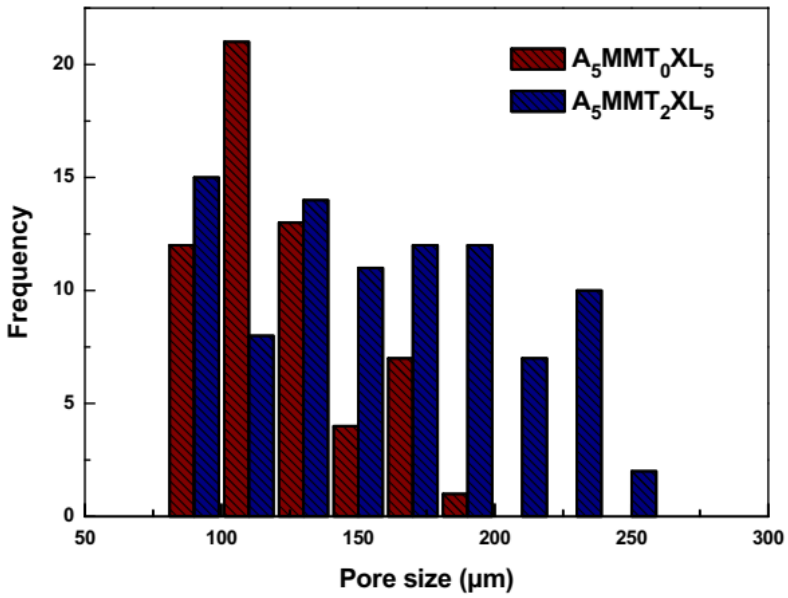


Figure 4.5 The effect of MMT presence on pore size distribution of post-crosslinked alginate/MMT composite hydrogels.

4.1.3 Gel Fraction and Swelling Ratio Measurements of Post-Crosslinked Macroporous Alginate/MMT Composite Hydrogels

Gel fraction measurements were conducted to understand the degree of crosslinked polymers in gel systems and swelling ratios were calculated for investigation of water uptake ability. Figure 4.6 shows the effect of MMT amount (a) and the effect of crosslinker amount (b) on both swelling ratio and gel fraction (%) data of post-crosslinked hydrogels.

According to Figure 4.6a, post-crosslinked alginate/MMT hydrogels possessed gel fraction (%) around 85 %. Thus, MMT enhanced gel fraction (%) of post-crosslinked hydrogels due to the possible electrostatic or ionic interactions between negatively charged MMT and Ca^{2+} ions in hydrogel system [129]. Post-crosslinked alginate/MMT hydrogels absorbed water approximately 13 times of their dry weights. MMT reduced water uptake capacity, as also reported previously [4]. MMT may cause depletion of flow of water inside the pores of hydrogel matrices thus resulting decreased swelling ratio [130].

As can be seen in Figure 4.6b, the change in crosslinker ratio did not significantly effect both gel fraction (%) and swelling ratio of post-crosslinked alginate/MMT hydrogels,

whereby their gel fraction (%) reached up to 85 % and they still absorbed 13 times of their dry weights. This is due to the fact that, when alginate/MMT matrices were inserted into crosslinker solutions with varying concentrations (1 (w/v) %- 5 (w/v) %), some part of the alginate and MMT were partially dissolved in each crosslinker solution. The remaining undissolved parts were equally crosslinked. As a result, the change in amount of crosslinker did not altered both gel fraction (%) and swelling ratio.

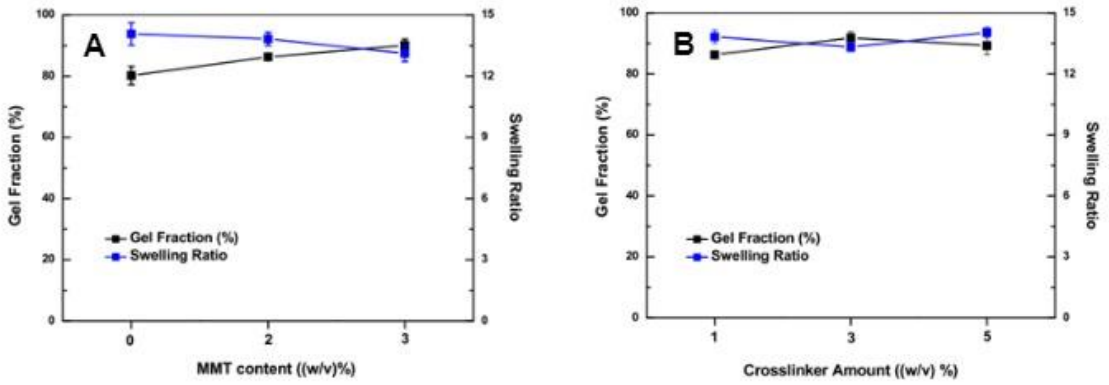


Figure 4.6 The effect of MMT content (a) and crosslinker amount (b) on gel fraction (%) and swelling ratio of post-crosslinked alginate/MMT hydrogels. ((a): Alginate ratio: 5 (w/v) %, crosslinker ratio: 5 (w/v) %, (b): Alginate ratio: 5 (w/v) %, MMT ratio: 2 (w/v) %).

4.1.4 Mechanical Testing of Post-Crosslinked Macroporous Alginate/MMT Composite Hydrogels

Uniaxial compression test was performed for investigation of the effect of MMT amount and crosslinker content on mechanical properties of post-crosslinked alginate/MMT composite hydrogels. Figure 4.7 illustrates typical stress-strain curves for post-crosslinked hydrogels with varying MMT amount (Figure 4.6a) and crosslinker content (Figure 4.2b).

As can be seen in Figure 4.7a, all post-crosslinked hydrogels were able to compress up to 80 % of initial size without crack or deformation. MMT also enhanced their compression stress limit by 3 % of strain that the sample containing 3 (w/v) % MMT ($A_5MMT_3XL_5$) was resisted up to 120 kPa stress values. Therefore, MMT acted as reinforcing agent for post-crosslinked alginate hydrogels. This could be related to interaction between MMT and crosslinker (Ca^{2+}) resulted in enhanced compression stress, as also reported previously [131]. Therefore, similar stress-strain curves for post-

crosslinked alginate sponges also reported by Lin et al. [23], which they reinforced post-crosslinked alginate hydrogels with cellulose nanocrystals.

Figure 4.7b shows stress-strain curves of post-crosslinked alginate/MMT composite hydrogels with varying crosslinker ratio. According to Figure 4.7b, alteration in crosslinker content did not significantly affect compression stress of post-crosslinked hydrogels. They can still compressed up to 80% of strain without deformation, whereby their compression limit did not also significantly altered. This observation is due to the fact that, when changing crosslinker amount in post-crosslinking process, some of the alginate and MMT dissolved in $CaCl_2$ solution, resulting crosslinking of retaining alginate equally in all crosslinker solution. Therefore, significant change in compression limit of post-crosslinked alginate/MMT composite hydrogels was observed.

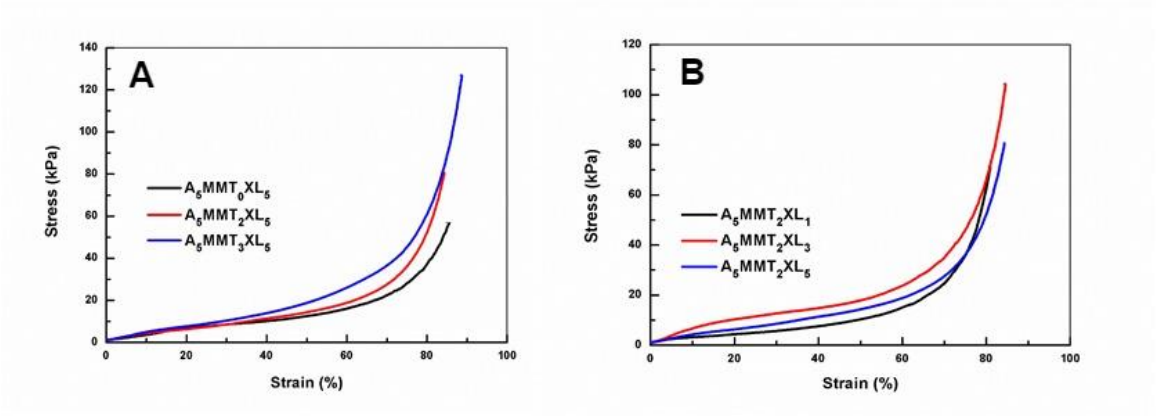


Figure 4.7 Typical stress-strain curves for post-crosslinked alginate/MMT composite hydrogels with varying MMT content (a) and crosslinker ratio (b).

Elastic modulus or stiffness of post-crosslinked alginate/MMT hydrogels were calculated by the slope of initial linear part of stress-strain curve for each specimen. Figure 4.8a and Figure 4.8b shows the effect of MMT amount and crosslinker ratio on elastic modulus (kPa) of post-crosslinked alginate/MMT composite hydrogels, respectively.

Figure 4.8a shows the effect of MMT amount on elastic modulus (kPa) of post-crosslinked alginate/MMT hydrogels. According to Figure 4.8a, incroporation of MMT enhanced elastic modulus of post-crosslinked alginate hydrogels, by 1.2 fold compared to MMT free sample ($A_5MMT_0XL_5$). This is due to the fact that, MMT mechanically reinforced pore walls of post-crosslinked alginate hydrogels and also reacted with Ca^{2+} ions and compacted the hydrogel backbone, resulting increased elastic modulus. Similar

results also reported by Afshar et al. [25] whereby they reinforced post-crosslinked alginate hydrogels with halloysite.

Figure 4.8b illustrates the effect of crossliker ratio on elastic modulus of each post-crosslinked alginate/MMT hydrogels. As also can be seen in Figure 4.8b, elastic moduli of post-crosslinked alginate/MMT hydrogels were remarkably altered with changing crosslinker ratio. More compact structure with highest elastic modulus was obtained around 48 kPa when crosslinker amount was adjusted to 3 (v/w) %. When crosslinker amount was 1 (w/v) %, crosslinking may not be fully achieved; however when crosslinker amount was 5 (v/w) %, there could be fast crosslinking. Therefore, we can conclude that, 3 (w/v) % of crosslinker ratio is optimum for formation of more compact post-crosslinked hydrogel formation.

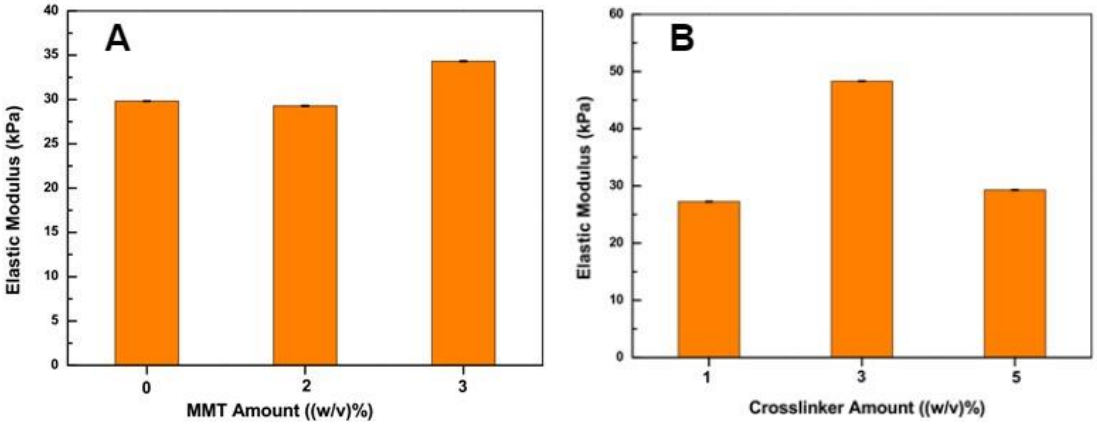


Figure 4.8 The effect of MMT content (a) and crosslinker ratio (b) on elastic moduli of post-crosslinked alginate/MMT hydrogels. ((a): Alginate: 5 (w/v) % and crosslinker concentration: 5 (w/v) %, (b): Alginate: 5 (w/v) % and MMT concentration 2 (w/v) %).

4.1.5 Adsorption of Methylene Blue by Post-Crosslinked Macroporous Alginate/MMT Composite Hydrogels

MB adsorption tests were conducted in both batch and kinetic procedure. Data obtained after experiments were used for non-linear fitting of either isotherm models or kinetic models to characterize adsorption of MB by alginate/MMT post-crosslinked composite hydrogels.

4.1.5.1 Batch Adsorption and Isotherm Models

Batch adsorption procedure was conducted for characterization of MB adsorption of post-crosslinked alginate/MMT composite hydrogels. Figure 4.9 and Figure 4.10 shows batch experimental data of post-crosslinked hydrogels and non-linear regression of Langmuir and Freundlich isotherm models. The parameters of these isotherm models are also listed in Table 4.1 and Table 4.2. The degree of non-linear fit of isotherm models onto experimental data was given by correlation coefficient (R^2).

According to Table 4.1 and Table 4.2, highest R^2 values obtained by non-linear fit of Langmuir isotherm model in all post-crosslinked composite hydrogels while Freundlich model gave a poor fit of experimental data. Therefore, we can conclude that post-crosslinked macroporous alginate/MMT composite hydrogels followed homogen adsorption where active sites for dye attachment are equally distributed all over the hydrogel network. Same observations were also reported by Almedia et al. [94] where they applied MMT clay for MB removal, and Belhouchat et al. [132] which they applied alginate/activated bentonite for MB removal and Lezehari et al. [84] where they used alginate/pillared clay beads for safranine (cationic dye) removal. Since all R_L values are between 0 and 1, adsorption is favorable for all post-crosslinked alginate/MMT hydrogels.

q_m values of each specimen is provided by Langmuir model. According to Table 4.1 and Table 4.2, maximum adsorption capacities (q_m) of post-crosslinked hydrogels were altered with MMT incorporation and changing crosslinker ratio. As can be seen in Table 4.1, incorporation of MMT enhanced q_m value due to its negative nature. However, further increased amount of MMT (3 (w/v) %) reduced q_m value, due to the fact that MMT may caused plugging of pore within $A_5MMT_3XL_5$ sample. As also illustrated in Table 4.2, q_m values were increased with enhanced crosslinker ratio. This is due to the fact that when introducing alginate/MMT matrices into high crosslinker containing solution (5 (w/v) %), alginate was rapidly crosslinked resulted in more free COO^- groups compared to other samples. By taking consideration of this, q_m value increased proportionally to crosslinker ratio.

Highest q_m value obtained as 1435.6 mg g^{-1} belonging to $A_5MMT_2XL_5$ sample. This q_m value is quite high compared to 137.2 mg g^{-1} obtained from poly(vinyl alcohol)-chitosan-

alginate-MMT hydrogel beads [133], 181.8 mg g^{-1} gathered from alginate-MMT quasi-cryogel beads [7], 452.3 mg g^{-1} revealed by alginate-clinoptilolite beads [4], 756.97 mg g^{-1} obtained by calcium alginate-bentonite-activated carbon beads [134]; however, low with respect to 2257.36 mg g^{-1} obtained by titanium and alginate loaded poly(acrylic acid) hydrogels [135].

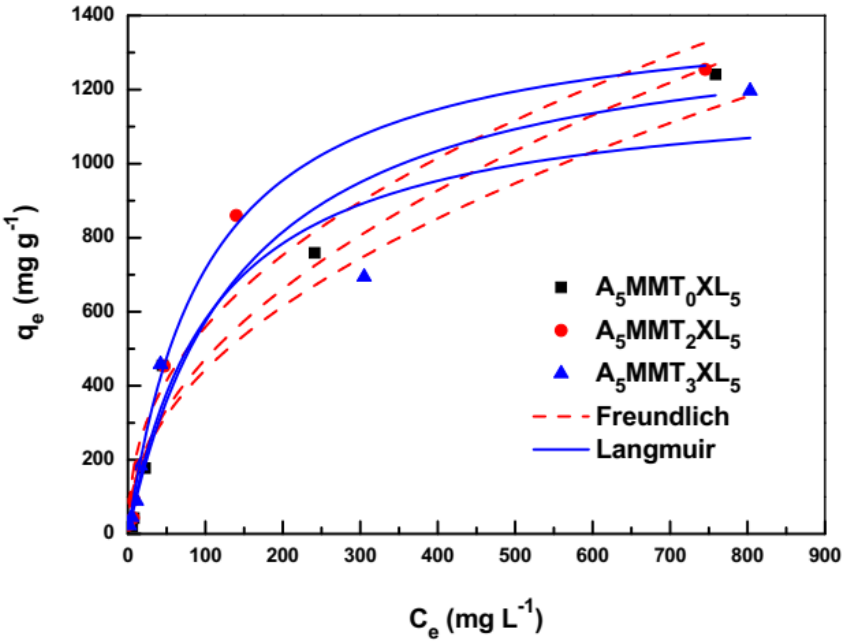


Figure 4.9 The effect of MMT onto batch adsorption data and non-linear fit of Langmuir and Freundlich isotherm models.

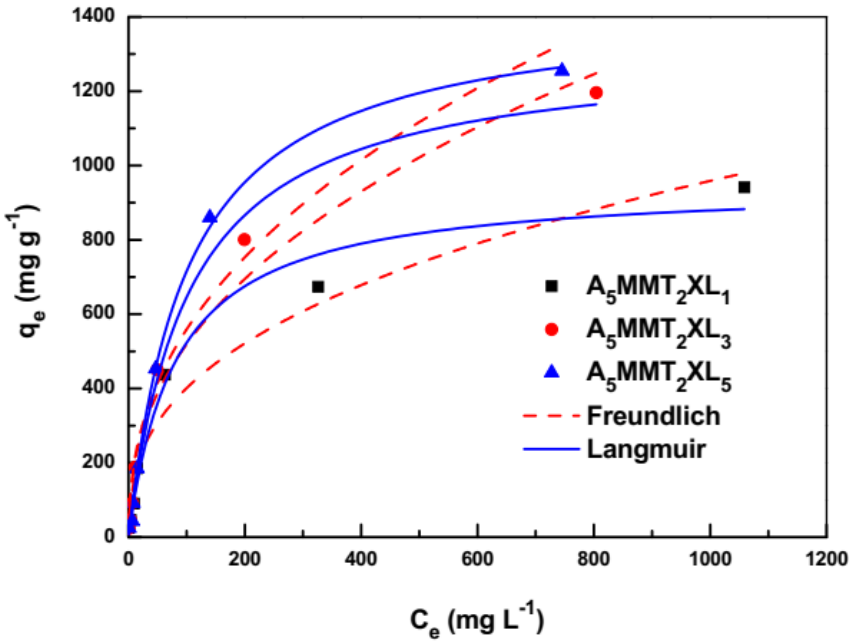


Figure 4.10 The effect of crosslinker amount onto batch adsorption data and non-linear regression of Langmuir and Freundlich isotherm models.

Table 4.1 The effect of MMT amount of post-crosslinked hydrogels on Langmuir and Freundlich isotherm constants.

Model	**Parameters**	**$A_5MMT_0XL_5$**	**$A_5MMT_2XL_5$**	**$A_5MMT_3XL_5$**
Langmuir	q_m, mg g^{-1}	1413.61	1435.58	1215.76
	K_L, L mg^{-1}	0.007	0.009	0.009
	R_L	0.38	0.44	0.39
	R^2	0.96	0.99	0.92
Freundlich	K_F, mg g^{-1}	49.85	76.99	50.46
	N	0.49	0.43	0.47
	R^2	0.96	0.92	0.96

Table 4.2 The effect of crosslinker amount of post-crosslinked hydrogels on Langmuir and Freundlich isotherm constants.

Model	**Parameters**	**$A_5MMT_2XL_1$**	**$A_5MMT_2XL_3$**	**$A_5MMT_2XL_5$**
Langmuir	q_m, mg g^{-1}	950.79	1314.12	1435.58
	K_L, L mg^{-1}	0.012	0.009	0.009
	R_L	0.29	0.32	0.43
	R^2	0.98	0.99	0.99
Freundlich	K_F, mg g^{-1}	70.26	74.76	76.98
	N	0.38	0.42	0.43
	R^2	0.96	0.96	0.92

4.1.5.2 Adsorption Kinetics and Kinetic Models

Kinetic studies or contact time experiments for MB adsorption by post-crosslinked alginate/MMT composite hydrogels were successfully carried out for investigation of characteristics of adsorption. Figure 4.11 and Figure 4.12 shows kinetic data of post-crosslinked hydrogels and non-linear fit of PFO and PSO kinetic models. As can be seen in Figure 4.11 and 4.12, all post-crosslinked hydrogels reached their equilibrium of dye removal about 3 hours contact with MB solution. Fast removal of MB was observed due

to macroporosity, interconnected porous structure and open-porous structure of the post-crosslinked alginate/MMT hydrogels.

Table 4.3 and Table 4.4 shows kinetic parameters of PFO and PSO models of post-crosslinked alginate/MMT hydrogels with varying MMT content (Table 4.3) and crosslinker ratio (Table 4.4), respectively. Considering high R^2 values, adsorption of MB is better characterized by PFO kinetics model. Therefore, the characteristics of adsorption followed physisorption, whereby the interactions between MB and post-crosslinked hydrogels could be Van der waals forces of electrostatic interactions. PFO model also predicted by Dragan et al. [5].

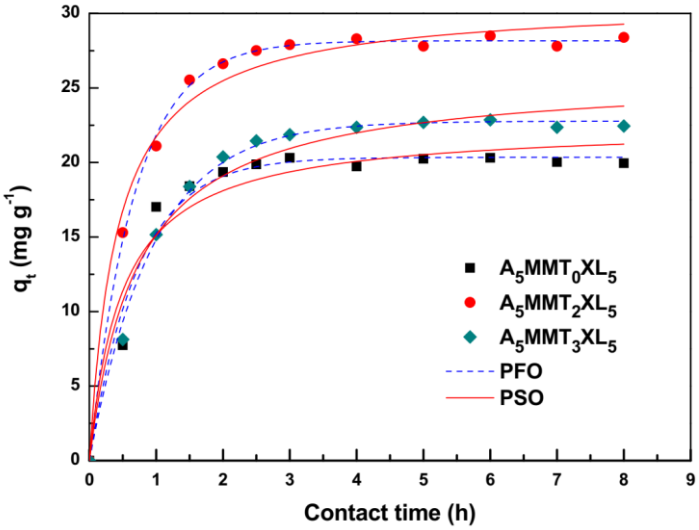


Figure 4.11 The effect of MMT amount on the kinetic data of post-crosslinked alginate/MMT hydrogels and non-linear fit of PFO and PSO kinetics models.

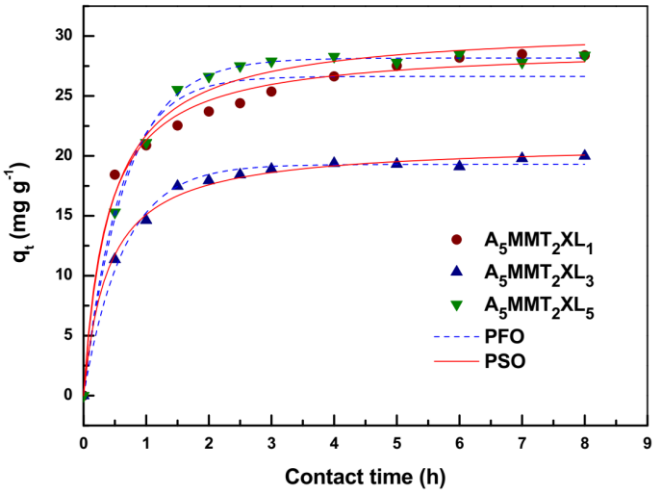


Figure 4.12 The effect of crosslinker amount on kinetic data of post-crosslinked alginate/MMT hydrogels and non-linear regression of PFO and PSO kinetics models.

Table 4.3 The effect of MMT amount on PFO and PSO kinetic parameters for MB adsorption

Adsorbent Parameter	**$A_5MMT_0XL_5$**	**$A_5MMT_2XL_5$**	**$A_5MMT_3XL_5$**
PFO Kinetic Model			
$q_{e,calc}$, mg g^{-1}	22.77	22.53	22.77
k_1, min^{-1}	0.017	0.025	0.018
R^2	0.99	0.99	0.99
PSO Kinetic Model			
$q_{e,calc}$, mg g^{-1}	22.53	24.64	25.90
k_2, min^{-1}	0.0015	0.0016	0.0009
R^2	0.94	0.98	0.97

Table 4.4 The effect of crosslinker amount on PFO and PSO kinetic parameters for MB adsorption

Adsorbent Parameter	**$A_5MMT_2XL_1$**	**$A_5MMT_2XL_3$**	**$A_5MMT_2XL_5$**
PFO Kinetic Model			
$q_{e,calc}$, mg g^{-1}	26.63	19.29	22.53
k_1, min^{-1}	0.029	0.026	0.025
R^2	0.98	0.99	0.99
PSO Kinetic Model			
$q_{e,calc}$, mg g^{-1}	29.13	21.06	24.64
k_2, h^{-1}	0.0015	0.0020	0.0016
R^2	0.95	0.99	0.98

4.1.5.3 Dye Removal Efficiency

Dye removal efficiencies of post-crosslinked alginate/MMT hydrogels were evaluted for investigation of the effect of MMT amount and crosslinker ratio on MB adsorption. Initial dye concentration was adjusted to 25 mg L^{-1}.

Figure 4.13a shows the effect of MMT content on dye removal efficiency. As can be seen in Figure 4.13a, MMT enhanced dye removal by 5 %, compared to MMT-free sample. Maximum dye removal efficiency obtained with 2 (w/v) % MMT-containing sample as that sample removed 97 % of initial dye concentration due to negative nature of MMT [136]. Further increasing the amount of MMT slightly reduced dye removal, due to plugged pores caused by excessive amount of MMT.

Figure 4.13b illustrates the effect of crosslinker ratio on dye removal (%). In this regard, increased crosslinker ratio gradually enhanced dye removal. This result can be explained by taking consideration of availability of more free COO^- groups on sample containing 5 (w/v) % of crosslinker which we assume fast-crosslinking observed. However, as can be seen in Figure 4.13b, no major changes observed in dye removal.

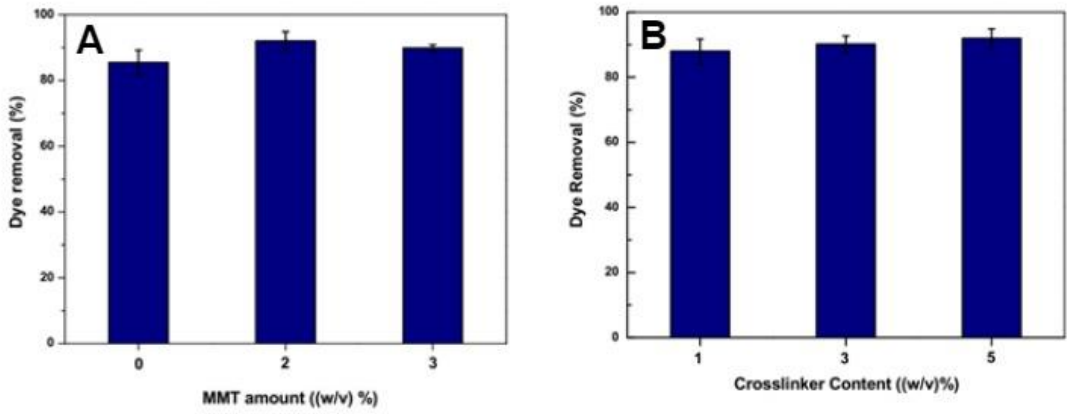


Figure 4.13 The effect of MMT content (a) and crosslinker ratio (b) on dye removal of post-crosslinked alginate/MMT hydrogels. ((a): Alginate: 5 (w/v) % and crosslinker concentration: 5 (w/v) %, (b): Alginate: 5 (w/v) % and MMT concentration 2 (w/v) %).

4.1.5.4 Desorption Study

Desorption study was conducted for regeneration of sorbents and reusability for multiple times. Figure 4.14 shows desorption efficiencies of various eluting agents with respect to dye adsorbed MMT-free sample ($A_5MMT_0XL_5$) and MMT-containing sample ($A_5MMT_2XL_5$).

According to Figure 4.14, 1 M HCl & 90 % methanol mixture is superior to remove MB from post-crosslinked hydrogels. This due to the fact that, when the pH of the medium has been changed by weak acids (suc as HCl), dye attached carboxylate groups turned

into free COO^- groups, resulting releasing of dye by breaking electrostatic interactions between dye and adsorbent [4].

Incorporation of MMT reduced dye releasing, due to activation and alteration of charges of MMT in acidic pH values [137].

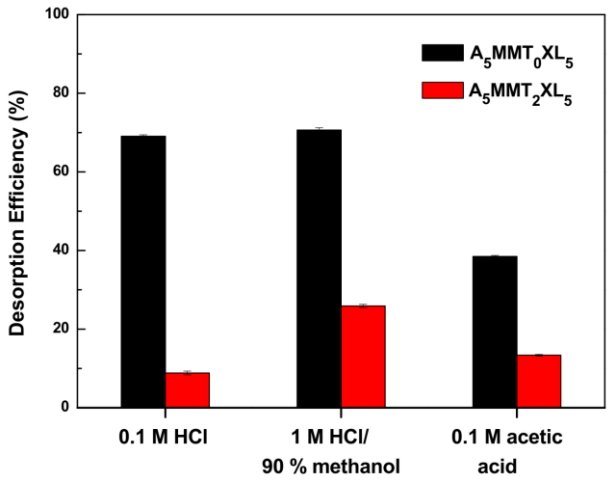


Figure 4.14 The effect of MMT presence on desorption efficiencies of various eluting agents for MB from post-crosslinked hydrogels.

Based on the adsorption tests, we can state that macroporous structure, open porosity and interconnected porous morphology of post-crosslinked alginate/MMT hydrogels made them superior adsorbent in MB removal compared to other adsorbents available in the literature. Therefore these post-crosslinked alginate/MMT composite hydrogels are promising low-cost alternatives for MB removal from waste waters.

4.2 MACROPOROUS ALGINATE/MMT COMPOSITE HYDROGELS OBTAINED BY CRYOGELATION METHOD

In the second part of the thesis, we generated macroporous alginate/MMT composite cryogels as adsorbents for MB removal. These cryogels were synthesized by cryogelation technique, where crosslinking of alginate chains was completed in moderately frozen state as also shown in schematic representation of cryogelation reaction (Figure 4.15).

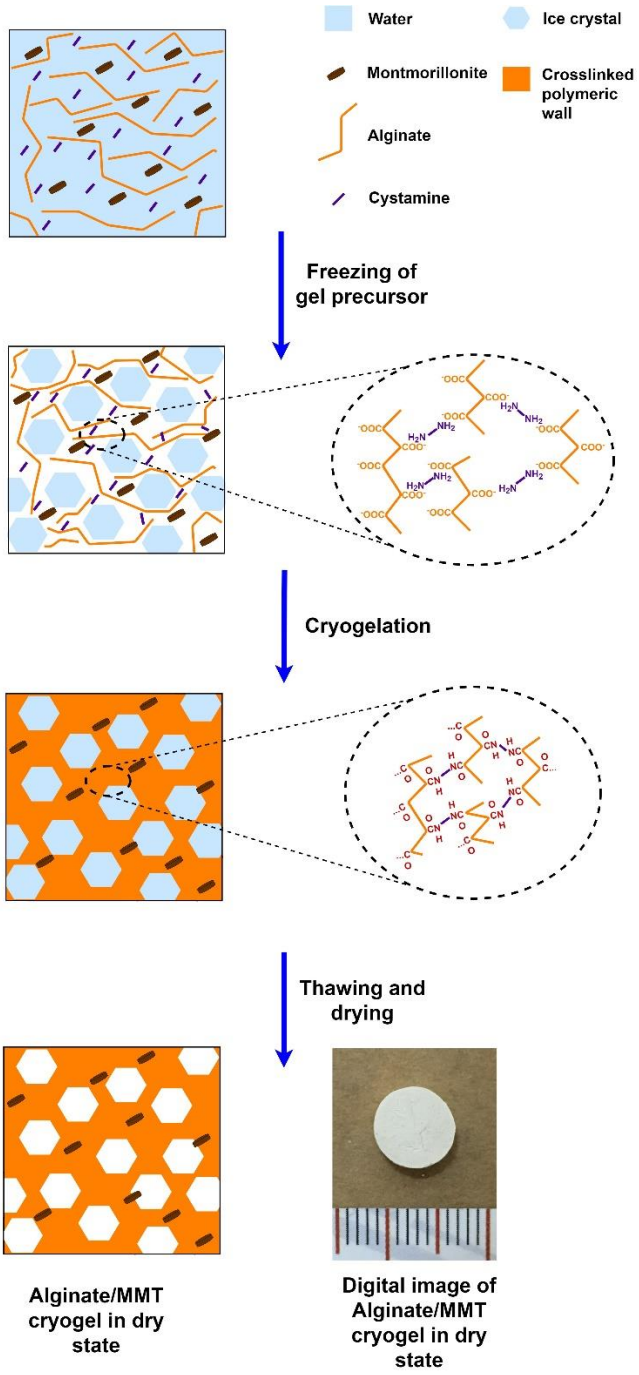


Figure 4.15 Schematic representation of macroporous alginate/MMT composite hydrogel preparation via cryogelation technique.

Crosslinking reaction of alginate chains was outlined in Figure 4.16 in three steps. In step 1, EDC was attached to carboxylate group of alginate to form unstable reactive O acylisourea ester of alginate. In Step 2, semi-stable amine reactive NHS-ester of alginate formed in presence of NHS. Later, amide bonds were formed between alginate chains due to amine groups of Cys in Step 3. As a result, crosslinking process was completely achieved via classical carbodiimide chemistry in frozen state.

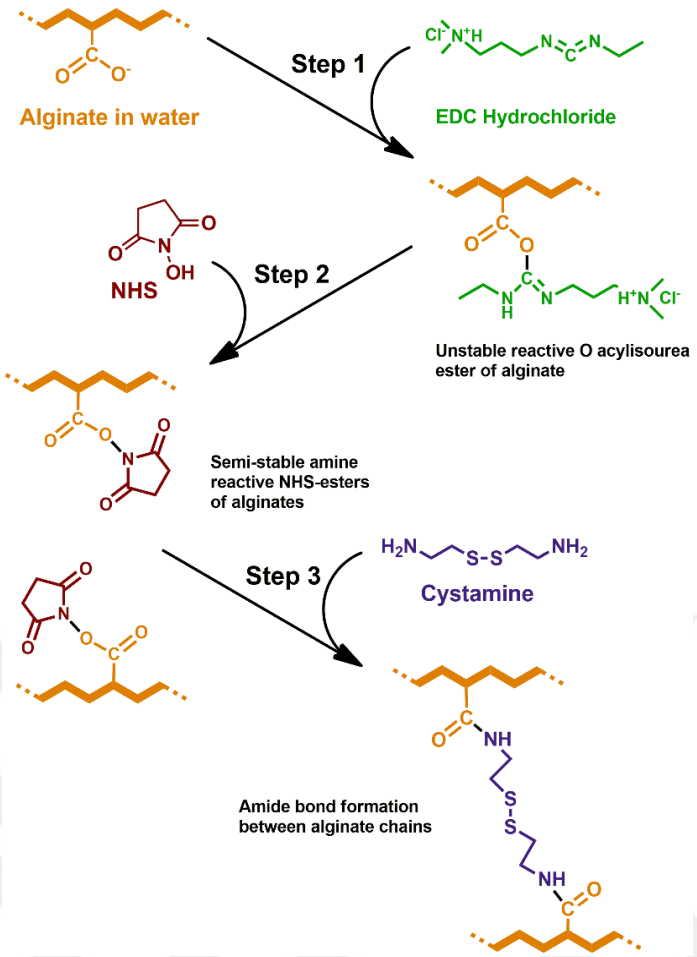


Figure 4.16 Covalent crosslinking of alginate chains with Cys via EDC/NHS coupling of carbodiimide chemistry. Adapted from [138].

4.2.1 FT-IR Analysis of Alginate/MMT Composite Cryogels

To investigate covalent crosslinking reaction between alginate chains and MMT incorporation, FT-IR analysis was performed. FT-IR spectrum for alginate, AMMT0 and AMMT3 samples were illustrated in Figure 4.17.

The spectrum of alginate exhibited broad peak between 3400 cm^{-1} and 3200 cm^{-1} referring O-H groups. C-O-O groups identified as C-O stretching at 1594 cm^{-1} and 1409 cm^{-1} [139]. The peak represented at 1030 cm^{-1} shows O-C-O stretching which is typical for polysaccharides.

The spectra of AMMT0 represents sharp peak at 1637 cm^{-1} which corresponds to amide I bond. Peaks at 1263 cm^{-1} and 1568 cm^{-1} show N-H bending of amide II bonds. Amide I and II bonds formation indicates amidation of carboxylic acid of alginate polymers [12].

By these findings, covalent bonding of alginates and Cys or crosslinking reaction in moderately frozen state was shown to be successfully achieved.

The spectra of AMMT3 differs from AMMT0 due to MMT addition. The spectra of AMMT3 involves 1620 cm^{-1}, due to H-O-H bending, 1040 cm^{-1} due to Si-O-Si, 917 cm^{-1} as for Al-Al-O-H and 816 cm^{-1} because of Al-Mg-O-H groups of MMT, respectively [126].

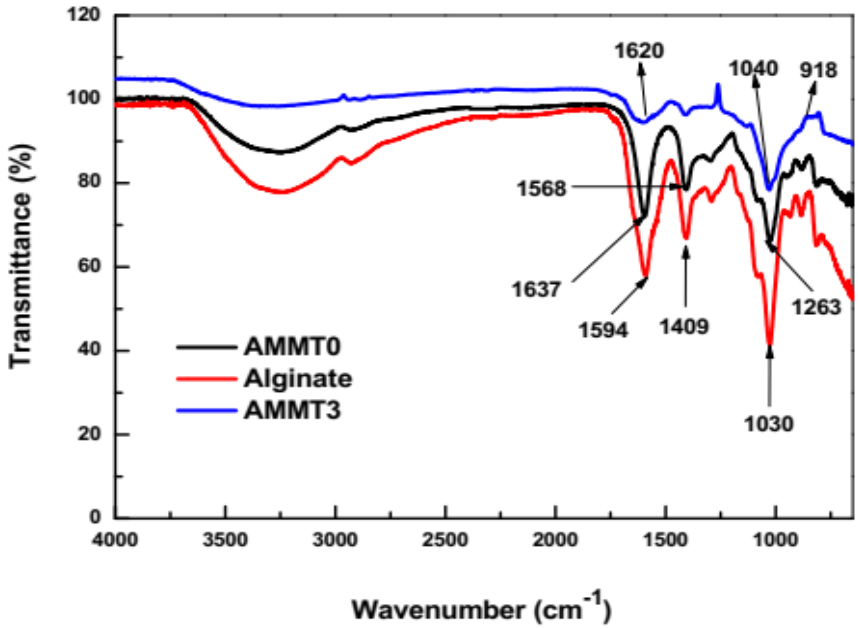


Figure 4.17 FT-IR spectrum of alginate, AMMT0 and AMMT3 samples. Crosslinking achieved by alteration of free COO^- groups of alginate into amide bonds.

4.2.2 Pore Size and Pore Size Distributions of Alginate/MMT Composite Cryogels

SEM measurements were conducted to investigate internal morphology and pore size of the alginate/MMT composite cryogels. Figure 4.18 reveals SEM images of alginate/MMT cryogels with different MMT ratio. According to Figure 4.18, all cryogels possess interconnected porosity, open porous struture and macroporous morphology. Incorporation of MMT particles into cryogels imparted roughness to the cryogel surfaces while smooth topology observed in MMT-free specimen (AMMT0).

MMT deposition into alginate cryogels also reduced pore size due to restriction of ice growth during freezing process in cryogelation, this observation also reported by Tuncaboylu et al. [124] and Koshy et al. [42]. Therefore, when MMT concentration was increased from 3 (w/v) % to 5 (w/v) %, pore size was further decreased. Uniform

distribution of MMT through matrices observed while MMT was mostly entrapped inside pore walls and slight aggregates occurred due to excessive amount of clay.

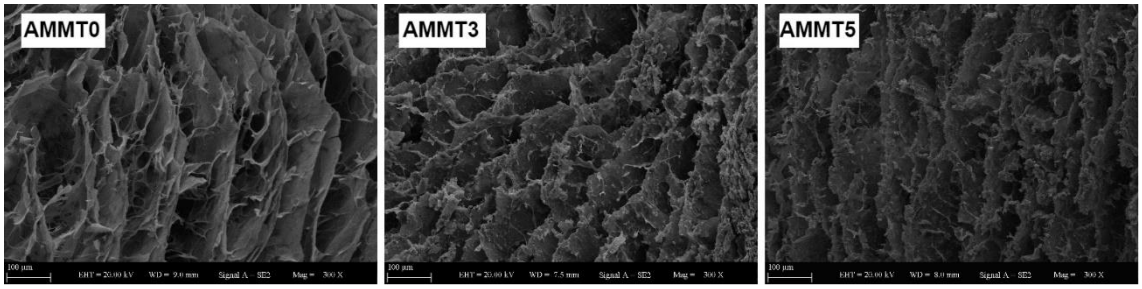


Figure 4.18 Cross-sectional SEM micrographs of AMMT0, AMMT3 and AMMT5 samples (Scale bar: 100 µm).

Image J analysis were performed on SEM images to investigate the effect of MMT amount on both pore size and pore size distributions. Figure 4.19 shows pore size distributions of alginate/MMT cryogels with altered MMT amount. As illustrated in Figure 4.19, pore size of each sample is mostly recoreded around 100 µm. MMT incorporation also altered pore size distribution of alginate/MMT cryogels, whereby MMT-incorporated samples (AMMT3 and AMMT5) exhibited broader pore size distribution compared to MMT-free sample (AMMT0). Average pore size for each sample was calculated as 143 $\pm$ 55 µm for AMMT0, 121 $\pm$ 33 µm for AMMT3 and 114 $\pm$ 28 µm for AMMT5 samples, respectively. As a conclusion, average pore size of alginate/MMT samples were gradually decreased with increased MMT amount due to restriction of ice growth during cryogelation method as negative replica of the pores [124].

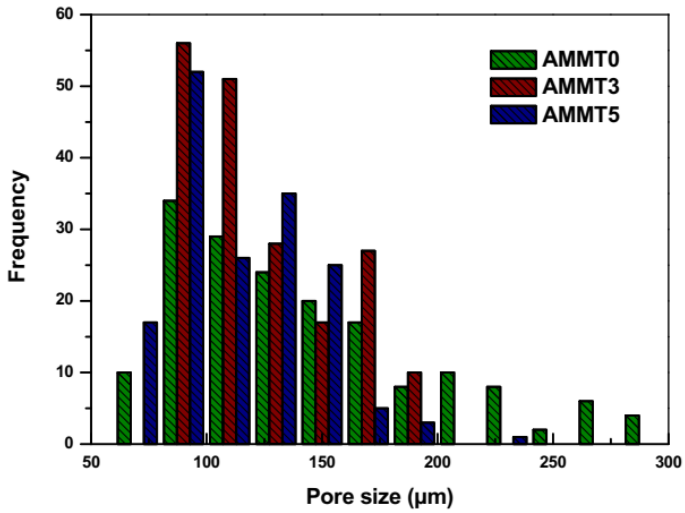


Figure 4.19 Pore size distributions of alginate/MMT composite cryogels with varying MMT content.

4.2.3 Gel Fraction and Swelling Ratio Measurements of Alginate/MMT Composite Cryogels

Gel fraction measurements were performed for evaluation of crosslinked polymer amount and swelling ratio measurements were conducted for estimation of water uptake capacity. Figure 4.20 shows gel fraction (%) and swelling ratio of alginate/MMT cryogels with different MMT ratio.

According to Figure 4.20, alginate/MMT cryogels exhibited gel fraction around 80 % meaning that 80 % of alginate used at the beginnig was crosslinked. Raising the amount of MMT slightly decreased gel fraction (%) of the composite cryogels. In this case, MMT could covered some of the crosslinking points (COO^-) of alginate chains or amine groups of Cys. Therefore, MMT had a negative effect on gel fraction (%).

As can be seen in Figure 4.20, alginate/MMT cryogels adsorbed huge amount of water, approximately 15 times of their dry weights. On the other hand, changing MMT amount from 0 (w/v) % to 5 (w/w) % decreased water uptake sharply, about 50 %. This is due to the fact that, excessive amount of MMT plugged the pores inside the cryogels and reduced pore size. And also, MMT exhibited slight aggregates on pore surfaces, reducing free-flow of water, as also reported previously [140].

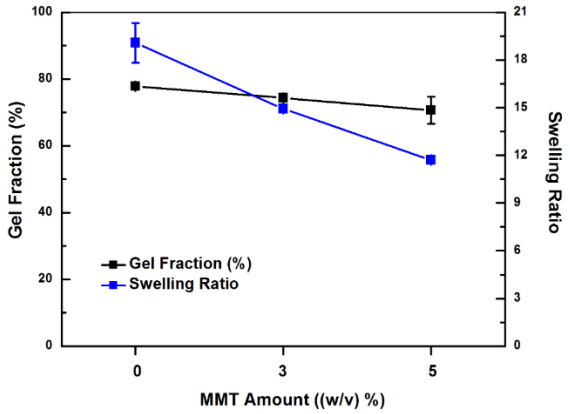


Figure 4.20 The effect of MMT amount ((w/v) %) on gel fraction (%) and swelling ratio of alginate/MMT composite cryogels.

4.2.4 Mechanical Testing of Alginate/MMT Composite Cryogels

Uniaxial compression test was performed on alginate/MMT composite cryogels to investigate the effect of MMT amount on mechanical behavious. Figure 4.21a shows

stress-strain curve of each alginate/MMT cryogel. As also illustrated in Figure 4.21a, concave upward curve for elastomeric materials were observed for all cryogels and they were able to compress up to 80% without any breakage [141]. After release of load in compression test, they quickly reabsorbed water released during compression (inner section of Figure 4.21a). MMT also enhanced compression stress of the cryogels, whereby their compression limit was attained to 160 kPa stress values. This is due to the fact that, in cryogel systems, denser and thin pore walls yields structural support for these alginate cryogels [142].

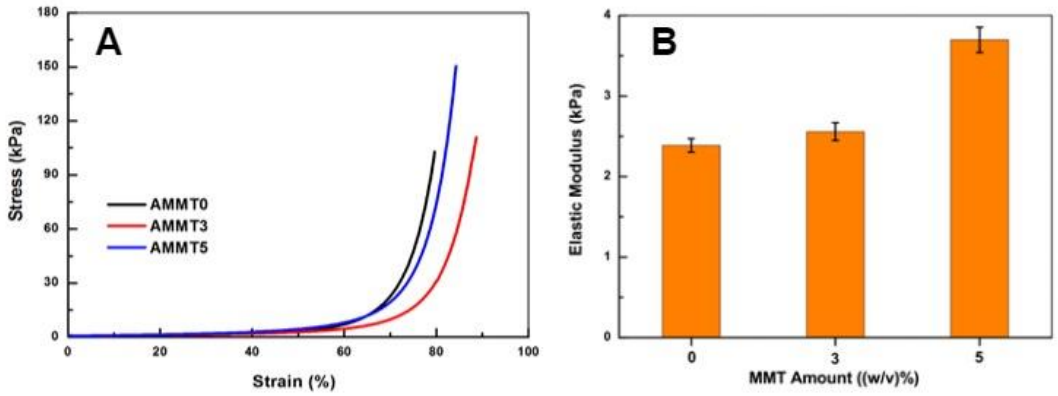


Figure 4.21 Typical stress-strain curves for cryogels (a) and elastic moduli of cryogels with varying MMT amount (b).

The elastic moduli or stiffness of cryogels were calculated from the slope of initial linear part of the each stress-strain curve for each sample. Figure 4.20b indicates elastic moduli (kPa) of each sample. Incorporation of MMT significantly enhanced elastic moduli values, approximately 1.5 fold. This is due to the fact that, huge amount of MMT led to thickening of the pore walls and acted as reinforcing agent. Same observations also reported by Suner et al. [143] and El-Naggar et al. [144] where they reinforced cryogels with clays. Thus, similar stress-strain curves for alginate cryogels also reported by Kumar et al. whereby they prepared agarose-alginate cryogel for biomedical applications [36].

4.2.5 Methylene Blue Adsorption by Alginate/MMT Composite Cryogels

4.2.5.1 Batch Adsorption and Isotherm Models

Batch adsorption procedure was conducted to understand the mechanism of adsorption of MB by alginate/MMT cryogels. Figure 4.22 shows data obtained by batch mode

adsorption and non-linear fitting of Freundlich and Langmuir isotherm models. According to Figure 4.22, sample containing 3 (w/v) % MMT (AMMT3) showed superior adsorption of MB, while others were limited due to either MMT absence (AMMT0) or excessive amount of MMT (AMMT5).

Table 4.5 shows parameters of Freundlich and Langmuir isotherms models. As can be seen in Table 4.5, based on R^2 values, Langmuir model showed better fitting onto experimental data whereby lower R^2 values obtained from non-linear fitting of Freundlich model. Therefore, we can report that all cryogels followed homogen adsorption where active sites for dye attachment were equally distributed all over the alginate/MMT cryogel networks.

As also can be inferred from Table 4.5, q_m values of alginate/MMT cryogels were enhanced with incroporation of MMT. On the other hand, excessive amount of MMT reduced q_m value due to pore-plugging property of MMT. Theoretical maximum adsorption capacity (q_m) for AMMT3 was found as 559.95 mg g^{-1} which is quite high compared to poly(vinyl alcohol)-chitosan-alginate-MMT hydrogel beads (137.2 mg g^{-1}) [133], alginate-MMT quasi-cryogel beads (181.8 mg g^{-1}) [7], alginate-clinoptilolite beads (452.25 mg g^{-1}) [4] and poly(acrylamide)-potato starch cryogel (443.7 mg g^{-1}) however, quite low compared to sodium vinyl sulfonate-co-2-acrylamido-2-me-[thylpropane sulfonic acid sodium salt-magnetite cryogel (788 mg g^{-1}) [145] and calcium alginate-bentonite-activated carbon beads (756.97 mg g^{-1}) [134].

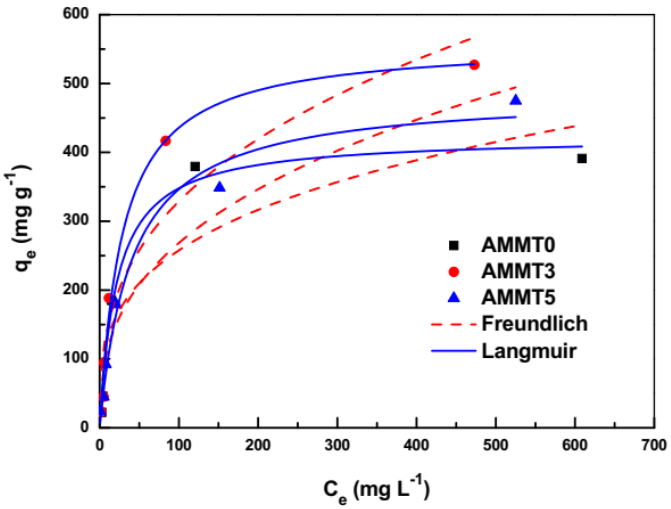


Figure 4.22 Batch adsorption data of cryogels and non-linear fitting of Freundlich and Langmuir isotherm models.

Table 4.5 Langmuir and Freundlich isotherm constants for MB adsorption onto composite cryogels.

Model	Parameters	AMMT0	AMMT3	AMMT5
Langmuir	q_m, mg g^{-1}	422.88	559.95	462.77
	K_L, L mg^{-1}	0.046	0.035	0.028
	R_L	0.46	0.53	0.59
	R^2	0.98	0.98	0.99
Freundlich	K_F, mg g^{-1}	65.9581	65.5833	51.1421
	N	0.2959	0.3502	0.3559
	R^2	0.79	0.87	0.95

4.2.5.2 Adsorption Kinetics and Kinetic Models

Kinetic study was completed for charaterization of MB adsorption by alginate/MMT composite cryogels. Figure 4.23 shows kinetic data and non-linear fitting of PFO and PSO models. According to Figure 4.23, all cryogel reached their equilibrium about 3 hours of contact with MB solution. Fast removal of MB by composite cryogels obtained due to open porous struture, interconnected porous moprhology and macroporosity of these cryogels which allowed flow of water through matrices and fast diffusion of dye particles [146]. However, extensive amount of MMT (5 (w/v) %, AMMT5) plugged the pores yielding negative effect on MB removal. As a result, reduced dye removal by AMMT5 sample observed, same phenomena also reported in a study related to composite cryogel for adsorption [147].

Table 4.6 illustrates kinetic parameters of PFO and PSO calculated from experimental data. According to Table 4.6, by taking consideration of high R^2 values, adsorption of MB is better described by PSO kinetic model revealing that adsorption of MB onto cryogels has a rate-limiting step and follows chemisorption [148]. In this regard, ionic interactions occured between MB particles and alginate/MMT cryogels. PSO kinetic model also found by Uyar et al. [7], which they applied alginate-MMT quasi-cryogel

beads for MB adsorption, and Belhouchat et al. [132], whereby they used alginate/bentonite composite for MB removal.

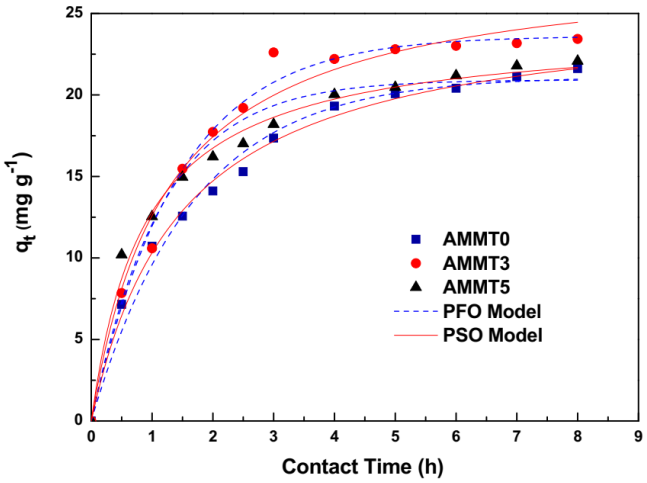


Figure 4.23 Non-linear regression of PFO and PSO kinetic models on the MB retention by alginate/MMT composite cryogels (Initial dye concentration: 25 mg L^{-1}, adsorbent dosage: 0.01 g, temperature: 25 °C).

Table 4.6 PFO and PSO kinetic parameters for MB adsorption onto AMMT0, AMMT3 and AMMT5 samples at the initial dye concentration of 25 mg L^{-1}.

Adsorbent Parameter	AMMT0	AMMT3	AMMT5
PFO Kinetic Model			
$q_{e,calc}$, mg g^{-1}	21.13	23,62	20.93
k_1, min^{-1}	0.0101	0.0177	0.0144
R^2	0.98	0.98	0.96
PSO Kinetic Model			
$q_{e,calc}$, mg g^{-1}	25.62	28.26	24.07
k_2, min^{-1}	0.0004	0.0005	0.0008
R^2	0.99	0.98	0.99

4.2.5.3 Dye Removal Efficiency

Dye removal efficiency (%) of alginate/MMT composite cryogels were evaluted for analyzing the effect of MMT amount on MB adsorption. Figure 4.24 shows dye removal (%) of alginate/MMT cryogels with different MMT amount. Regarding of Figure 4.23, all

cryogels removed 90 % of initial MB concentration due to negatively charged free COO^- groups of alginate. The presence of free COO^- groups also provided by gel fraction, which almost 20 % of COO^- groups on polymer backbone is unbound. Same observations also provided by Dinu et al. [4] and Dragan et al. [5].

As also can be inferred from Figure 4.24, the negative nature of MMT enhanced dye removal (%) where the ratio of MMT increased from 0 (w/v) % to 3 (w/v) %, removal improved by 4 %. When the ratio of MMT increased by 5 (w/v) %, slight decrease of dye removal observed. This alteration could be explained by less swelling ratio resulting reduced interactions with MB. Same results also observed in a study related to inorganic composite cryogel for adsorption adsorption [140].

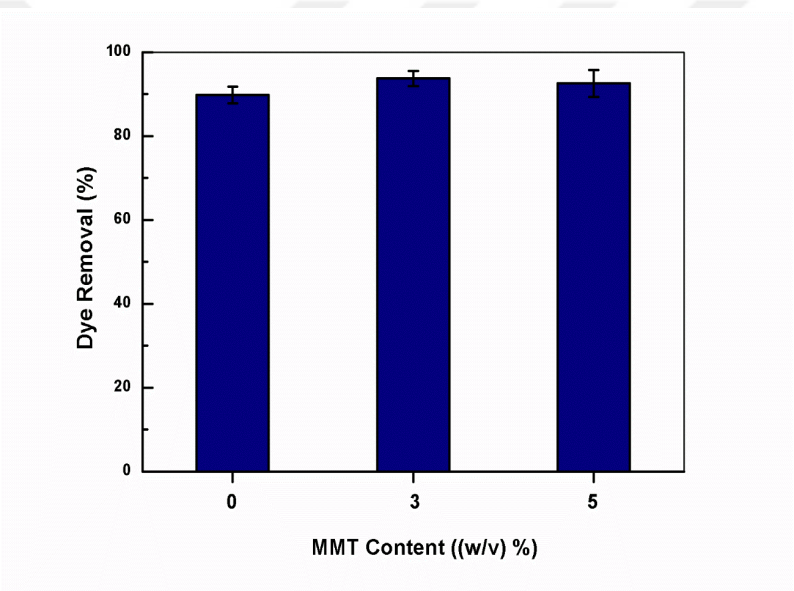


Figure 4.24 The effect of MMT content ((w/v) %) on dye removal (%) of alginate/MMT composite cryogels.

4.2.5.4 Desorption Study

Desorption study was carried out to investigate regeneration of adsorbents and their reusability. Figure 4.25 shows desorption efficiencies of different eluting agents on dye adsorbed alginate/MMT cryogels. Each adsorption and desorption was conducted for 1 hour.

Taking consideration of Figure 4.25, acetic acid as organic acid showed superior desorption of AMMT0 sample. This is due to the fact that, adsorption was also driven by chemisorption process for this sorbent. However, MMT decreased dye release

characteristics in all desorbing agents. This due the fact that, the surface of MMT alters with pH change, specifically in acidic pH values [137].

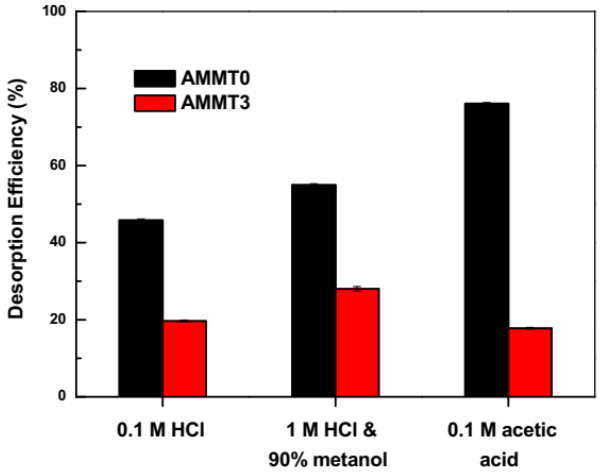


Figure 4.25 The effect of MMT presence of cryogels on desorption efficiencies of different eluting agents for MB.

4.3 Comparision of Composite Post-Crosslinked Hydrogels and Cryogels

In this thesis, we prepared macroporous alginate/MMT hydrogels via two separate methods, post-crosslinking approach and cryogelation technique. In the post-crosslinking approach, we prepared alginate/MMT macroporous hydrogels by physical crosslinking. On the other hand, in cryogelation technique, we employed covalent crosslinking to form true alginate/MMT cryogels via carbodiimide chemistry. Each technique possessed excellent performance for production of macroporous alginate/MMT composite hydrogels. In the following paragraphs the difference between the obtained post-crosslinked hydrogels and cryogels are discussed.

SEM measurements revealed formation of macroporosity, since both technique uses freezing part as a step to form hydrogel. Looking through post-crosslinked hydrogels, MMT incorporation resulted larger pores on the contrary to MMT incorporated cryogels. This separation is originated from preparation technique. In post-crosslinking approach, porosity was imparted while freezing of alginate/MMT mixture. In this freezing process, ice crystals have grown more freely due to depletion of freezing point of water [127]. Since post-crosslinking system does not involve any crosslinking during freezing, post-crosslinked hydrogels showed different property compared to cryogels. On the contrary, in the cryogel systems, incorporation of MMT reduced pore size. This is also related to

freezing and gelation in moderately frozen state. Therefore, due to MMT, the growth of ice crystals restricted and reduced pore size in all over the cryogel network [124].

According to pore size distributions, post-crosslinked hydrogels exhibited narrower pore size distribution compared to alginate/MMT cryogels. While average pore size of post-crosslinked alginate/MMT hydrogels are between 120 µm and 162 µm, the average pore size for the cryogels are between 114 µm and 143 µm. The difference between pore size distributions and average pore size were due to their crosslinking temperature and reaction medium.

Gel fraction results revealed the ratio of polymer crosslinked over polymer used. Both post-crosslinked hydrogels and cryogels exhbited gel fraction around 80 %-85 %. Incorporation of MMT enhanced gel fraction of post-crosslinked hydrogels by 5 %, on the other hand, MMT reduced gel fraction of cryogels. Since post-crosslinking path used Ca^{2+} for crosslinking of alginate, MMT also participated to Ca^{2+} due to negatively charged hydroxyl groups of MMT. However, in cryogelation system, MMT blocked covalent crosslinking points of alginate and reduced gel fraction slightly.

Swelling ratio measurements elucidated the water uptake capacity of macroporous alginate/MMT hydrogels. Both macroporous hydrogels swelled in water approximately 14 times of their dry weight. While swelling of post-crosslinked composite hydrogels slightly affected by MMT, significant changes are observed in composite cryogels. When MMT did not involve in crosslinking of cryogels covalently, they also acted as pore wall thickening agent and resulted in decrease of pore size [42]. Thus it reduced water uptake capacity of composite cryogels.

Uniaxial compression tests were elucidated to understand mechanical behavior of macroporous alginate/MMT composite hydrogels. Both gels were compressed up to 80 % of their initial length without crack or deformation. After release of compression, they also reabsorbed water that they released during compression. Both gels showed upward concave curve as stress-strain curve which is typical for elastomeric materials. While elastic moduli of post-crosslinked hydrogels were reached up to 48 kPa, cryogels were attained to 4 kPa. More compact hydrogels were obtained with post-crosslinking route. This observation is related to their crosslinking temperature and time. Since post-crosslinked hydrogels were prepared at room temperature and crosslinking conducted

for 72 h, cryogels synthesized at -18°C for 48 h. Thus, crosslinking time and temperature may alter the crosslinking performance of these gels.

In batch mode adsorption experiment, MB adsorption via macroporous composite hydrogels were characterized. Post-crosslinked hydrogels were shown to be superior compared to cryogels in MB removal. Both macroporous hydrogels followed monolayer adsorption based on high R^2 values obtained by Langmuir model. Theoretical maximum adsorption capacities were found as 1435.58 mg g^{-1} for post-crosslinked hydrogels and 559.95 mg g^{-1} for cryogels, respectively. It should be noted that, post-crosslinking strategy with physical crosslinking is more suitable for production of alginate adsorbent in comparison with cryogelation method. However, physical crosslinking causes disassociation under physiological condition yielding disrupted hydrogel integrity, as reported in the literature [11]. When post-crosslinked hydrogels were introduced to MB solution, they partially dissolved and owned more free carboxylate groups. Therefore, maximum adsorption capacity of post-crosslinked hydrogels for MB removal was more than two-times of cryogels which they chemically crosslinked. However, they both showed remarkable dye removal compared to other adsorbent in the literature for MB removal.

In kinetic experiments, the route for MB adsorption was also characterized. Both post-crosslinked hydrogels and cryogels removed MB within 3 hours contact with the benefit of macroporosity, open-porous structure and interconnected porosity revealed by their preparation techniques [146]. Post-crosslinked hydrogels with physical crosslinking and reduced MMT amount retained MB via physical electrostatic interactions. However, cryogels with covalent crosslinking and huge amount of MMT resulted attachment of MB via ion-exchange. As a result, while post-crosslinked hydrogels followed PFO model, cryogels continued PSO model. Desorption study was also give information about if adsorption is chemisorption or physisorption. Therefore, while MB is discharged form post-crosslinked hydrogels via weak acids, MB elimination from cryogels accomplished by organic acids. Once more it has been proved that, while post-crosslinked hydrogels followed physisorption, cryogels followed chemisorption route.

4.4 CONCLUSION

In this thesis, we prepared macroporous alginate/MMT hydrogels as adsorbents for MB removal. Post-crosslinking approach and cryogelation techniques were employed to prepare such composite hydrogels.

The following conclusions can be drawn from our experimental results:

I) Post-crosslinking strategy was successfully applied to prepare macroporous alginate/MMT composite hydrogels. Post-crosslinked alginate/MMT hydrogels exhibited interconnected porous morphology. Their pore size ranged between 75 µm to 250 µm. Average pore size for MMT free sample ($A_5MMT_0XL_5$) and MMT-containing sample ($A_5MMT_2XL_5$) samples were found as 120 $\pm$ 27 µm and 162 $\pm$ 50 µm, respectively. They retained huge amount of water, approximately 13 times with respect to their dry weights, whereby at the same time, their gel fractions was around 85 %.

III) Post-crosslinked alginate/MMT hydrogels showed upward concave stress-strain curve specialized for elastomeric materials. They compressed up to 80 % of their initial length without crack or deformation. Their elastic modulus values reached around to 48 kPa.

IV) Post-crosslinked hydrogels exhibited super adsorption ability against MB. They removed up to 95% of initial dye concentration within 24 hour of contact with dye. Monolayer adsorption was found to be characteristics of MB adsorption via post-crosslinked hydrogels. Theoretical maximum adsorption capacity for post-crosslinked alginate/MMT hydrogels was obtained as 1435.58. mg g^{-1}.

VI) PFO kinetic model showed better fitting onto kinetic experimental data which post-crosslinked alginate/MMT hydrogels followed physisorption way.

VII) MMT reduced dye releasing behavior of post-crosslinked hydrogels, yet weak acids showed better elution performance for MB.

VIII) Cryogelation technique was precisely used to accomplish to prepare macroporous alginate/MMT cryogels. FT-IR results revealed both covalent crosslinking and MMT incorporation.

IX) Interconnected porosity obtained as a result of cryogelation technique. Their pore size were obtained between 50 µm to 300 µm. Average pore size of the samples were calculated as 143 ± 55 µm for AMMT0, 121 ± 33 µm for AMMT3 and 114 ± 28 µm for AMMT5, respectively.

X) Gel fraction values were calculated around 80%. Thus, alginate/MMT cryogels also hold 15 times of water of their dry weights.

XI) MMT enhanced elastic limit of alginate cryogels. Elastic modulus of alginate cryogels was found around 4 kPa.

XII) Alginate/MMT cryogels recovered 95 % of initial MB amount within 24 h of contact. Langmuir isotherm model gave better fitting onto batch experimental data and maximum adsorption capacity for alginate/MMT cryogels was found as 559.95 mg g^{-1}.

XIII) Alginate/MMT cryogels reached their dye removal equilibrium in 3 h duration while they followed chemisorption path for MB removal.

XIV) MMT restricted dye releasing of MB adsorbed alginate/MMT cryogels. Still, organic acids showed superior dye elution from alginate/MMT cryogels.

As a consequence, both post-crosslinked hydrogels and cryogels possessed unique properties as adsorbents. Therefore, they have assigned as alternatives to current adsorbents for MB removal.

As future studies, the thermodynamic modelling of these adsorbents can be conducted. Also, among being adsorbent for MB removal, both post-crosslinked hydrogels and cryogels may also be used to remove heavy metals or organic pollutants from waste waters.

Alginate cryogels would also have potential to be used in biomedical applications such as drug and protein delivery, tissue engineered scaffold etc. Thus, by incorporation of different additives such as polymeric or metallic nanoparticles, they also could be preferred in bioseparation (e.g. purification of antibodies, proteins), energy production (e.g. H_2 generation), biosensor or antibacterial applications, regarding nanoparticle type. Both post-crosslinked alginate hydrogels and cryogels may have potential to be employed in cell culturing. They may be applied as matrices for cell preservation for long-time use.

Furthermore, by incorporating conductive materials such as graphene oxide or carbon nanotubes, they could be utilized in nerve tissue engineering or biosensor applications. Also, bacterial cells could be immobilized onto these alginate gels for biocatalytic purposes.

REFERENCES

[1] Yagub, M.T. Sen, T.K. Afroze, S. ve Ang, H.M., (2014). "Dye and its removal from aqueous solution by adsorption: A review", Advances in Colloid and Interface Science, 209: 172-184.

[2] Ahmad, A. Mohd-Setapar, S.H. Chuong, C.S. Khatoon, A. Wani, W.A. Kumar, R. ve Rafatullah, M., (2015). "Recent advances in new generation dye removal technologies: novel search for approaches to reprocess wastewater", RSC Advances, 5: 30801-30818.

[3] Fil, B.A. Ozmetin, C. ve Korkmaz, M., (2012). "Cationic dye (methylene blue) removal from aqueous solution by montmorillonite", Bulletin of the Korean Chemical Society, 33: 3184-3190.

[4] Dinu, M.V. Lazar, M.M. ve Dragan, E.S., (2017). "Dual ionic cross-linked alginate/clinoptilolite composite microbeads with improved stability and enhanced sorption properties for methylene blue", Reactive and Functional Polymers, 116: 31-40.

[5] Dragan, E.S. ve Apopei Loghin, D.F., (2013). "Enhanced sorption of methylene blue from aqueous solutions by semi-IPN composite cryogels with anionically modified potato starch entrapped in PAAm matrix", Chemical Engineering Journal, 234: 211-222.

[6] Zhou, C. Wu, Q. Lei, T. ve Negulescu, I.I., (2014). "Adsorption kinetic and equilibrium studies for methylene blue dye by partially hydrolyzed polyacrylamide/cellulose nanocrystal nanocomposite hydrogels", Chemical Engineering Journal, 251: 17-24.

[7] Uyar, G. Kaygusuz, H. ve Erim, F.B., (2016). "Methylene blue removal by alginate–clay quasi-cryogel beads", Reactive and Functional Polymers, 106: 1-7.

[8] Lu, T. Xiang, T. Huang, X.-L. Li, C. Zhao, W.-F. Zhang, Q. ve Zhao, C.-S., (2015). "Post-crosslinking towards stimuli-responsive sodium alginate beads for the removal of dye and heavy metals", Carbohydrate Polymers, 133: 587-595.

[9] Liu, L. Wan, Y. Xie, Y. Zhai, R. Zhang, B. ve Liu, J., (2012). "The removal of dye from aqueous solution using alginate-halloysite nanotube beads", Chemical Engineering Journal, 187: 210-216.

[10] Shang, K. Liao, W. Wang, J. Wang, Y.-T. Wang, Y.-Z. ve Schiraldi, D.A., (2016). "Nonflammable Alginate Nanocomposite Aerogels Prepared by a Simple Freeze-Drying and Post-Cross-Linking Method", ACS Applied Materials & Interfaces, 8: 643-650.

[11] Petrenko, Y.A. Ivanov, R.V. Petrenko, A.Y. ve Lozinsky, V.I., (2011). "Coupling of gelatin to inner surfaces of pore walls in spongy alginate-based scaffolds facilitates the adhesion, growth and differentiation of human bone marrow mesenchymal stromal cells", Journal of Materials Science: Materials in Medicine, 22: 1529-1540.

[12] Zhao, Y. Gao, S. Zhao, S. Li, Y. Cheng, L. Li, J. ve Yin, Y., (2012). "Synthesis and characterization of disulfide-crosslinked alginate hydrogel scaffolds", Materials Science and Engineering: C, 32: 2153-2162.

[13] Béduer, A. Braschler, T. Peric, O. Fantner, G.E. Mosser, S. Fraering, P.C. Benchérif, S. Mooney, D.J. ve Renaud, P., (2015). "A compressible scaffold for minimally invasive delivery of large intact neuronal networks", Advanced healthcare materials, 4: 301-312.

[14] Tillet, G. Boutevin, B. ve Ameduri, B., (2011). "Chemical reactions of polymer crosslinking and post-crosslinking at room and medium temperature", Progress in Polymer Science, 36: 191-217.

[15] Katsen-Globa, A. Meiser, I. Petrenko, Y.A. Ivanov, R.V. Lozinsky, V.I. Zimmermann, H. ve Petrenko, A.Y., (2014). "Towards ready-to-use 3-D scaffolds for regenerative medicine: adhesion-based cryopreservation of human mesenchymal stem cells attached and spread within alginate–gelatin cryogel scaffolds", Journal of Materials Science. Materials in Medicine, 25: 857-871.

[16] Pan, T. Song, W. Cao, X. ve Wang, Y., (2016). "3D Bioplotting of Gelatin/Alginate Scaffolds for Tissue Engineering: Influence of Crosslinking Degree and Pore Architecture on Physicochemical Properties", Journal of Materials Science & Technology, 32: 889-900.

[17] Kim, Y. ve Kim, G., (2013). "Collagen/alginate scaffolds comprising core (PCL)–shell (collagen/alginate) struts for hard tissue regeneration: fabrication, characterisation, and cellular activities", Journal of Materials Chemistry B, 1: 3185-3194.

[18] Nguyen, V.-T. Ko, S.-C. Oh, G.-W. Heo, S.-Y. Jeon, Y.-J. sun Park, W. Choi, I.-W. Choi, S.-W. ve Jung, W.-K., (2016). "Anti-inflammatory effects of sodium alginate/gelatine porous scaffolds merged with fucoidan in murine microglial BV2 cells", International Journal of Biological Macromolecules, 93: 1620-1632.

[19] Ki, S.B. Singh, D. Kim, S.C. Son, T.W. ve Han, S.S., (2013). "Effect of cross-linkers in fabrication of carrageenan–alginate matrices for tissue engineering application", Biotechnology and applied biochemistry, 60: 589-595.

[20] Li, Z. Leung, M. Hopper, R. Ellenbogen, R. ve Zhang, M., (2010). "Feeder-free self-renewal of human embryonic stem cells in 3D porous natural polymer scaffolds", biomaterials, 31: 404-412.

[21] Liu, M. Dai, L. Shi, H. Xiong, S. ve Zhou, C., (2015). "In vitro evaluation of alginate/halloysite nanotube composite scaffolds for tissue engineering", Materials Science and Engineering: C, 49: 700-712.

[22] Puetzer, J.L. Ballyns, J.J. ve Bonassar, L.J., (2012). "The Effect of the Duration of Mechanical Stimulation and Post-Stimulation Culture on the Structure and Properties of Dynamically Compressed Tissue-Engineered Menisci", Tissue Engineering Part A, 18: 1365-1375.

[23] Lin, N. Bruzzese, C.c. ve Dufresne, A., (2012). "TEMPO-oxidized nanocellulose participating as crosslinking aid for alginate-based sponges", ACS applied materials & interfaces, 4: 4948-4959.

[24] Darder, M. Matos, C.R.S. Aranda, P. Gouveia, R.F. ve Ruiz-Hitzky, E., (2017). "Bionanocomposite foams based on the assembly of starch and alginate with sepiolite fibrous clay", Carbohydrate Polymers, 157: 1933-1939.

[25] Afshar, H.A. ve Ghaee, A., (2016). "Preparation of aminated chitosan/alginate scaffold containing halloysite nanotubes with improved cell attachment", Carbohydrate Polymers, 151: 1120-1131.

[26] Wang, Y. Feng, Y. Zhang, X.-F. Zhang, X. Jiang, J. ve Yao, J., (2018). "Alginate-based attapulgite foams as efficient and recyclable adsorbents for the removal of heavy metals", Journal of Colloid and Interface Science, 514: 190-198.

[27] Ceylan, D. Ozmen, M. ve Okay, O., (2006). Swelling-Deswelling Kinetics of Ionic Poly (acrylamide) Hydrogels and Cryogels.

[28] Dinu, M.V. Ozmen, M.M. Dragan, E.S. ve Okay, O., (2007). "Freezing as a path to build macroporous structures: Superfast responsive polyacrylamide hydrogels", Polymer, 48: 195-204.

[29] Shan, L. Gao, Y. Zhang, Y. Yu, W. Yang, Y. Shen, S. Zhang, S. Zhu, L. Xu, L. ve Tian, B., (2016). "Fabrication and use of alginate-based cryogel delivery beads loaded with urea and phosphates as potential carriers for bioremediation", Industrial & Engineering Chemistry Research, 55: 7655-7660.

[30] Fatoni, A. Dwiasi, D.W. ve Hermawan, D., (2016). "Alginate cryogel based glucose biosensor": IOP Publishing.

[31] Zhang, W. Yang, Y. Guan, T. Guan, J. Zheng, S. Chen, B. ve Yun, J., (2018). "Formation Dynamics of Cell-Loading Alginate Droplets in the Microtube Dripping and Cryo-Cross-Linking Process for Cell-Entrapped Cryogel Beads as the Biocatalysts toward Phenyllactic Acid Biosynthesis", Industrial & Engineering Chemistry Research, 57: 7291-7300.

[32] Petrenko, Y.A. Ivanov, R. Lozinsky, V. ve Petrenko, A.Y., (2011). "Comparison of the methods for seeding human bone marrow mesenchymal stem cells to macroporous alginate cryogel carriers", Bulletin of experimental biology and medicine, 150: 543-546.

[33] Brovko, O. Palamarchuk, I. Val'chuk, N. Chukhchin, D. Bogolitsyn, K. ve Boitsova, T., (2017). "Gels of sodium alginate–chitosan interpolyelectrolyte complexes", Russian Journal of Physical Chemistry A, 91: 1580-1585.

[34] Tripathi, A. Vishnoi, T. Singh, D. ve Kumar, A., (2013). "Modulated crosslinking of macroporous polymeric cryogel affects in vitro cell adhesion and growth", Macromolecular bioscience, 13: 838-850.

[35] Tripathi, A. Sami, H. Jain, S.R. Viloria-Cols, M. Zhuravleva, N. Nilsson, G. Jungvid, H. ve Kumar, A., (2010). "Improved bio-catalytic conversion by novel immobilization process using cryogel beads to increase solvent production", Enzyme and Microbial Technology, 47: 44-51.

[36] Tripathi, A. ve Kumar, A., (2011). "Multi-Featured Macroporous Agarose–Alginate Cryogel: Synthesis and Characterization for Bioengineering Applications", Macromolecular bioscience, 11: 22-35.

[37] Tripathi, A. Hadapad, A.B. Hire, R.S. Melo, J.S. ve D'Souza, S.F., (2013). "Polymeric macroporous formulations for the control release of mosquitocidal Bacillus sphaericus ISPC-8", Enzyme Microb Technol, 53: 398-405.

[38] Tripathi, A. Melo, J.S. ve D'Souza, S.F., (2013). "Uranium (VI) recovery from aqueous medium using novel floating macroporous alginate-agarose-magnetite cryobeads", Journal of hazardous materials, 246-247: 87-95.

[39] Bencherif, S.A. Sands, R.W. Ali, O.A. Li, W.A. Lewin, S.A. Braschler, T.M. Shih, T.-Y. Verbeke, C.S. Bhatta, D. ve Dranoff, G., (2015). "Injectable cryogel-based whole-cell cancer vaccines", Nature communications, 6: 7556.

[40] Bencherif, S.A. Sands, R.W. Bhatta, D. Arany, P. Verbeke, C.S. Edwards, D.A. ve Mooney, D.J., (2012). "Injectable preformed scaffolds with shape-memory properties", Proceedings of the National Academy of Sciences, 109: 19590-19595.

[41] Shih, T.Y. Blacklow, S.O. Li, A.W. Freedman, B.R. Bencherif, S. Koshy, S.T. Darnell, M.C. ve Mooney, D.J., (2018). "Injectable, Tough Alginate Cryogels as Cancer Vaccines", Advanced healthcare materials, 7: 1701469.

[42] Koshy, S.T. Zhang, D.K. Grolman, J.M. Stafford, A.G. ve Mooney, D.J., (2018). "Injectable nanocomposite cryogels for versatile protein drug delivery", Acta biomaterialia, 65: 36-43.

[43] Balkız, G. Pingo, E. Kahya, N. Kaygusuz, H. ve Bedia Erim, F., (2018). "Graphene Oxide/Alginate Quasi-Cryogels for Removal of Methylene Blue", Water, Air, & Soil Pollution, 229: 131.

[44] Waring, D.R. ve Hallas, G., (2013). The chemistry and application of dyes: Springer Science & Business Media.

[45] Gupta, V., (2009). "Application of low-cost adsorbents for dye removal–a review", Journal of environmental management, 90: 2313-2342.

[46] Chequer, F.M.D. de Oliveira, G.A.R. Ferraz, E.R.A. Cardoso, J.C. Zanoni, M.V.B. ve de Oliveira, D.P., (2013). Textile dyes: dyeing process and environmental impact, ed. Eco-friendly textile dyeing and finishing. IntechOpen.

[47] Benkhaya, S. El Harfi, S. ve Elharfi, A., (2017). Classifications, properties and applications of textile dyes: A review.

[48] Rafatullah, M. Sulaiman, O. Hashim, R. ve Ahmad, A., (2010). "Adsorption of methylene blue on low-cost adsorbents: a review", Journal of hazardous materials, 177: 70-80.

[49] Katheresan, V. Kansedo, J. ve Lau, S.Y., (2018). "Efficiency of various recent wastewater dye removal methods: A review", Journal of Environmental Chemical Engineering, 6: 4676-4697.

[50] Barakat, M.A. ve Kumar, R., (2015). CHAPTER 10 Modified and New Adsorbents for Removal of Heavy Metals from Wastewater, ed. Heavy Metals In Water: Presence, Removal and Safety. The Royal Society of Chemistry, 193-212.

[51] Bonilla-Petriciolet, A. Mendoza-Castillo, D.I. ve Reynel-Ávila, H.E., (2017). Adsorption processes for water treatment and purification: Springer.

[52] Al-Anber, M.A., (2011). Thermodynamics approach in the adsorption of heavy metals, ed. Thermodynamics-Interaction Studies-Solids, Liquids and Gases. InTech.

[53] Worch, E., (2012). Adsorption technology in water treatment: fundamentals, processes, and modeling: Walter de Gruyter.

[54] Limousin, G. Gaudet, J.P. Charlet, L. Szenknect, S. Barthès, V. ve Krimissa, M., (2007). "Sorption isotherms: A review on physical bases, modeling and measurement", Applied Geochemistry, 22: 249-275.

[55] Foo, K.Y. ve Hameed, B.H., (2010). "Insights into the modeling of adsorption isotherm systems", Chemical Engineering Journal, 156: 2-10.

[56] Benavente, M., (2008). Adsorption of metallic ions onto chitosan: equilibrium and kinetic studies, ed^eds.: KTH.

[57] Largitte, L. ve Pasquier, R., (2016). "A review of the kinetics adsorption models and their application to the adsorption of lead by an activated carbon", Chemical Engineering Research and Design, 109: 495-504.

[58] Liu, C. Omer, A.M. ve Ouyang, X.-k., (2018). "Adsorptive removal of cationic methylene blue dye using carboxymethyl cellulose/k-carrageenan/activated montmorillonite composite beads: Isotherm and kinetic studies", International Journal of Biological Macromolecules, 106: 823-833.

[59] Aichour, A. Zaghouane-Boudiaf, H. Iborra, C.V. ve Polo, M.S., (2018). "Bioadsorbent beads prepared from activated biomass/alginate for enhanced removal of cationic dye from water medium: Kinetics, equilibrium and thermodynamic studies", Journal of Molecular Liquids, 256: 533-540.

[60] Samiey, B. Cheng, C.-H. ve Wu, J., (2014). "Organic-inorganic hybrid polymers as adsorbents for removal of heavy metal ions from solutions: a review", Materials, 7: 673-726.

[61] Kyzas, G.Z. ve Kostoglou, M., (2014). "Green adsorbents for wastewaters: a critical review", Materials, 7: 333-364.

[62] Wang, Y. Wang, W. ve Wang, A., (2013). "Efficient adsorption of methylene blue on an alginate-based nanocomposite hydrogel enhanced by organo-illite/smectite clay", Chemical Engineering Journal, 228: 132-139.

[63] Li, L. Xiao, J. Liu, P. ve Yang, G., (2015). "Super adsorption capability from amorphousization of metal oxide nanoparticles for dye removal", Scientific reports, 5: 9028.

[64] González, J.A. Villanueva, M.E. Piehl, L.L. ve Copello, G.J., (2015). "Development of a chitin/graphene oxide hybrid composite for the removal of pollutant dyes: adsorption and desorption study", Chemical Engineering Journal, 280: 41-48.

[65] Kaur, S. Rani, S. Mahajan, R. Asif, M. ve Gupta, V.K., (2015). "Synthesis and adsorption properties of mesoporous material for the removal of dye safranin: kinetics, equilibrium, and thermodynamics", Journal of Industrial and Engineering Chemistry, 22: 19-27.

[66] Caló, E. ve Khutoryanskiy, V.V., (2015). "Biomedical applications of hydrogels: A review of patents and commercial products", European Polymer Journal, 65: 252-267.

[67] Li, L. Wang, Y. Pan, L. Shi, Y. Cheng, W. Shi, Y. ve Yu, G., (2015). "A nanostructured conductive hydrogels-based biosensor platform for human metabolite detection", Nano letters, 15: 1146-1151.

[68] Hoffman, A.S., (2012). "Hydrogels for biomedical applications", Advanced drug delivery reviews, 64: 18-23.

[69] Liang, Y.Y. Zhang, L.M. Jiang, W. ve Li, W., (2007). "Embedding Magnetic Nanoparticles into Polysaccharide-Based Hydrogels for Magnetically Assisted Bioseparation", ChemPhysChem, 8: 2367-2372.

[70] Zhou, G. Liu, C. Chu, L. Tang, Y. ve Luo, S., (2016). "Rapid and efficient treatment of wastewater with high-concentration heavy metals using a new type of hydrogel-based adsorption process", Bioresource Technology, 219: 451-457.

[71] Liu, D. Martinez-Sanz, M. Lopez-Sanchez, P. Gilbert, E.P. ve Gidley, M.J., (2017). "Adsorption behaviour of polyphenols on cellulose is affected by processing history", Food Hydrocolloids, 63: 496-507.

[72] Liu, C. Omer, A. ve Ouyang, X.-k., (2018). "Adsorptive removal of cationic methylene blue dye using carboxymethyl cellulose/k-carrageenan/activated montmorillonite composite beads: Isotherm and kinetic studies", International Journal of Biological Macromolecules, 106: 823-833.

[73] Hu, X.-S. Liang, R. ve Sun, G., (2018). "Super-adsorbent hydrogel for removal of methylene blue dye from aqueous solution", Journal of Materials Chemistry A, 6: 17612-17624.

[74] Dai, H. ve Huang, H., (2016). "Modified pineapple peel cellulose hydrogels embedded with sepia ink for effective removal of methylene blue", Carbohydrate Polymers, 148: 1-10.

[75] Melo, B.C. Paulino, F.A. Cardoso, V.A. Pereira, A.G. Fajardo, A.R. ve Rodrigues, F.H., (2018). "Cellulose nanowhiskers improve the methylene blue adsorption capacity of chitosan-g-poly (acrylic acid) hydrogel", Carbohydrate Polymers, 181: 358-367.

[76] Chatterjee, S. Tran, H.N. Godfred, O.-B. ve Woo, S.H., (2018). "Supersorption capacity of anionic dye by newer chitosan hydrogel capsules via green surfactant exchange method", ACS Sustainable Chemistry & Engineering, 6: 3604-3614.

[77] Saber-Samandari, S. Saber-Samandari, S. Joneidi-Yekta, H. ve Mohseni, M., (2017). "Adsorption of anionic and cationic dyes from aqueous solution using gelatin-based magnetic nanocomposite beads comprising carboxylic acid functionalized carbon nanotube", Chemical Engineering Journal, 308: 1133-1144.

[78] Das, S. Chakraborty, P. Ghosh, R. Paul, S. Mondal, S. Panja, A. ve Nandi, A.K., (2017). "Folic acid-polyaniline hybrid hydrogel for adsorption/reduction of chromium (VI) and selective adsorption of anionic dye from water", ACS Sustainable Chemistry & Engineering, 5: 9325-9337.

[79] Kanmani, P. Aravind, J. Kamaraj, M. Sureshbabu, P. ve Karthikeyan, S., (2017). "Environmental applications of chitosan and cellulosic biopolymers: A comprehensive outlook", Bioresource Technology, 242: 295-303.

[80] Rehm, B. ve Fata Moradali, M., (2018). Alginates and Their Biomedical Applications.

[81] Zare, M. Ramezani, Z. ve Rahbar, N., (2016). "Development of zirconia nanoparticles-decorated calcium alginate hydrogel fibers for extraction of organophosphorous pesticides from water and juice samples: Facile synthesis and application with elimination of matrix effects", Journal of Chromatography A, 1473: 28-37.

[82] Katsen-Globa, A. Meiser, I. Petrenko, Y.A. Ivanov, R.V. Lozinsky, V.I. Zimmermann, H. ve Petrenko, A.Y., (2014). "Towards ready-to-use 3-D scaffolds for regenerative medicine: adhesion-based cryopreservation of human mesenchymal stem cells attached and spread within alginate–gelatin cryogel scaffolds", Journal of Materials Science: Materials in Medicine, 25: 857-871.

[83] Lee, K.Y. Rowley, J.A. Eiselt, P. Moy, E.M. Bouhadir, K.H. ve Mooney, D.J., (2000). "Controlling mechanical and swelling properties of alginate hydrogels independently by cross-linker type and cross-linking density", Macromolecules, 33: 4291-4294.

[84] Lezehari, M. Basly, J.-P. Baudu, M. ve Bouras, O., (2010). "Alginate encapsulated pillared clays: removal of a neutral/anionic biocide (pentachlorophenol) and a cationic dye (safranine) from aqueous solutions", Colloids and Surfaces A: Physicochemical and Engineering Aspects, 366: 88-94.

[85] Li, Y. Du, Q. Liu, T. Sun, J. Wang, Y. Wu, S. Wang, Z. Xia, Y. ve Xia, L., (2013). "Methylene blue adsorption on graphene oxide/calcium alginate composites", Carbohydrate Polymers, 95: 501-507.

[86] Mahmoodi, N.M. Hayati, B. Arami, M. ve Bahrami, H., (2011). "Preparation, characterization and dye adsorption properties of biocompatible composite (alginate/titania nanoparticle)", Desalination, 275: 93-101.

[87] Jlassi, K. Krupa, I. ve Chehimi, M.M., (2017). Chapter 1 - Overview: Clay Preparation, Properties, Modification, K. Jlassi Chehimi, M.M. ve Thomas, S., ed. Clay-Polymer Nanocomposites. Elsevier, 1-28.

[88] Zoveidavianpoor, M., (2018). Current Topics in the Utilization of Clay in Industrial and Medical Applications.

[89] Steinmetz, D.R., (2007). "Texture evolution in processing of polystyrene-clay nanocomposites".

[90] Zhu, R. Chen, Q. Zhou, Q. Xi, Y. Zhu, J. ve He, H., (2016). "Adsorbents based on montmorillonite for contaminant removal from water: A review", Applied Clay Science, 123: 239-258.

[91] Akpomie, K.G. Dawodu, F.A. ve Adebowale, K.O., (2015). "Mechanism on the sorption of heavy metals from binary-solution by a low cost montmorillonite and its desorption potential", Alexandria Engineering Journal, 54: 757-767.

[92] Rathnayake, S.I. Xi, Y. Frost, R.L. ve Ayoko, G.A., (2016). "Environmental applications of inorganic–organic clays for recalcitrant organic pollutants removal: Bisphenol A", Journal of Colloid and Interface Science, 470: 183-195.

[93] Shattar, S. Zakaria, N. ve Foo, K., (2016). "Feasibility of montmorillonite-assisted adsorption process for the effective treatment of organo-pesticides", Desalination and Water Treatment, 57: 13645-13677.

[94] Almeida, C.A.P. Debacher, N.A. Downs, A.J. Cottet, L. ve Mello, C.A.D., (2009). "Removal of methylene blue from colored effluents by adsorption on montmorillonite clay", Journal of Colloid and Interface Science, 332: 46-53.

[95] Wang, W. Zhao, Y. Bai, H. Zhang, T. Ibarra-Galvan, V. ve Song, S., (2018). "Methylene blue removal from water using the hydrogel beads of poly (vinyl alcohol)-sodium alginate-chitosan-montmorillonite", Carbohydrate Polymers, 198: 518-528.

[96] Li, H. Zhang, S. Liang, Y. Liu, Q. Mao, X. ve Li, Y., (2018). "Trimeric Surfactant Modified Montmorillonite Immobilized in Alginate Beads: An Efficient Adsorbent for Removal of Cu 2+ and Methyl Orange from Aqueous Solution", Russian Journal of Physical Chemistry A, 92: 2802-2810.

[97] Saavedra-Labastida, E. Díaz-Nava, M. Illescas, J. ve Muro, C., (2019). "Comparison of the Removal of an Anionic Dye from Aqueous Solutions by Adsorption with Organically Modified Clays and their Composites", Water, Air, & Soil Pollution, 230: 88.

[98] Remigio-Reyes, G.D. Illescas, J. ve del Carmen Díaz-Nava, M., (2018). "Removal of bromophenol blue dye from aqueous solutions through the synthesis and characterization of a polymer-clay composite", MRS Advances, 3: 3751-3755.

[99] Hassani, A. Soltani, R.D.C. Karaca, S. ve Khataee, A., (2015). "Preparation of montmorillonite–alginate nanobiocomposite for adsorption of a textile dye in aqueous phase: isotherm, kinetic and experimental design approaches", Journal of Industrial and Engineering Chemistry, 21: 1197-1207.

[100] Taleb, M.F.A. Hegazy, D.E. ve Ismail, S.A., (2012). "Radiation synthesis, characterization and dye adsorption of alginate–organophilic montmorillonite nanocomposite", Carbohydrate Polymers, 87: 2263-2269.

[101] Pawar, R.R. Gupta, P. Sawant, S.Y. Shahmoradi, B. ve Lee, S.-M., (2018). "Porous synthetic hectorite clay-alginate composite beads for effective adsorption of methylene blue dye from aqueous solution", International Journal of Biological Macromolecules, 114: 1315-1324.

[102] Oussalah, A. Boukerroui, A. Aichour, A. ve Djellouli, B., (2019). "Cationic and anionic dyes removal by low-cost hybrid alginate/natural bentonite composite beads: Adsorption and reusability studies", International Journal of Biological Macromolecules, 124: 854-862.

[103] Fabryanty, R. Valencia, C. Soetaredjo, F.E. Putro, J.N. Santoso, S.P. Kurniawan, A. Ju, Y.-H. ve Ismadji, S., (2017). "Removal of crystal violet dye by adsorption using bentonite – alginate composite", Journal of Environmental Chemical Engineering, 5: 5677-5687.

[104] Porada, S. Zhao, R. van der Wal, A. Presser, V. ve Biesheuvel, M., (2013). Review on the science and technology of water desalination by capacitive deionization.

[105] Sen, T. Ozcelik, B. Qiao, G.G. ve Ozmen, M.M., (2017). "Hierarchical porous hybrid chitosan scaffolds with tailorable mechanical properties", Materials Letters, 209: 528-531.

[106] Shang, K. Liao, W. Wang, J. Wang, Y.-T. Wang, Y.-Z. ve Schiraldi, D.A., (2015). "Nonflammable alginate nanocomposite aerogels prepared by a simple freeze-drying and post-cross-linking method", ACS applied materials & interfaces, 8: 643-650.

[107] Petrenko, Y.A. Ivanov, R. Petrenko, A.Y. ve Lozinsky, V., (2011). "Coupling of gelatin to inner surfaces of pore walls in spongy alginate-based scaffolds facilitates the adhesion, growth and differentiation of human bone marrow mesenchymal stromal cells", Journal of Materials Science: Materials in Medicine, 22: 1529-1540.

[108] Sen, T. Ozcelik, B. ve Ozmen, M.M., (2019). "Tough and hierarchical porous cryogel scaffolds preparation using n-butanol as a non-solvent", International Journal of Polymeric Materials and Polymeric Biomaterials, 68: 411-416.

[109] Bencherif, S.A. Braschler, T.M. ve Renaud, P., (2013). "Advances in the design of macroporous polymer scaffolds for potential applications in dentistry", J Periodontal Implant Sci, 43: 251-261.

[110] Ozmen, M.M. Dinu, M.V. Dragan, E.S. ve Okay, O., (2007). "Preparation of Macroporous Acrylamide-Based Hydrogels: Cryogelation Under Isothermal Conditions", Journal of Macromolecular Science, Part A: Pure and Applied Chemistry, 44: 1195-1202.

[111] Shirbin, S.J. Lam, S.J. Chan, N.J.-A. Ozmen, M.M. Fu, Q. O'Brien-Simpson, N. Reynolds, E.C. ve Qiao, G.G., (2016). "Polypeptide-based macroporous cryogels

with inherent antimicrobial properties: the importance of a macroporous structure", ACS Macro Letters, 5: 552-557.

[112] Ozmen, M.M. ve Okay, O., (2005). "Superfast responsive ionic hydrogels with controllable pore size", Polymer, 46: 8119-8127.

[113] Kumar, A. ve Srivastava, A., (2010). "Cell separation using cryogel-based affinity chromatography", Nature protocols, 5: 1737.

[114] Dragan, E.S. ve Loghin, D.F.A., (2013). "Enhanced sorption of methylene blue from aqueous solutions by semi-IPN composite cryogels with anionically modified potato starch entrapped in PAAm matrix", Chemical Engineering Journal, 234: 211-222.

[115] Loo, S.-L. Fane, A.G. Lim, T.-T. Krantz, W.B. Liang, Y.-N. Liu, X. ve Hu, X., (2013). "Superabsorbent cryogels decorated with silver nanoparticles as a novel water technology for point-of-use disinfection", Environmental science & technology, 47: 9363-9371.

[116] Fatoni, A. Numnuam, A. Kanatharana, P. Limbut, W. Thammakhet, C. ve Thavarungkul, P., (2013). "A highly stable oxygen-independent glucose biosensor based on a chitosan-albumin cryogel incorporated with carbon nanotubes and ferrocene", Sensors and Actuators B: Chemical, 185: 725-734.

[117] Tripathi, A. ve Kumar, A., (2011). "Multi-Featured Macroporous Agarose–Alginate Cryogel: Synthesis and Characterization for Bioengineering Applications", Macromolecular bioscience, 11: 22-35.

[118] Koshy, S.T. Zhang, D.K.Y. Grolman, J.M. Stafford, A.G. ve Mooney, D.J., (2018). "Injectable nanocomposite cryogels for versatile protein drug delivery", Acta biomaterialia, 65: 36-43.

[119] Kumari, J. Karande, A.A. ve Kumar, A., (2015). "Combined effect of cryogel matrix and temperature-reversible soluble–insoluble polymer for the development of in vitro human liver tissue", ACS applied materials & interfaces, 8: 264-277.

[120] Dragan, E.S. Lazar, M.M. Dinu, M.V. ve Doroftei, F., (2012). "Macroporous composite IPN hydrogels based on poly (acrylamide) and chitosan with tuned swelling and sorption of cationic dyes", Chemical Engineering Journal, 204: 198-209.

[121] Sahiner, N. Yildiz, S. ve Sagbas, S., (2018). "Graphene oxide embedded P (4-VP) cryogel composites for fast dye removal/separations", Polymer Composites, 39: 1694-1703.

[122] Al-Hussain, S.A. Ezzat, A.O. Gaffer, A.K. ve Atta, A.M., (2018). "Removal of organic water pollutant using magnetite nanomaterials embedded with ionic copolymers of 2-acrylamido-2-methylpropane sodium sulfonate cryogels", Polymer International, 67: 166-177.

[123] Dragan, E.S. ve Dinu, M.V., (2015). Interpenetrating Polymer Network Composite Cryogels with Tailored Porous Morphology and Sorption Properties,

S. Reichelt, ed. Affinity Chromatography: Methods and Protocols. New York, NY: Springer New York, 239-252.

[124] Tuncaboylu, D.C. ve Okay, O., (2010). "Hierarchically macroporous cryogels of polyisobutylene and silica nanoparticles", Langmuir, 26: 7574-7581.

[125] Tan, W.S. ve Ting, A.S.Y., (2014). "Alginate-immobilized bentonite clay: Adsorption efficacy and reusability for Cu(II) removal from aqueous solution", Bioresource Technology, 160: 115-118.

[126] Etcheverry, M. Cappa, V. Trelles, J. ve Zanini, G., (2017). "Montmorillonite-alginate beads: Natural mineral and biopolymers based sorbent of paraquat herbicides", Journal of Environmental Chemical Engineering, 5: 5868-5875.

[127] Birgersson, M. Karnland, O. ve Nilsson, U., (2008). "Freezing in saturated bentonite–A thermodynamic approach", Physics and Chemistry of the Earth, Parts A/B/C, 33: S527-S530.

[128] Strachotová, B. Matějka, L. Sikora, A. Spevacek, J. Konefał, R. Zhigunov, A. ve Slouf, M., (2016). Insight into the cryopolymerization to form poly(N-isopropylacrylamide) / clay macroporous gel. Structure and phase evolution.

[129] Zlopasa, J. Norder, B. Koenders, E.A.B. ve Picken, S.J., (2016). "Rheological investigation of specific interactions in Na Alginate and Na MMT suspension", Carbohydrate polymers, 151: 144-149.

[130] Lee, W.F. ve Fu, Y.T., (2003). "Effect of montmorillonite on the swelling behavior and drug-release behavior of nanocomposite hydrogels", Journal of Applied Polymer Science, 89: 3652-3660.

[131] Su, X. ve Chen, B., (2018). "Transparent, UV-proof and mechanically strong montmorillonite/alginate/Ca2+ nanocomposite hydrogel films with solvent sensitivity", Applied Clay Science, 165: 223-233.

[132] Belhouchat, N. Zaghouane-Boudiaf, H. ve Viseras, C., (2017). "Removal of anionic and cationic dyes from aqueous solution with activated organo-bentonite/sodium alginate encapsulated beads", Applied Clay Science, 135: 9-15.

[133] Wang, W. Zhao, Y. Bai, H. Zhang, T. Ibarra-Galvan, V. ve Song, S., (2018). "Methylene blue removal from water using the hydrogel beads of poly(vinyl alcohol)-sodium alginate-chitosan-montmorillonite", Carbohydrate Polymers, 198: 518-528.

[134] Benhouria, A. Islam, M.A. Zaghouane-Boudiaf, H. Boutahala, M. ve Hameed, B.H., (2015). "Calcium alginate–bentonite–activated carbon composite beads as highly effective adsorbent for methylene blue", Chemical Engineering Journal, 270: 621-630.

[135] Thakur, S. Pandey, S. ve Arotiba, O.A., (2016). "Development of a sodium alginate-based organic/inorganic superabsorbent composite hydrogel for adsorption of methylene blue", Carbohydrate Polymers, 153: 34-46.

[136] Wang, L. Zhang, J. ve Wang, A., (2008). "Removal of methylene blue from aqueous solution using chitosan-g-poly(acrylic acid)/montmorillonite

superadsorbent nanocomposite", Colloids and Surfaces A: Physicochemical and Engineering Aspects, 322: 47-53.

[137] Mahdavinia, G.R. Aghaie, H. Sheykhloie, H. Vardini, M.T. ve Etemadi, H., (2013). "Synthesis of CarAlg/MMt nanocomposite hydrogels and adsorption of cationic crystal violet", Carbohydrate Polymers, 98: 358-365.

[138] H., U., Applications of Carbodiimides, ed. Chemistry and Technology of Carbodiimides.

[139] Voo, W.-P. Lee, B.-B. Idris, A. Islam, A. Tey, B.-T. ve Chan, E.-S., (2015). "Production of ultra-high concentration calcium alginate beads with prolonged dissolution profile", RSC Advances, 5: 36687-36695.

[140] Önnby, L. Svensson, C. Mbundi, L. Busquets, R. Cundy, A. ve Kirsebom, H., (2014). "γ-Al2O3-based nanocomposite adsorbents for arsenic (v) removal: Assessing performance, toxicity and particle leakage", Science of the Total Environment, 473: 207-214.

[141] Zhao, X. Guo, B. Wu, H. Liang, Y. ve Ma, P.X., (2018). "Injectable antibacterial conductive nanocomposite cryogels with rapid shape recovery for noncompressible hemorrhage and wound healing", Nature communications, 9: 2784.

[142] Shirbin, S.J. Karimi, F. Chan, N.J.-A. Heath, D.E. ve Qiao, G.G., (2016). "Macroporous hydrogels composed entirely of synthetic polypeptides: biocompatible and enzyme biodegradable 3D cellular scaffolds", Biomacromolecules, 17: 2981-2991.

[143] Suner, S.S. Demirci, S. Yetiskin, B. Fakhrullin, R. Naumenko, E. Okay, O. Ayyala, R.S. ve Sahiner, N., (2019). "Cryogel composites based on hyaluronic acid and halloysite nanotubes as scaffold for tissue engineering", International Journal of Biological Macromolecules.

[144] El-Naggar, M.E. Abdelgawad, A.M. Tripathi, A. ve Rojas, O.J., (2017). "Curdlan cryogels reinforced with cellulose nanofibrils for controlled release", Journal of Environmental Chemical Engineering, 5: 5754-5761.

[145] Al-Hussain, S. Atta, A. Al-Lohedan, H. Ezzat, A. ve Tawfeek, A., (2018). "Application of New Sodium Vinyl Sulfonate–co-2-Acrylamido-2-me [thylpropane Sulfonic Acid Sodium Salt-Magnetite Cryogel Nanocomposites for Fast Methylene Blue Removal from Industrial Waste Water", Nanomaterials, 8: 878.

[146] Loo, S.-L. Lim, T.-T. Krantz, W.B. Fane, A.G. ve Hu, X., (2015). "Potential evaluation and perspectives on using sponge-like superabsorbent cryogels for onsite water treatment in emergencies", Desalination and Water Treatment, 53: 1506-1515.

[147] Shu, Y. Huang, R. Wei, X. Liu, L. ve Jia, Z., (2017). "Pb (II) Removal Using TiO2-Embedded Monolith Composite Cryogel as an Alternative Wastewater Treatment Method", Water, Air, & Soil Pollution, 228: 375.

[148] Tan, W.S. ve Ting, A.S.Y., (2014). "Alginate-immobilized bentonite clay: adsorption efficacy and reusability for Cu (II) removal from aqueous solution", Bioresource technology, 160: 115-118.

CIRRICULUM VITAE

PERSONAL INFORMATION

Name Surname : Serap HAFIZOGLU

Date of Birth and Place : 14.02.1995 Giresun

Foreing Languages : English

E-mail : seraph1903@gmail.com

EDUCATION

Degree	Department	School/University	Date of Graduation
Master of Science	Bioengineering	Yildiz Technical University	2019
Undergraduate	Bioengineering	Yildiz Technical University	2017
High School	Quantitative	Halil Gurel Anatolian High School	2012

PUBLISHMENTS

Conference Papers

1. Hafızoğlu, S., Ozmen, M., (2019). ''Post-Crosslinked Alginate/Montmorillonite Composite Hydrogels for Methylene Blue Removal'', 4th International Mediterranean Science and Engineering Congress, 25-27.04.2019, Antalya.

2. Hafızoğlu, S., Ozmen, M., (2019). ''Highly Effective Alginate-based Composite Cryogels as Adsorbents for Dye Removal'', 2nd International Eurasian Conference on Biological and Chemical Sciences, 28-29.06.2019, Ankara.

Projects

1. ''Adsorbent Olarak Aljinat Hidrojellerinin Eldesi için Kontra Hazırlama Yöntemlerinin Kullanılması'', (FYL-3432), Scientific Research Projects Coordination Department of Yildiz Technical University, 2018.

AWARDS

1. Highest Ranked Student Award of Bioengineering Department, Yıldız Technical University, 2017.

2. Higher Education Success Award, Turkish Educational Foundation, 2016.

SCHOLARSHIPS

1. Hafizoglu S., ''Adsorbent Olarak Aljinat Hidrojellerinin Eldesi için Kontra Hazırlama Yöntemlerinin Kullanılması'' (2019), TUBITAK-BIDEB, 2210-C National Post-Graduate Scholarship Program for Priority Areas.

2. Undergraduate Scholarship (2013), Turkish Educational Foundation.